R-06-24

Hydrogeological DFN modelling using structural and hydraulic data from KLX04

Preliminary site description Laxemar subarea – version 1.2

Sven Follin, SF GeoLogic AB

Martin Stigsson, Svensk Kärnbränslehantering AB

Urban Svensson, Computer-aided Fluid Engineering AB

April 2006

Svensk Kärnbränslehantering AB
Swedish Nuclear Fuel
and Waste Management Co
Box 5864
SE-102 40 Stockholm Sweden
Tel 08-459 84 00
+46 8 459 84 00
Fax 08-661 57 19
+46 8 661 57 19

ISSN 1402-3091
SKB Rapport R-06-24

Hydrogeological DFN modelling using structural and hydraulic data from KLX04

Preliminary site description Laxemar subarea – version 1.2

Sven Follin, SF GeoLogic AB

Martin Stigsson, Svensk Kärnbränslehantering AB

Urban Svensson, Computer-aided Fluid Engineering AB

April 2006

Notation

a	Power-law coefficient in $T = a\ r^{\,b}$
b	Power-law exponent in $T = a\ r^{\,b}$
k_r	Shape parameter for a power-law fit to $G[r' > r]$
k_T	Shape parameter for a power-law fit to $G[T' > T]$
m_r	Value of r at $G[r' > r] = 1$
m_T	Value of T at $G[T' > T] = 1$
r	Fracture radius
r_0	Location parameter
r_w	Core-drilled borehole radius in SKB's site investigations
s	Standard deviation
t	Outcrop fracture trace length
$G[X' > X]$	Complementary cumulative density function (= $1 - P[X' < X]$)
L	Side length of a square-shaped fracture
N_{CAL}	No. of Open and Partly open fractures
N_{CON}	No. of connected Open and Partly open fractures
N_{PFL}	No. of flowing Open and Partly open fractures with $T > (1–2)\times10^{-9}$ m^2/s
P_{10}	Observed fracture frequency
$P_{10,corr}$	Terzaghi corrected fracture frequency
$P_{32}[r > r_{min}]$	Total fracture surface are per unit volume of rock of all fractures $r > r_{min}$
T	Transmissivity
T_g	Geometric mean transmissivity
α_{DT}	DarcyTools fracture intensity
κ	Fisher concentration
λ	Inverse of the expected value for an exponentially distributed size model

Executive summary

SKB is conducting site investigations for a high-level nuclear waste repository in fractured crystalline rocks at two coastal areas in Sweden. The two candidate areas are named Forsmark and Simpevarp. The investigations started in 2002 and have been planned since the late 1990's. The site characterisation work is divided into two phases, an initial site investigation phase (ISI) and a complete site investigation phase (CSI). The results of the ISI phase are used as a basis for deciding on the subsequent CSI phase. On the basis of the CSI investigations a decision is made as to whether detailed characterisation will be performed (including sinking of a shaft).

An integrated component in the site characterisation work is the development of site descriptive models. These comprise basic models in three dimensions with an accompanying text description. Central in the modelling work is the geological model which provides the geometrical context in terms of a model of deformation zones and the rock mass between the zones. Using the geological and geometrical description models as a basis, descriptive models for other disciplines (surface ecosystems, hydrogeology, hydrogeochemistry, rock mechanics, thermal properties and transport properties) will be developed. Great care is taken to arrive at a general consistency in the description of the various models and assessment of uncertainty and possible needs of alternative models.

The main objective of this study is to support the development of a hydrogeological DFN model for the Preliminary Site Description of the Laxemar area on a regional-scale (SDM version L1.2). A more specific objective of this study is to assess the propagation of uncertainties in the geological DFN modelling reported for L1.2 into the groundwater flow modelling. An improved understanding is necessary in order to gain credibility for the Site Description in general and the hydrogeological description in particular. The latter will serve as a basis for describing the present-day hydrogeological conditions on a local scale as well as predictions of future hydrogeological conditions. A final aim of this study is to document the hydrogeological DFN modelling approach used during modelling stage 1.2 by the DarcyTools modelling team.

The body of the geological DFN modelling reported for modelling stage L1.2 focuses on investigating the scaling properties of three regional steeply dipping fracture sets in rock domain A, which is the dominating rock domain in the Simpevarp regional model area. There are hydraulic data from four core-drilled boreholes in the Laxemar subarea, KLX01–04. Two of these are fully located in rock domain A, KLX01 and KLX04. The other two penetrate two or more rock domains. KLX03 does not penetrate rock domain A at all. KLX04 is the only borehole in the Laxemar subarea that is densely investigated for fracture transmissivities with both high resolution Posiva Flow Log (difference flow) measurements (PFL-f; 0.1 m) and PSS injection tests (PSS 5 m). The work reported here uses the methodology developed by the DarcyTools modelling team in support of the Preliminary Site Descriptions of the Simpevarp subarea and Forsmark. A cornerstone in this methodology is the detailed difference flow measurements (PFL-f; 0.1 m). The modelling assumes a correlated transmissivity-size model and the results derived are checked against the (PSS 5 m) data. In conclusion, the hydrogeological DFN modelling reported here is limited to treat the geological DFN modelling reported for rock domain A and the geological and hydraulic data for the KLX04 borehole.

Structural and hydraulic data in the KLX04 borehole

Six intervals in the KLX04 borehole are interpreted to have deformation zone type properties in the single-hole geological interpretation. The intervals are denoted by DZ1–DZ6 in Figure S-1. Two of the intervals are correlated with lineaments at surface and are deterministically modelled in the 1.2 deformation zone model as ZSMEW007A (DZ5) and ZSMNW929A (DZ6), respectively. The remaining four intervals with deformation zone like properties are not associated with interpreted lineaments at surface, hence not incorporated into the deformation zone model. Figure S-1 shows the positions of the six intervals with deformation zone like properties together with the available hydraulic information; double-packer injection tests (PSS) and difference-flow anomalies (PFL).

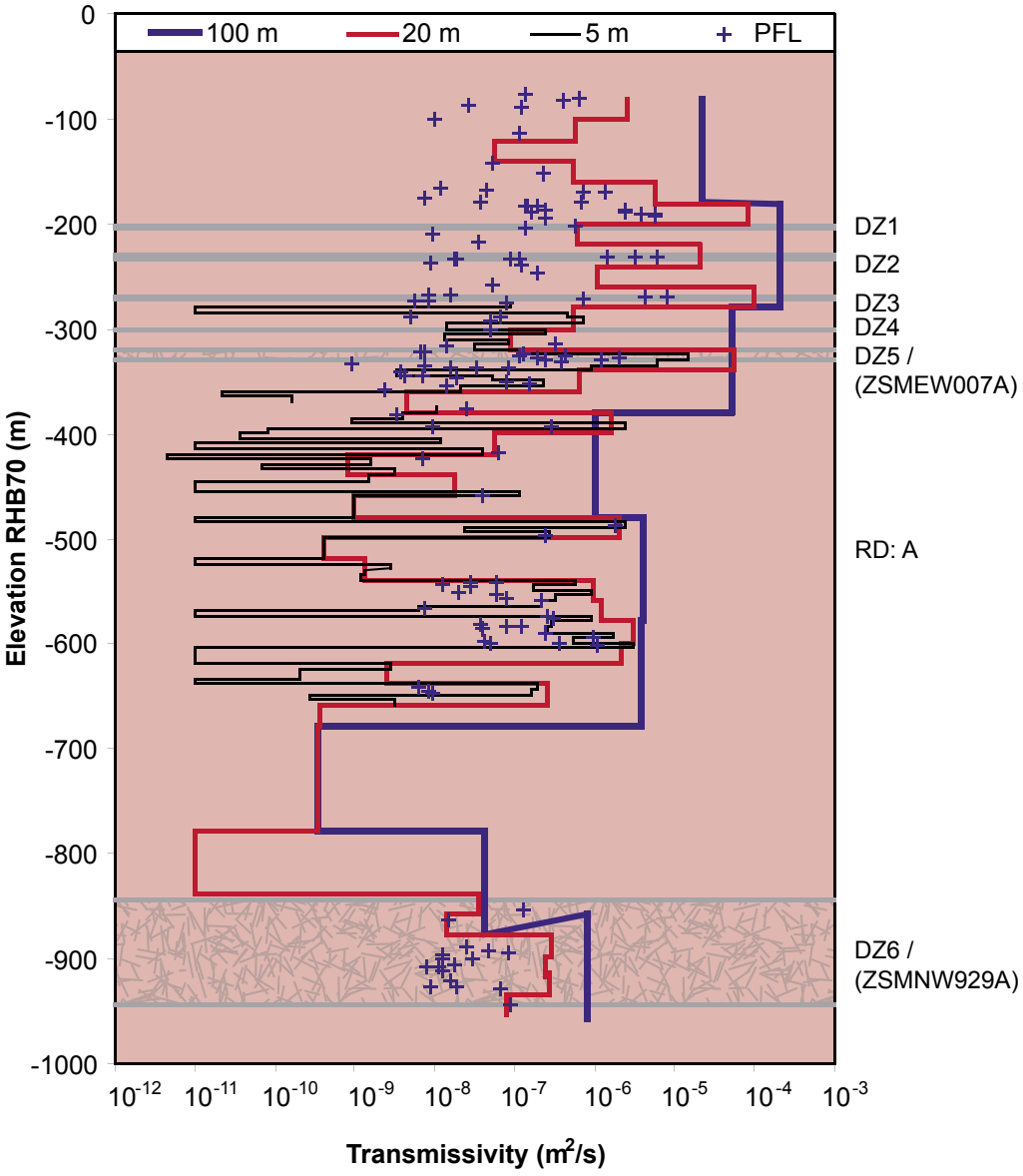

Figure S-1. *Positions of the six intervals with deformation zone like properties DZ1–DZ6 in the KLX04 borehole together with the hydraulic testing conducted; PSS = Pipe String System data: 100 m, 20 m, 5 m and PFL = Posiva Flow Log data (1 m; 0.1 m).*

Geological DFN model in rock domain A

The rock mass outside the deformation zones is modelled geologically by the Discrete Fracture Network (DFN) approach, which conveys a stochastic treatment of the heterogeneity between individual features. Table S-1 shows the orientations, densities and sizes of the five sets of fractures determined to be characteristic for the rock mass in rock domain A within the Laxemar subarea.

Table S-1. Distribution parameters for the geological DFN model in rock domain A within the Laxemar subarea.

Laxemar subarea, Domain A								
Set ID	Orientation[1]			Intensity[2]		Size		
	Trend	Plunge	κ	P_{32} [$r > r_0$]	% Open	Distribution[3]	λ or k_r	r_0
S_A	338.1	4.5	13.06	1.31–1.43	42.5	Power-law	2.85	0.328
S_B	100.4	0.2	19.62	1.03–1.69	37.9	Power-law	3.04	0.977
S_C	212.9	0.9	10.46	0.97–1.52	41.3	Power-law	3.01	0.858
S_d	3.3	62.1	10.13	2.32	40.1	Exponential	4	–
S_f	243	24.4	23.52	1.40	42.1	Power-law	3.6	0.4

[1] Fisher.

[2] Uniformly and randomly distributed.

[3] The parameter λ of the exponential distribution is given as λ = mean^{-1}. The parameters of the power-law distribution are the shape parameter k_r and the location parameter r_0.

Hydrogeological DFN modelling of KLX04 data

Figure S-2 shows a hard sector plot of the orientations in Table S-1. The hard sector algorithm is used in the work reported here to determine the fracture set belonging of mapped fractures in the KLX04 borehole. The algorithm is explained in Appendix B.

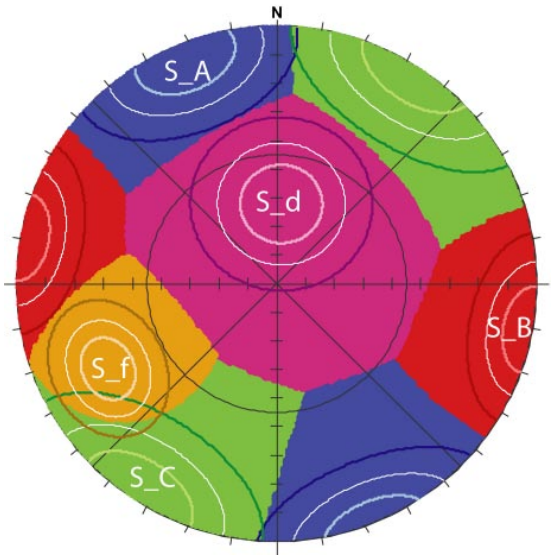

Figure S-2. *Hard sector division of the five fracture sets shown in Table S-1. The mean trend and plunge of each Fisher distribution is close to the position of its label. The contours show the 25%, 50% and 75% probability percentiles for each set, e.g. 25% of the fractures of fracture set S_C are found inside the innermost contour, 50% inside the next contour and 75% inside the outermost contour.*

Figure S-3 shows a complementary cumulative density function plot of all rock mass PFL fracture transmissivities in the KLX04 borehole together with the lumped transmissivity values within the DZ1–DZ4 intervals. The appearance is interpreted as a power-law distribution in the work reported here:

$$G[T' > T] = (1 - P[T' \leq T]) = \left(\frac{m_T}{T} \right)^{k_T} \quad \text{(S-1)}$$

where m_T is the transmissivity value where the power-law regression intersects $G[T' > T] = 1$ and k_T is the slope of the power-law regression.

The Terzaghi correction method is used in the work reported here to correct the P_{10} borehole fracture frequency for the borehole's orientation bias; each fracture is weighted by a factor $1/\cos(\vartheta)$, where ϑ is the angle between the pole to the fracture plane and the borehole trajectory.

The $P_{10,corr}$ Terzaghi corrected fracture frequency of Open fractures varies by elevation in the KLX04 borehole. In effect, the rock masses outside the DZ1–DZ6 intervals are divided into three parts denoted by Volumes I–III, see Tables S-2 through S-4. Volumes I and II are considerably more fractured than Volume III, and Volume II is somewhat more fractured than Volume I.

The $P_{10,corr}$ Terzaghi corrected fracture frequency is used in the work reported here as an estimate of the fracture surface area per unit volume $P_{32}[r > r_0]$. The soundness of this approximation is discussed in the report.

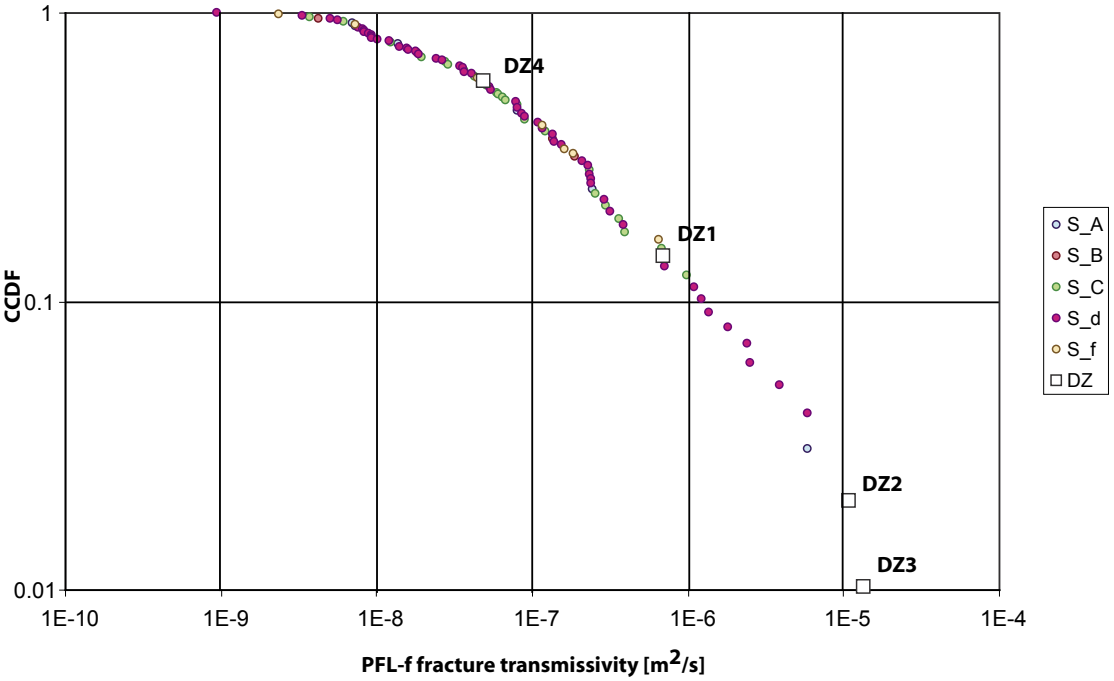

Figure S-3. *CCDF plot the of hydraulic data outside the deterministically treated deformation zones. The data points in the rock mass are coloured according to their set belonging, see Table S-1.*

Tabell S-2. Intensity and hydraulic data for Volume I (–77.43 to –415.78 m.a.s.l.).

Secup (m)	Seclow (m)	Z up (m.a.s.l.)	Z low (m.a.s.l.)	P_{10} (m^{-1})	$P_{10,corr}$ (m^{-1})
102	442	–77.43	–415.78	2.1	3.25
Object	**Set S_A**	**Set S_B**	**Set S_C**	**Set S_d**	**Set S_f**
$P_{10,corr}$ (%)	14.9	10.9	11.7	52.2	10.3
N_{PFL} (–)	6	4	6	45	6
$P_{10,PFL}$ (m^{-1})	0.018	0.012	0.018	0.132	0.018
T_{max} (m^2/s) †	5.9E–6	1.9E–7	6.8E–7	5.8E–6	6.6E–7
T_{min} (m^2/s)	7.0E–9	4.3E–9	3.7E–9	9.4E–10	2.3E–9
T_g (m^2/s)	6.6E–8	3.8E–8	7.8E–8	6.3E–8	7.9E–8
s_{logT} (–)	1.14	0.774	0.796	0.891	1.15

† The maximum transmissivity value in Volume I is 1.3E–5 m^2/s. However, this value is associated with the stochastically treated deformation zone DZ3, see Figure S-1.

Tabell S-3. Intensity and hydraulic data for Volume II (–475.51 to –647.70 m.a.s.l.).

Secup (m)	Seclow (m)	Z up (m.a.s.l.)	Z low (m.a.s.l.)	P_{10} (m^{-1})	$P_{10,corr}$ (m^{-1})
502	675	–475.51	–647.70	2.0	5.40
Object	**Set S_A**	**Set S_B**	**Set S_C**	**Set S_d**	**Set S_f**
$P_{10,corr}$ (%)	12.0	3.0	57.0	23.0	5.0
N_{PFL} (–)	0	0	16	9	1
$P_{10,PFL}$ (m^{-1})	N/A	N/A	0.092	0.052	0.006
T_{max} (m^2/s)	N/A	N/A	9.8E–7	1.8E–6	7.4E–9
T_{min} (m^2/s)	N/A	N/A	6.2E–9	8.4E–9	7.4E–9
T_g (m^2/s)	N/A	N/A	7.1E–8	1.0E–7	7.4E–9
s_{logT} (–)	N/A	N/A	0.595	0.820	N/A

Tabell S-4. Intensity and hydraulic data for Volume III (–721.27 to –952.61 m.a.s.l.).

Secup (m)	Seclow (m)	Z up (m.a.s.l.)	Z low (m.a.s.l.)	P_{10} (m^{-1})	$P_{10,corr}$ (m^{-1})
749	982	–721.27	–952.61	0.36	0.91
Object	**Set S_A**	**Set S_B**	**Set S_C**	**Set S_d**	**Set S_f**
$P_{10,corr}$ (%)	55.4	14.7	11.5	17.2	1.2
N_{PFL} (–)	0	0	1	0	0
$P_{10,PFL}$ (m^{-1})	N/A	N/A	0.004	N/A	N/A
T_{max} (m^2/s)	N/A	N/A	9.0E–8	N/A	N/A
T_{min} (m^2/s)	N/A	N/A	9.0E–8	N/A	N/A
T_g (m^2/s)	N/A	N/A	9.0E–8	N/A	N/A
s_{logT} (–)	N/A	N/A	N/A	N/A	N/A

The data in Tables S-2 through S-4 are commented below:

- In Volume I c 10% of the Open fractures are associated with PFL-f flow anomalies, i.e. have transmissivity values greater than the lower measurement limit of the Posiva Flow Log, which is c (1–2)×10^{-9} m^2/s. In Volume II c 7% of the Open fractures are associated with PFL-f flow anomalies. The fracture intensity in Volume II is c 66% greater than in Volume I, however. In Volume III there is only one (1) PFL-f flow anomaly. The anomaly is located c 0.2 m below the deterministically treated deformation zone interval ZSMNW929A (DZ6). It is advocated that this flow anomaly should be treated as a feature of the ZSMNW929A deformation zone rather than a feature of the rock mass.
- Volume I has five flowing fracture sets. The differences between the sets in terms of T_g geometric means are judged to be insignificant. It is noted that c 62% of the fractures in Volume I are gently dipping (S_d + S_f) and the gently dipping fractures comprise c 76% of the PFL-f flow anomalies.
- Volume II indicates a geometrical anisotropy compared to Volume I with c 57% of the fracture intensity associated with steeply dipping fractures striking NW (set S_C). The second largest fracture set is the gently dipping set S_d with c 23% of the corrected fracture intensity. The two fracture sets have together c 96% of the PFL-f flow anomalies. This suggests that the geometric anisotropy is accompanied by a hydraulic anisotropy.
- In spite of the visible structural and hydraulic differences between Volume I and Volume II the most significant difference in the KLX04 borehole data is that between Volume I and Volume II on one hand and Volume III on the other. If the observations in the KLX04 borehole are considered representative for rock domain A in general, the uppermost c 650 m of data will render a fairly water conductive rock mass. It is suggested that more borehole data at other locations in rock domain A are acquired before the generality of the KLX04 borehole is concluded.

The geological DFN modelling conducted throughout the 1.2 modelling stage (i.e. all areas; Simpevarp, Forsmark and Laxemar) is based on two significant assumptions:

1. a single, continuous, power-law size distribution that spans all scales of observation (from borehole fractures to lineaments), and
2. an uniform and random (Poisson) process for the spatial distribution of fracture centres in the rock masses between the deterministically treated deformation zones.

For the derivation of the location parameter in the Laxemar subarea the geological DFN modelling is supplemented by two additional assumptions not previously used in the geological DFN modelling conducted in the Simpevarp and Forsmark areas:

3. the core-drilled boreholes are perfect scanlines, and
4. all deformation zones with traces at ground surface greater than 1,000 m reaches the bottom of the model volume at –1,100.

These assumptions were used to derive set-specific values of the shape parameter k_r, the location parameter r_0 and the fracture surface area per unit volume $P_{32}[r > r_0]$.

The methodology used in the geological DFN modelling put constraints on what may be suggested in terms of parameter combinations of k_r and r_0, either fairly high values or fairly low values of both k_r and r_0 have to be assumed. For the three steeply dipping fracture sets the geological DFN suggests values of k_r between 2.85–3.04 and values of r_0 between 0.328–0.977. Size distributions are also suggested for the gently dipping fracture sets despite the scarcity of pertinent field observations.

For the sake of understanding how the uncertainties in the geological DFN modelling propagate into the hydrogeological DFN modelling, two parameter combinations that are along the results of the geological DFN modelling are explored in the work reported here. The two combinations simplify the geological DFN modelling in Table S-1:

A. k_r = 2.90 and r_0 = 0.282 m B. k_r = 2.56 and r_0 = 0.038 m

Parameter combination A mimics the parameter values of the geological DFN modelling fairly well. However, this parameter combination produces only 24 deformations zone trace lines greater than 1,000 m within the local model domain. In comparison, there are c 80 lineaments greater than 1,000 m in the deformation zone model. Parameter combination B produces a more correct number of trace lines greater than 1,000 m, but does not meet the assumption that all of them reach the bottom of the model volume at –1,100 m above sea level (cf assumption no. 4 above). The simulation results for parameter combinations A and B are summarised in Table S-5.

- Parameter combination A renders a well connected DFNs; c 100% of the Open fractures are connected in Volumes I and II and c 81% in Volume III.
- Parameter combination B leads to a somewhat less connected DFN; c 91% of the Open fractures in Volume I are connected, c 98% in Volume II, and c 12% in Volume III.

In conclusion, both parameter combinations render well connected DFNs in the more intensely fractured Volumes I and II. In Volume III the difference between the two parameter combinations is much greater because of the lower value of $P_{32}[r > r_0]$, which suggests that the magnitude of $P_{32}[r > r_0]$ affects the role of r_0 on the connectivity.

Table S-5. Results of the connectivity analysis in Volumes I–III. N_{CON} is the number of connected Open and Partly open fractures after calibration against N_{CAL}, which is the total number of Open and Partly open fractures. P_{10CON} is the interval frequency matching N_{CON}. $P_{32}[r > r_0]$ is approximated by the Terzaghi corrected P_{10corr}, which is first estimated from N_{CAL} and then adjusted to match the variability in k_r between the five fractures sets, see Chapter 5. P_{32CON} [%] is N_{CON}/N_{CAL}. All values shown represent mean values of ten realisations.

Case	k_r [–]	r_0 [m]	N_{CON} [–]	P_{10CON} [100 m]	$P_{32}[r > r_0]^{\dagger}$ [m²/m³]	P_{32CON} [%]	P_{32CON} [m²/m³]	$P_{32CON} < T_{min}$ [% of P_{32CON}]	$P_{32CON} > T_{min}$ [% of P_{32CON}]
Volume I: N_{CAL} = 704									
A	2.90	0.28	702	205	3.73	99.8	3.86	90	10
B	2.56	0.038	638	187	3.79	90.6	3.55	89	11
Volume II: N_{CAL} = 351									
A	2.90	0.282	351	202	5.38	100	5.38	93	7
B	2.56	0.038	344	198	5.53	98.1	5.43	92	8
Volume III: N_{CAL} = 84									
A	2.90	0.282	68	29	0.98	81.2	0.79	99	1
B	2.56	0.038	10	4	1.10	12.3	0.14	90	10

† The values shown are the arithmetic averages of ten realisations and should be equal within each volume regardless of the values of k_r and r_0. The differences are caused by too few simulations.

The work reported here uses the methodology developed in support of the Preliminary Site Descriptions of the Simpevarp subarea and Forsmark. A cornerstone in this methodology is the detailed difference flow measurements (PFL-f; 0.1 m). The modelling postulates a correlated transmissivity-size model

$$T = a\, r^{\,b} \qquad \text{(S-2)}$$

where a and be b are deduced by means of numerical simulations. The simulations couple the geological DFN model to the hydraulic testing with the PFL-f method. The results derived are checked against the (PSS 5 m) data. Figure S-4 shows the outcome of ten realisations for each parameter combination (A and B) and Volume (I–III). The variability between the realisations means that there is an uncertainty in the exact shape of the correlation between the fracture transmissivity and the fracture size.

Figures S-5 and S-6 demonstrate that both parameter combinations give fair fits in the transmissivity range 10^{-9}–10^{-5} m^2/s when the outcome of a correlated transmissivity-size model derived from the PFL-f transmissivity data is compared with measured PSS 5 m (Pipe String System) transmissivity data.

The matching against PSS 5 m data is not very sensitive to the tested parameter combinations. This is interpreted to be due to the high fracture intensity and the postulated correlated transmissivity-size model. That is, in each simulation the largest fractures are associated with the N_{PFL} observed inflows (transmissivities). Hence, the major difference between different parameter combinations is in lower end of the size distribution where the number of connected fractures N_{CON} differs depending on the assumed values of k_r and r_0. The contribution of flow from small fractures is difficult to appreciate hydraulically, however, because of the magnitude of lower measurement limit of the PFL-f method, which is c (1–2)×10^{-9} m^2/s. If this threshold value is sufficient for Safety Assessment, a key figure is that c 7–10% of all Open fractures are associated with flow greater than the lower measurement limit of the PFL-f method according to the data shown in Tables S-2 and S-3.

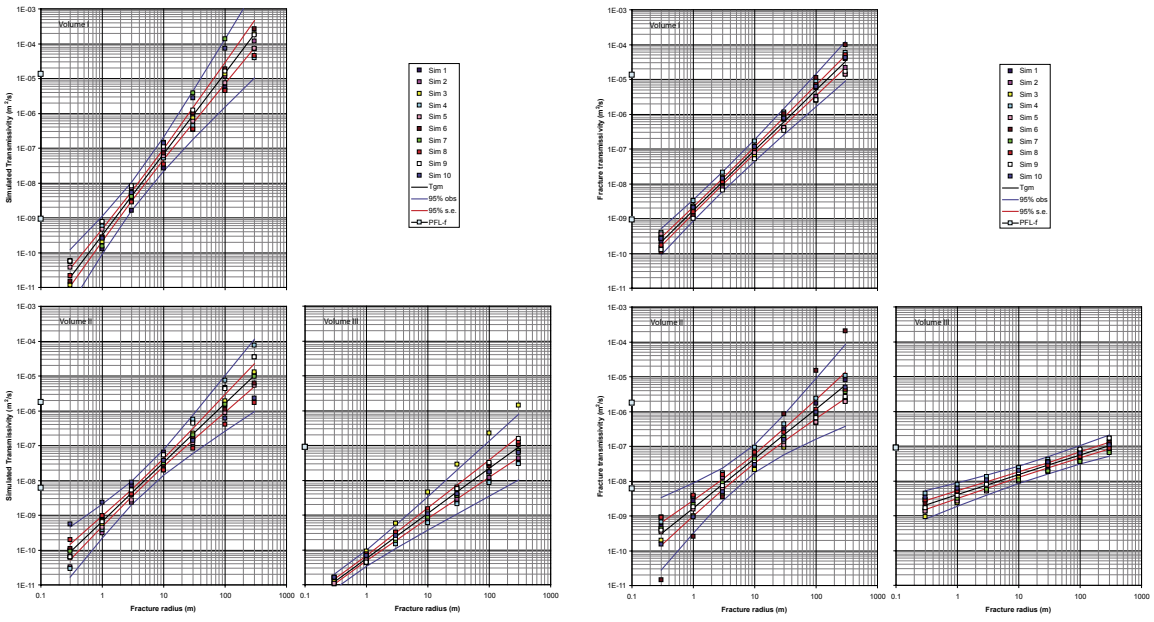

Figure S-4. *Simulation results for Volumes I–III using parameter combination A (left) and B (right).*

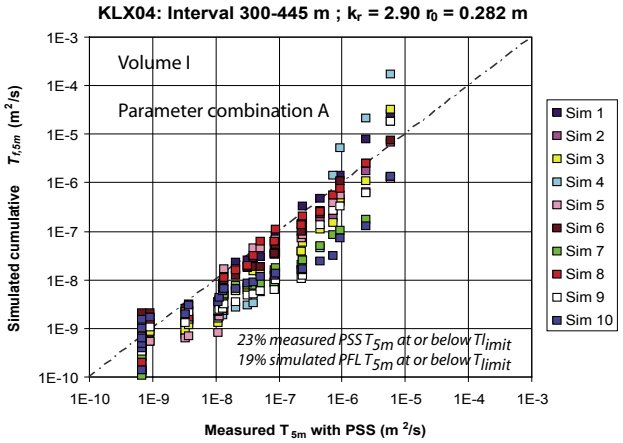

Figure S-5. *Cross plot of simulated T_{5m} versus measured T_{5m} in Volume I using a correlated transmissivity-size model and parameter combination A.*

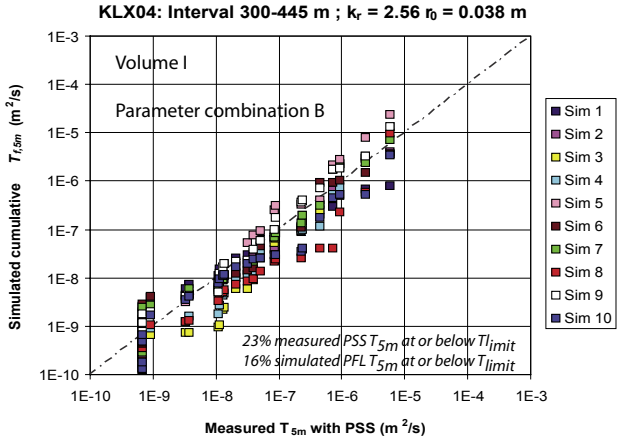

Figure S-6. *Cross plot of simulated T_{5m} versus measured T_{5m} in Volume I using a correlated transmissivity-size model and parameter combination B.*

Discussion and conclusions

The spatial variation of the fracture intensity is a key issue for the hydrogeological DFN modelling. Throughout the 1.2 modelling stage, the statistics of outcrop fractures have been used as input data as well as calibration targets in the geological DFN modelling. Based on the work reported form the geological DFN modelling and the work reported here we advocate that the usefulness of fracture intensity measures from outcrop data should be used with care. We consider the fracture frequency P_{10} in core-drilled boreholes a much more important entity. The Terzaghi correction, which is used in the work reported here, is a simplistic method to correct for borehole orientation bias, although it often proves to serve its purpose. We note that other methods exist but we have not explored them in the work reported here.

The modelling experiences gained from the hydrogeological DFN modelling in the Simpevarp subarea and in Forsmark area suggest that the value of the location parameter r_0 is important for the deduced fracture connectivity. However, it is observed in the modelling reported here that the role of r_0 for the fracture connectivity also depends highly on the magnitude of P_{10}. For a high value of P_{10} the fracture connectivity is less sensitive to the value of r_0.

The mean spacing between Open and Partly open in the KLX04 borehole, i.e. P_{10}^{-1}, is c 0.5 m above –650 m above sea level and c 2.8 m below. For the suggested range of the location parameter in the geological DFN modelling, i.e. 0.328–0.977 m, the hydrogeological DFN modelling conducted in the work report here renders a mean spacing between *connected* Open and Partly open fractures of c 0.5 m above –650 m above sea level and c 3.5 m below, hence implying a well connected DFN of Open and Partly open fractures. Using a value of the location parameter that is significantly lower than the value suggested by the geological DFN modelling, e.g. 0.038 m, renders a somewhat greater mean spacing, i.e. a somewhat less connected fracture network. However, the mean spacing between connected Open and Partly open fractures cannot exceed the observed spacing between the PFL-f anomalies if the latter are a subset of all connected Open and Partly open fractures. The PFL-f measurements conducted in the KLX04 borehole show that the maximum mean spacing between flowing fractures greater than the lower measurement limit, which is c $(1–2)\times10^{-9}$ m^2/s, is c 5–7 m above –650 m above sea level and c 250 m below. In conclusion, the frequency of PFL-f flow anomalies in the KLX04 borehole indicate already a fairly well connected network of flowing fractures in rock mass around this borehole down to c –650 m above sea level and a poorly connected network of flowing fractures in the rock mass below this elevation.

The observed range of the PFL-f transmissivities in the KLX04 borehole associated with the hydrogeological DFN modelling in the work reported here is c 10^{-9}–10^{-5} m^2/s. Together with the aforementioned spacing of the PFL-f flow anomalies this implies a fairly permeable rock mass above –650 m above sea level. In conclusion, if the observations in the KLX04 borehole are considered representative for the rock mass in general in rock domain A, the bedrock at repositiory depth in the Laxemar subarea is fairly permeable. However, we question if the KLX04 borehole is representative for rock domain A given the outcome of the hydraulic testing in the KLX01–KLX03 boreholes. It is suggested that more borehole data at other locations in rock domain A are acquired before the generality of the KLX04 borehole data is concluded or used in a regional flow model.

The postulated correlated transmissivity-size model used in the work reported here is demonstrated to render results that compare well with measured PSS 5 m (Pipe String System) transmissivity data including the number of 5 m sections below transmissivity threshold of the PSS 5 m tests, which is c 6.5×10^{-10} m^2/s. It is noted that the choice of parameter values of the power-law size distribution model does not seem to have a crucial impact on the fit if a correlated transmissivity-size model is postulated. This is interpreted to be due to the high fracture intensity and the postulated correlated transmissivity-size model. That is, in each simulation the largest fractures are associated with the N_{PFL} observed inflows (transmissivities). Hence, the difference between the different power-law parameter combinations studied here (denoted by A and B in the report) is predominantly in the lower end of the size distribution. It is in this segment of the power-law size distribution the number of connected fractures differs depending on the assumed values of k_r and r_0. The contribution of flow from low-transmissivity fractures is difficult to appreciate, however, because of the magnitude of the lower measurement limit of the PFL-f method.

In conclusion, if the magnitude of the lower measurement limit of the PFL-f method is sufficient, e.g. from a Safety Assessment point of view, the spacing of the PFL-f anomalies is already a good indicator of the hydrogeological DFN connectivity. If the magnitude of the lower measurement limit of the PFL-f method is too large, however, e.g. an order of magnitude or so, the spacing between the hydrogeologically connected fractures is smaller than the spacing between the PFL-f anomalies, which means that the connectivity of important features increases. In such case the spacing between the features of interest is probably better represented by $P_{10,CON}^{-1}$, which is the mean spacing of the *connected* Open and Partly open fractures. However, $P_{10,CON}^{-1}$ depends on the values of r_0, hence an uncertain model parameter.

Contents

1 Introduction

1.1 Background

SKB is conducting site investigations for a high-level nuclear waste repository in fractured crystalline rocks at two coastal areas in Sweden. The two candidate areas are named Forsmark and Simpevarp. The investigations started in 2002 and have been planned since the late 1990's. The site characterisation work is divided into two phases, an initial site investigation phase (ISI) and a complete site investigation phase (CSI). The results of the ISI phase are used as a basis for deciding on the subsequent CSI phase. On the basis of the CSI investigations a decision is made as to whether detailed characterisation will be performed (including sinking of a shaft).

An integrated component in the site characterisation work is the development of site descriptive models. These comprise basic models in three dimensions with an accompanying text description. Central in the modelling work is the geological model which provides the geometrical context in terms of a model of deformation zones and the less fractured rock mass between the zones.

Using the geological and geometrical description models as a basis, descriptive models for other disciplines (surface ecosystems, hydrogeology, hydrogeochemistry, rock mechanics, thermal properties and transport properties) will be developed. Great care is taken to arrive at a general consistency in the description of the various models and assessment of uncertainty and possible needs of alternative models.

1.2 Scope and objectives

During the course of the initial site investigations the geological discrete fracture network (DFN) modelling of the rock mass fracturing has revealed an increasing degree of complexity /SKB 2004ab, 2005ab/. In parts, this complexity results from the growing amount of data gathered as more boreholes are being drilled and investigated, but there is also a substantial component of methodology development invoked. The methodology used at start of the site investigations was primarily based on data and experiences gained from the investigations at Äspö, the conditions of which are probably not fully compatible with those studied in the Simpevarp subarea, Laxemar subarea or Forsmark. A potential site specific factor that contributes to the need for methodology development of the geological DFN modelling concerns the assessment of hydraulic anisotropy and spatial variability, which may be different in Simpevarp, Laxemar and Forsmark.

The main objectives of the work reported here are:

- to review the concepts used in the geological DFN modelling conducted by /Hermanson et al. 2005/ in support of the development of a Preliminary Site Description of the Laxemar subarea (denoted by SDM L1.2), and
- to investigate if the identified uncertainties in the geological DFN modelling are important for the development of a hydrogeological DFN model at Laxemar, i.e. contribute to the assessment of how the uncertainties in the geological DFN modelling propagate into the groundwater flow modelling.

1.3 Limitations

The body of the geological DFN modelling focuses on investigating the scaling properties of three regional steeply dipping fracture sets in rock domain A, which is the dominating rock domain, see Figure 1-1.

There are hydraulic data from four core-drilled boreholes in the Laxemar subarea, KLX01–04, see Table 1-1. Two of these are fully located in rock domain A, KLX01 and KLX04. The other two penetrate two or more rock domains. KLX03 does not penetrate rock domain A at all. Figure 1-2 shows an overview of the single-hole hydraulic test data in KLX01–04 available at the time of the L1.2 Data Freeze, 2005-11-01.

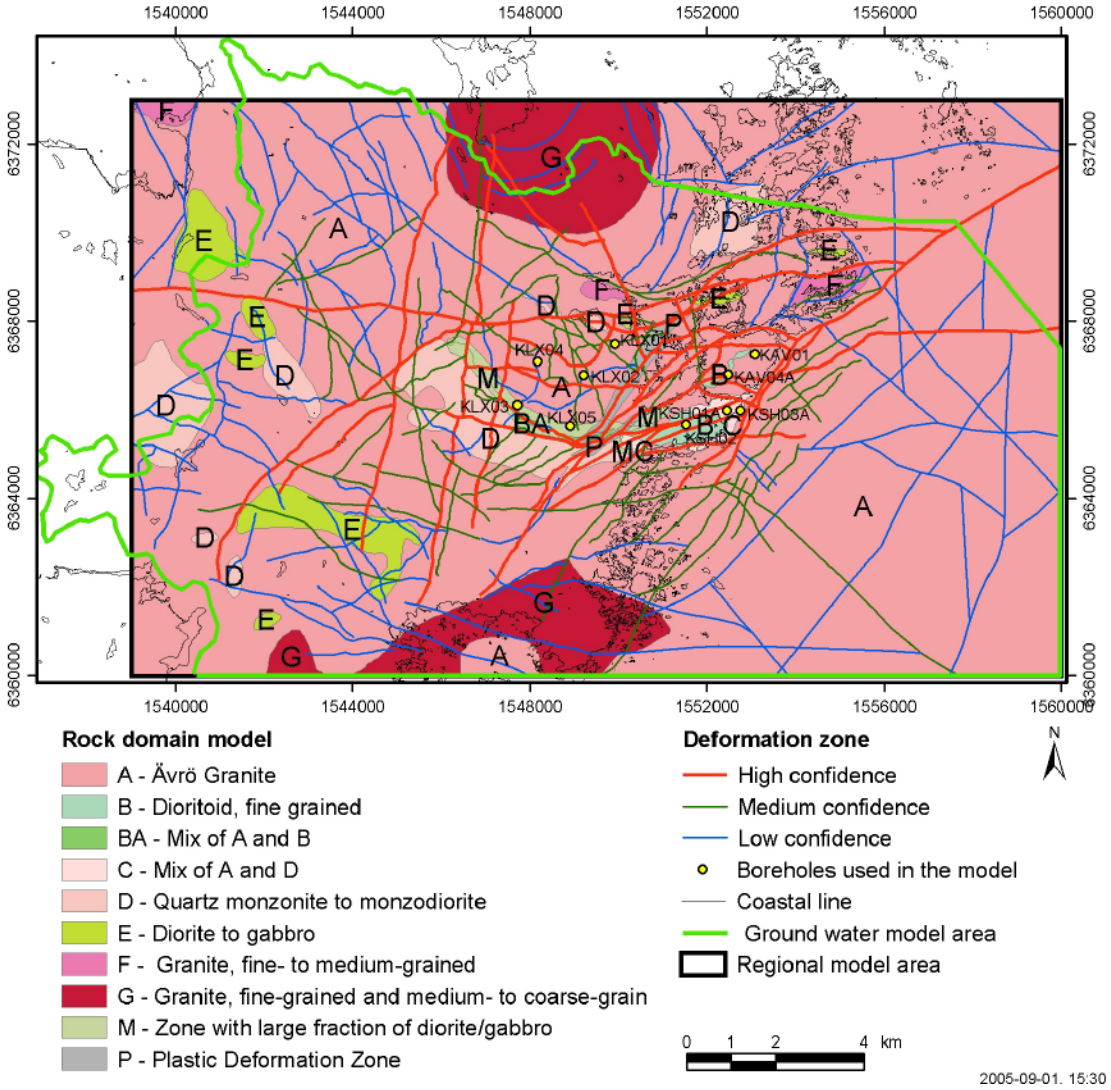

Figure 1-1. *Geological map of the regional model area showing ten rock domains A–P and three kinds of deformation zones. The curved polygon represents the ground water model area /Hermanson et al. 2005/.*

Table 1-1. Overview of the hydraulic tests methods conducted in KLX01–04.

Borehole	PFL-f 0.1 m	PFL 3 m	PSS 3 m	PSS 5 m	PSS 20 m	PSS 30 m	PSS 100 m
KLX01	–	–	Yes	–	–	Yes	–
KLX02	–	Yes	–	Yes	Yes	–	Yes
KLX03	Yes	–	–	–	–	–	Yes
KLX04	Yes	–	–	Yes†	Yes	–	Yes

† PSS 5 m data exist between c –300 to –700 m.a.s.l., see Figure 1-2.

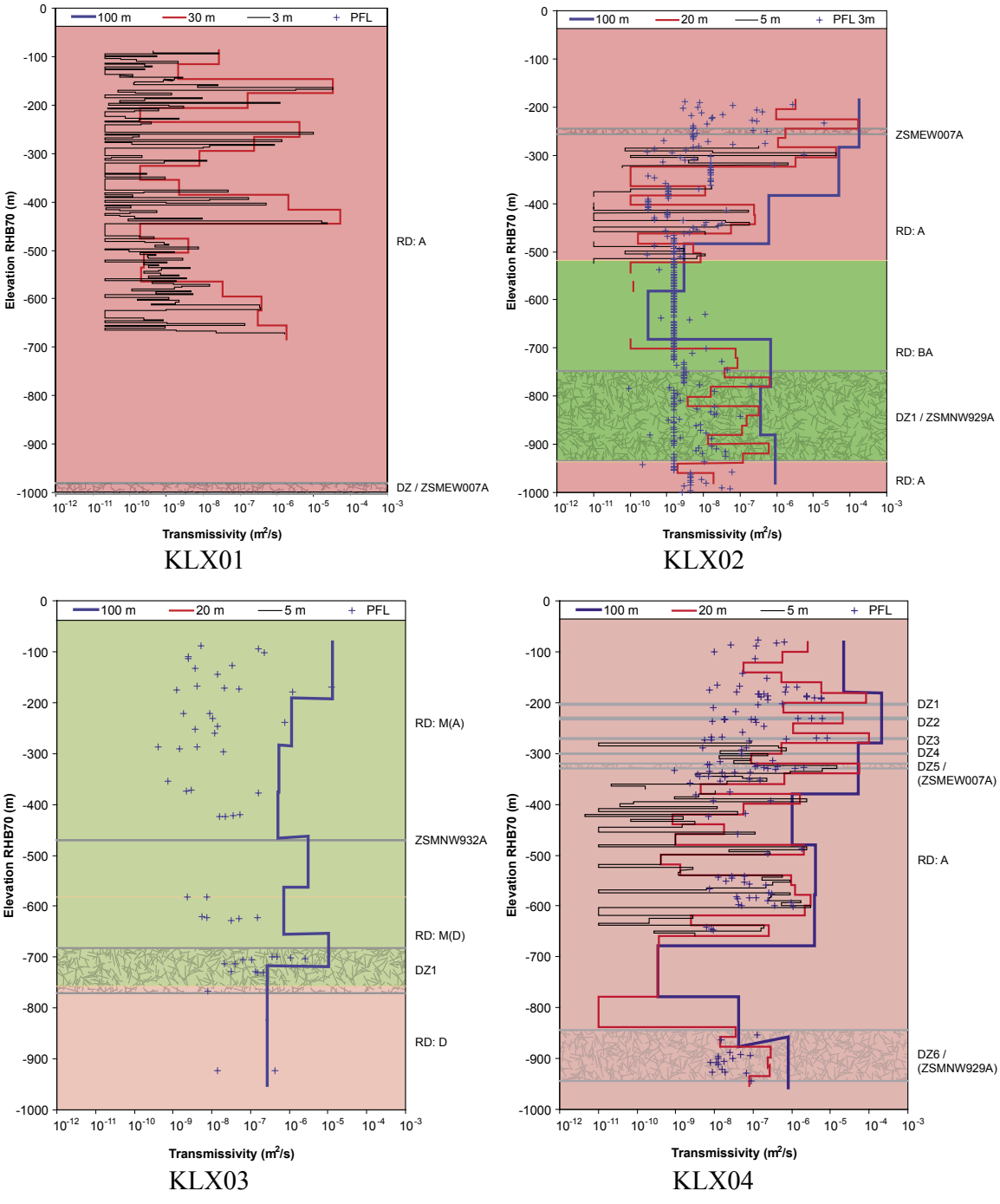

Figure 1-2. *Overview of the single-hole hydraulic test data in KLX01–04 available at the time of the Data Freeze L1.2 (2005-11-01). The borehole analysed in the work reported here is KLX04.*

The work reported here uses the methodology developed by /Follin et al. 2005ab/ in support of the Preliminary Site Descriptions of the Simpevarp subarea /SKB 2005a/ and Forsmark /SKB 2005b/. A cornerstone in this methodology is the detailed difference flow measurements (PFL-f; 0.1 m). The modelling assumes a correlated transmissivity-size model

$$T = a\, r^{b} \qquad (1\text{-}1)$$

where a and be b are deduced by means of numerical simulations. The simulations couple the geological DFN model to the hydraulic testing with the PFL-f method. The results derived are checked against the (PSS 5 m) data.

It is noted that KLX04 is the only borehole in the Laxemar subarea that is densely investigated for fracture transmissivities with both high resolution Posiva Flow Log measurements (PFL-f; 0.1 m) and PSS injection tests (PSS 5 m). In conclusion, the hydrogeological DFN modelling reported here is limited to treat the geological DFN modelling reported for rock domain A by /Hermanson et al. 2005/ and the geological and hydraulic data for borehole KLX04.

1.4 Organisation of work and structure of report

The work presented in this report was conducted by the DarcyTools Team involving hydrogeologists from SF GeoLogic, Swedish Nuclear Fuel and Waste Management Company and Computer-aided Fluid Engineering. The DarcyTools code is developed and maintained by Computer-aided Fluid Engineering /Svensson et al. 2004, Svensson and Ferry 2004, Svensson 2004/. The structure of the report is as follows:

- Chapter 2 presents the primary DFN concepts and assumptions used in the geological DFN modelling throughout modelling stage 1.2 at Simpevarp, Forsmark and Laxemar. Chapter 2 also reviews some of the additional assumptions invoked in support of the geological DFN modelling conducted for Laxemar.
- Chapter 3 presents the structural and hydraulic data in the KLX04 borehole available for hydrogeological DFN modelling.
- Chapter 4 presents the primary concepts and assumptions used in the structural and hydraulic modelling by the DarcyTools Team. Chapter 4 also presents and comments the cases treated in the work reported here.
- Chapter 5 demonstrates the methodology of the hydrogeological DFN modelling and the application to the KLX04 data.
- Chapter 6 discusses the results and concludes the study.

2 DFN concepts in the 1.2 modelling stage

Sections 2.1, 2.2 and 2.3 present the primary DFN concepts used in the geological DFN modelling throughout the 1.2 modelling stage in Simpevarp, Forsmark and Laxemar /La Pointe and Hermanson 2005, La Pointe et al. 2005, Hermanson et al. 2005/. Section 2.4 reviews the additional assumptions invoked in support of the geological DFN for Laxemar.

2.1 Fracture size distribution

One of the most difficult fracture characteristics to measure directly in the subsurface is fracture size. Fracture trace lengths can be measured on outcrops for fractures on the scale of centimetres to several metres, and interpretations of so called deformation zones, i.e. elongated swarms of fractures, are often available on the scale of 500 m to several kilometres. This leaves a gap between the scales and a widely used assumption in geology is one of a continuum of fractures that spans all scales and that can be described by a power-law relationship between fracture intensity and size. The illustration shown in Figure 2-1 demonstrates the approach.

Figure 2-1 illustrates also the conceptual relationship between deterministically treated deformation zones and the stochastic geological DFN as used in the initial site investigations. Deformation zones interpreted to be at least 1,000 m long are treated as deterministic structures, whereas the uncertainty about the position and frequency of zones/fractures less than 1,000 m are treated stochastically. The deterministically treated deformation zones are essentially treated as squares, whereas all stochastic structures are generally treated as circular discs in the geological DFN modelling. In the flow modelling conducted by the DarcyTools Team and the ConnectFlow Team stochastic structures are simulated as squares. The equivalent radius r of a square of size L is shown in Equation (2-1):

$$r = L/\sqrt{\pi} \qquad (2\text{-}1)$$

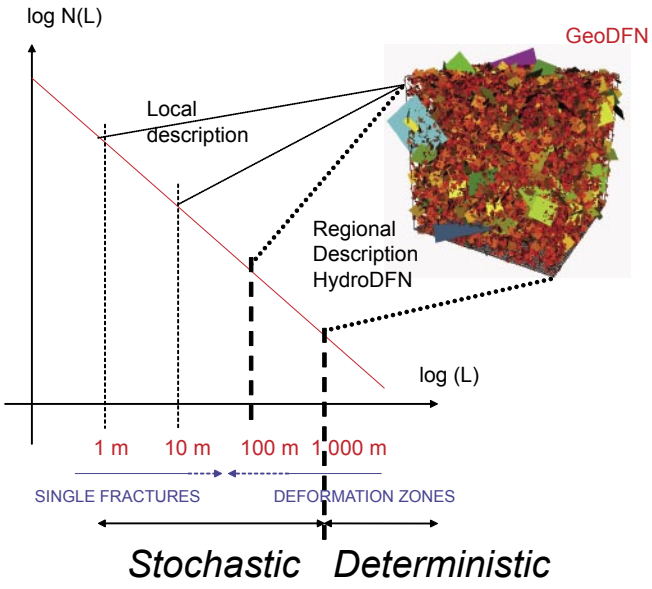

Figure 2-1. *Illustration of the power-law size distribution and the conceptual relationship between deterministically treated deformation zones and the stochastic geological DFN.*

During the initial site investigations the flow modelling is regional and the stochastic simulations use a power-law size distribution model, however, truncated $r_{min} < r < r_{max}$, where r_{min} is set to be of the order of the resolution of the computational grid 50–100 m and r_{max} is set to 1,000 m. Discussions of the role of the chosen value of r_{min} are provided by /Follin et al. 2005b, Hartley et al. 2005b/.

The key parameters of a power-law size population providing the number of fractures of different sizes are the shape parameter k_r and the location parameter r_0, where $k_r > 2$ and $r_0 > 0$ m, i.e.

$$f(r) = \frac{k_r \; r_0^{k_r}}{r^{k_r+1}}, \; r_0 \le r < \infty \qquad (2\text{-}2)$$

The primary method used in the geological DFN modelling for the determination of the shape parameter is to plot fracture trace length and lineament data in so called area-normalised frequency plots. The method allows for a combined analysis of structural data gathered on different scales of observation, i.e. outcrops and lineament maps.

The determination of the shape parameter may be sensitive to the fact that fracture trace lengths and lineament lengths are both subjected to truncation and/or censoring effects as well as substantial subjective ("expert judgement") interpretations. For example, outcrop fracture data are generally mapped to the greatest detail possible, which means that each feature is treated as a single object. In contrast, lineaments are made long by linking clusters of short fractures together. It is therefore possible that some outcrops would yield longer traces than reported, had linking been applied to outcrops too. Finally, it is noted that in some cases the definition of a lineament is not based on direct fracture observations but represent a geophysical anomaly.

The location parameter of a particular data set is by definition the smallest value in the data set. However, the window of observation may vary several orders of magnitude, which means that the minimum values observed in borehole data, outcrop data and lineament data also vary several orders of magnitude, see Table 2-1 and Figure 2-2. Moreover, it vital to note that it is not fracture size, r, that is observed in the field but trace length, t, and that both large and small fractures can produce short trace lengths.

Most probably one cannot observe very small fractures on rough outcrop surfaces but, if present, they will probably show up more easily in the core-drilled borehole as the surface of a cored rock cylinder is very smooth and the resolution of the borehole observation scale is high; the borehole radius, r_w, is 0.038 m in SKB's site investigation, see Figure 2-3. This means that the scale of observation of borehole data is close to one order of magnitude smaller than the scale of observation associated with outcrop surveys. Trace length cannot be observed in core-drilled boreholes, however.

Table 2-1. Range of the minimum and maximum trace length values [t_{min}, t_{max}] associated with the three scales of fracture observations shown in Figure 2-2.

Scale of observation	t_{min} [m]	t_{max} [m]
Core	Centimetres	Decimetres
Outcrop	Several decimetres	Several metres
Lineament map	Several tens of metres	Kilometres

In the work presented here we assume that the data set available for modelling is a representative sample of the population parameters, i.e. $k_r \approx k_r^*$ and $r_0 \approx r_0^*$, where k_r^* and r_0^* denote sample parameters. Moreover, we assume that r_0 is the smallest value possible in the three scale of observation shown in Figure 2-2, e.g. the radius of a core-drilled borehole, r_w. To simplify the notation we use k_r and r_0 from now on.

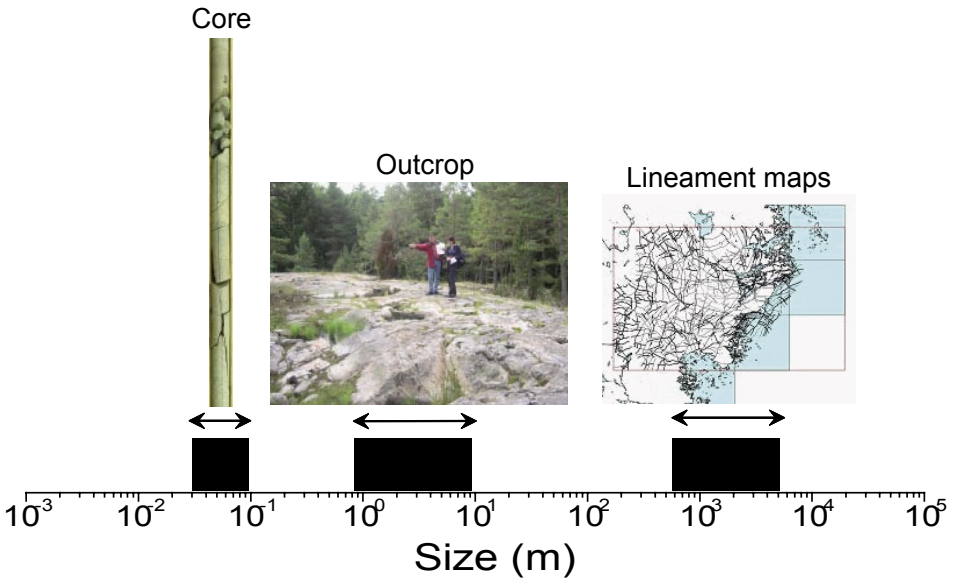

Figure 2-2. *Three scales of fracture trace observations. Only Outcrop and Lineament traces are used for the construction of a fracture size model in the geological DFN. The missing scales of observation in between constitute a significant source of uncertainty.*

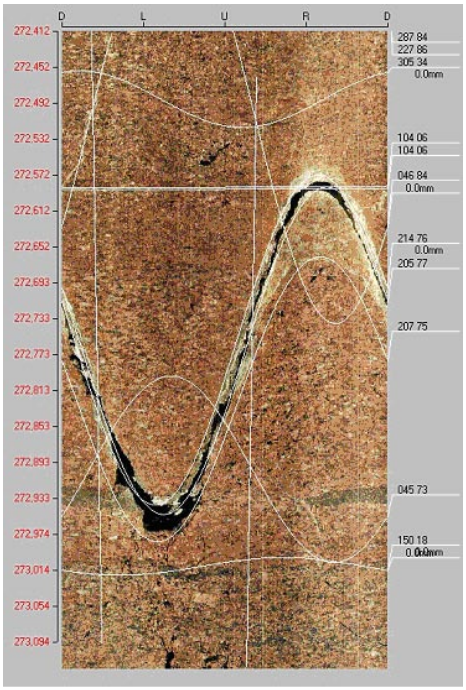

Figure 2-3. *BIPS image showing a c 0.7 m long borehole section in borehole KLX04A. The fracture in the centre is associated with a flow anomaly determined by the Posiva Flow Log. The fracture transmissivity is 1.9×10^{-7} m²/s. The borehole radius is 0.038 m. Reproduced from /Forssman et al. 2005/.*

2.2 Fracture intensity

If $P_{32}[r > r_0]$ denote the fracture surface area of all fractures greater than the location parameter we can write:

$$P_{32}[r > r_1] = P_{32}[r > r_0]\left(\frac{r_0}{r_1}\right)^{(k_r-2)} \tag{2-3}$$

where $P_{32}[r > r_1]$ is the fracture surface area of all fractures r greater than the size r_1. log $P_{32}[r > r_{min}]$ vs log r plots as a straight line with a slope of $(k_r–2)$, see Figure 2-4.

From a modelling point of view it is necessary to decide the size range $[r_{max}, r_{min}]$ that will be used in the numerical simulations and, equally important, the intensity value $P_{32}[r > r_0]$ that corresponds to the smallest value of the underlying data set. As already stated in Section 2.1 we assume in the work reported here that $r_0 \approx r_0^*$ where $r_0^* \approx r_w$. In conclusion, the fracture intensity of a DFN model with fractures in the size interval $[r_{min}, r_{max}]$ may be written as:

$$P_{32}[r_{min}, r_{max}] = P_{32}[r > r_0]\left(\frac{(r_{min})^{(2-k_r)} - (r_{max})^{(2-k_r)}}{(r_0)^{(2-k_r)}}\right) \tag{2-4}$$

The fracture intensity term in DarcyTools is denoted by α_{DT}. Its relation to P_{32}, r, and $(k_r–2)$ may be written as:

$$\alpha_{DT} = P_{32}[r > r_{min}]\frac{(k_r-2)}{\pi} r_{min}^{(k_r-2)} r_{ref}^{k^{-1}} \tag{2-5}$$

Equation (2-3) implies that the product $P_{32}[r > r_{min}]\ r_{min}^{(k_r-2)} = const.$, hence the intensity value α_{DT} is constant-valued for any fixed value of $P_{32}[r > r_0]$, see Figure 2-4.

Figure 2-5 shows the dependence of P_{32} on r_{min}, k_r and α_{DT}. The value of r_{ref} may be set arbitrarily in DarcyTools. Commonly a value of $r_{ref} = 1$ m is used.

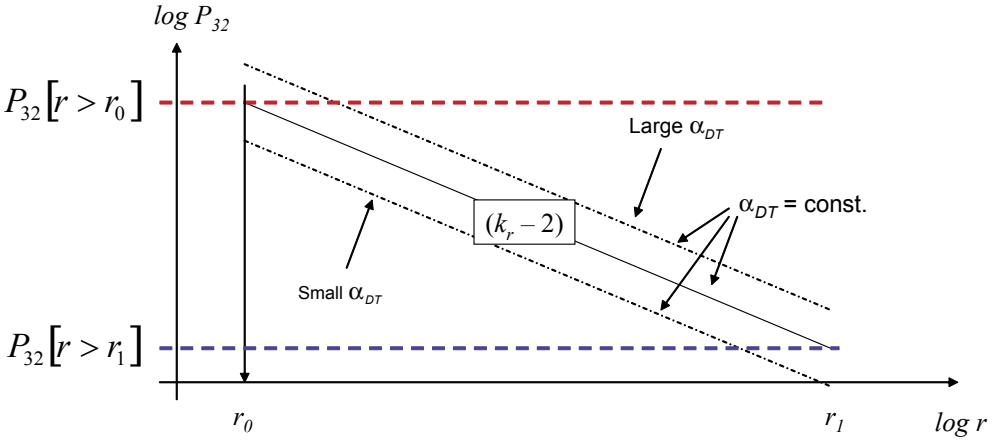

Figure 2-4. *Graph showing the relationship between P_{32} and r in Equation (2-3). log$P_{32}[r > r_{min}]$ vs log r plots as a straight line with a slope of $(k_r–2)$. α_{DT} denotes the intensity parameter used in DarcyTools. Its relation to P_{32}, r, and $(k_r–2)$ is explained in the text.*

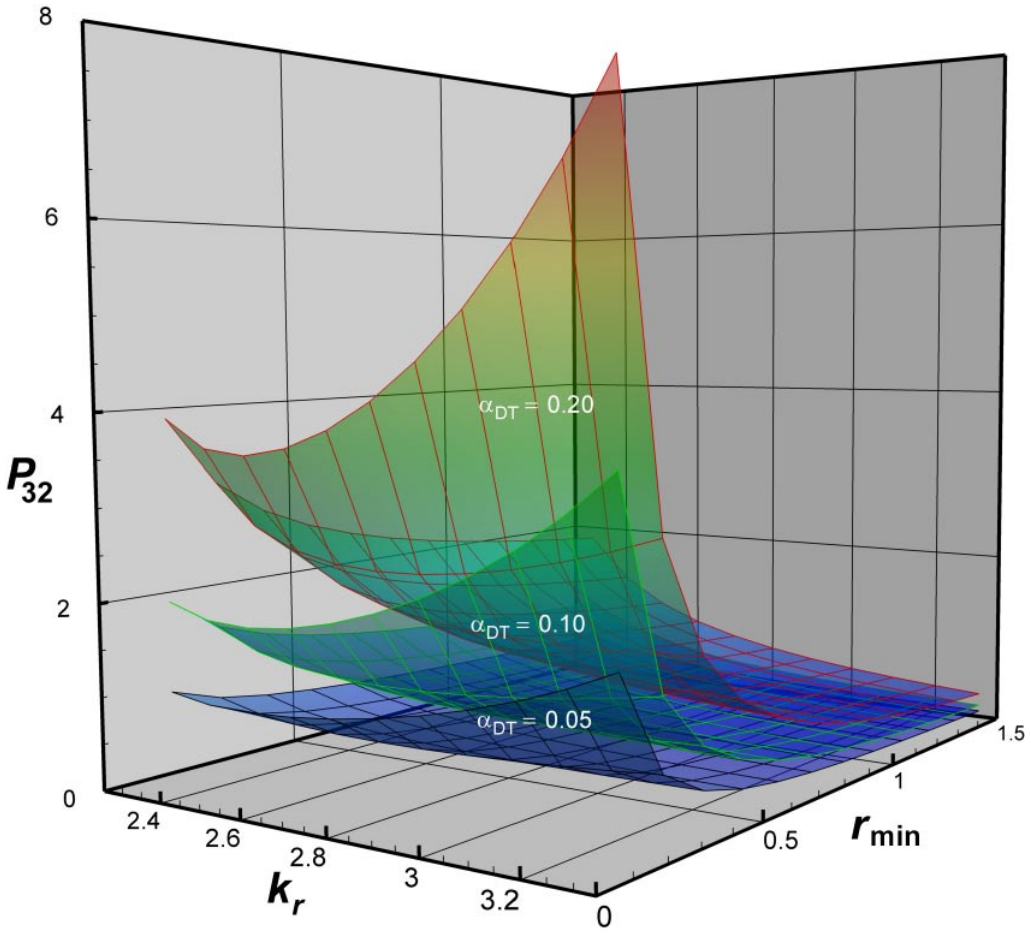

Figure 2-5. *Illustration of the dependence of P_{32} on r_{min}, k_r and α_{DT}. The surfaces show that the value of $P_{32}[r > r_{min}]$ is less sensitive to uncertainties in k_r and r_{min} for $k_r > 2.6$ and $r_{min} > 0.25$ m.*

Figure 2-6 demonstrates the dependence of $P_{32}[r > r_0]$ on k_r for two different values of α_{DT}, 0.1 and 0.3, and two different values of r_0, 0.038 m and 0.282 m. The two settings for r_0 were discussed in the hydrogeological DFN modelling conducted in Simpevarp and Forsmark, see /Follin et al. 2005ab, Hartley et al. 2005ab/. These studies indicate that α_{DT}, k_r and r_0 are all important for the performance of the hydrogeological DFN. Figure 2-6 indicates that the fracture surface area per unit volume of rock $P_{32}[r > r_0]$ is more sensitive to uncertainties in the determination of k_r if r_0 is small than if r_0 is large regardless of the value of α_{DT}. The effect of r_0 on the $P_{32}[r > r_0]$ available for flow is not demonstrated by Figure 2-6, however. The $P_{32}[r > r_0]$ shown in Figure 2-6 is the total fracture surface area of all fractures regardless of their connectivity. Means for estimating the connected fracture surface area per volume of rock $P_{32}[r > r_0]_{CON}$ is discussed in Section 2.3.

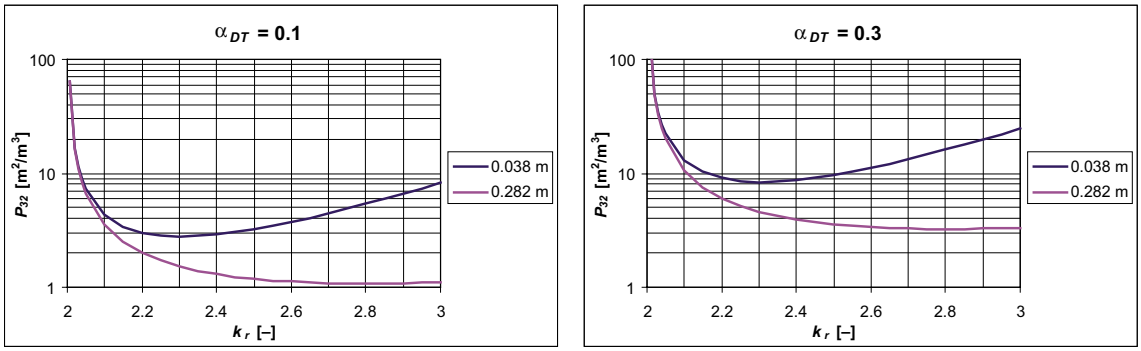

Figure 2-6. *Illustration of the dependence of the fracture surface area per unit volume of rock $P_{32}[r > r_0]$ on k_r for two different values of α_{DT} and two different values of r_0.*

2.3 Spatial correlation

/La Pointe and Hermanson 2005, La Pointe et al. 2005, Hermanson et al. 2005/ combine area-normalised frequency plots with a mass dimension analysis to study if the number of fractures of different sizes scales linearly with the size of the area of observation or not.

The assumption of a Poisson process implies that the positions of the fracture centres in three dimensions are random and uncorrelated. In fractal terminology a Poisson process can be described by an integer dimension, i.e. a fractal dimension of $D = 3$ in three dimensions, $D = 2$ in two dimensions and $D = 1$ in one dimension[1].

The assumption of a Poisson process is a considerable simplification but it does not necessarily imply a uniform distribution of the fracture centres in space. Typically, individual realisations of a Poisson process often possess random clusters, i.e. statistical homogeneity is only valid for the ensemble of realisations. In practice, it is almost impossible to discriminate between a Poisson process and a fractal process, particularly for small data sets.

It is important to note that a Poissonian geological DFN does not imply that the connected DFN is Poissonian. This is demonstrated in Appendix C. Geometrically isolated fractures or isolated clusters of fractures do not contribute to flow between the modelled boundaries. This means that it is mostly the large fractures that are potential candidates for flow as they connect more easily. In addition, if fracture transmissivity is heterogeneous a geometrically constrained DFN realisation, which contains connected fractures only, becomes also hydraulically constrained as some of the connected potential flow paths may be tight.

Figure 2-7 illustrates the conceptual model used in the work reported here to define fracture connectivity of all Open and Partly open fractures observed in a core-drilled borehole, N_{CAL}. The limitation to Open and Partly open fractures is explained in Chapter 4.

[1] When the mass dimension of fracture trace lengths has a value of 2 (two), the number of fractures per unit area (P_{20}) scales linearly to area and the spatial pattern of the subvertical fracture sets can be characterised by a uniform random density function, which inherently has no spatial correlation among the fractures. The calculation of the mass dimension from the number of fractures per unit borehole length (P_{10}) generally contain a bias but may be used to estimate the spatial model in the vertical direction provided that the intensities of all the fracture sets are stationary. A value of 1 (one) is then considered characteristic for a Poissonian process.

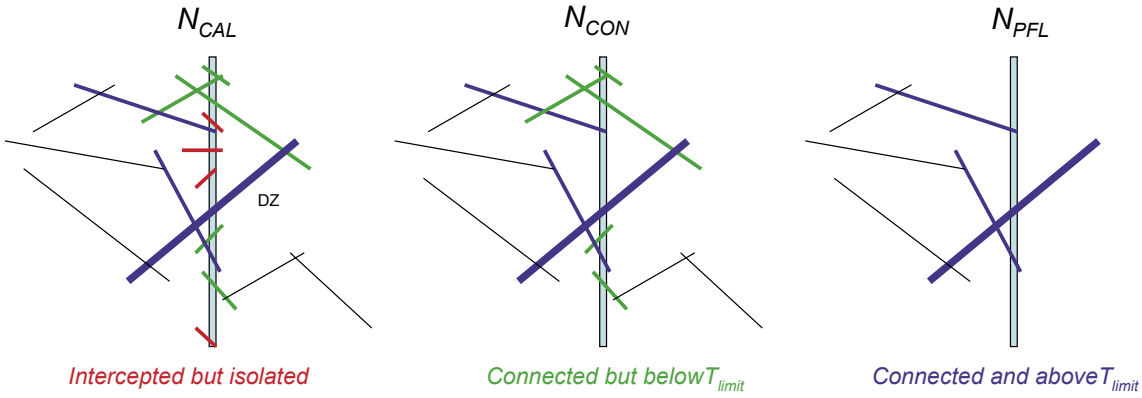

Figure 2-7. *The definition of N_{CAL}, N_{CON} and N_{PFL} of Open fractures. T_{limit} denotes the lower measurement limit for transmissivity, which is typically (1–2)×10^{-9} m^2/s for the Posiva Flow Log (PFL-f).*

Figure 2-7 illustrates that the number of flowing fractures in a core-drilled borehole detected by the Posiva Flow Log, N_{PFL}, is regarded as a subset of the geometrically connected Open fractures, N_{CON}, which in turn is a subset of N_{CAL}, i.e.

$$N_{PFL} < N_{CON} < N_{CAL} \tag{2-6}$$

In the work reported here we consider the ratio between N_{CON} and N_{CAL} as an estimator of the Open fracture connectivity. Hence, the connected fracture surface area per unit volume of Open fractures may approximately be written as:

$$P_{32}[r > r_0]_{CON} = \frac{N_{CON}}{N_{CAL}} P_{32}[r > r_0]_{CAL} \tag{2-7}$$

By the same token, the ratio between N_{PFL} and N_{CON} is an estimator of the flowing fracture connectivity of fractures with trans$T \geq T_{limit}$. Thus, the flowing fracture surface area per unit volume of fractures $T \geq T_{limit}$ may approximately be written as:

$$P_{32}[r > r_0]_{PFL} = \frac{N_{PFL}}{N_{CON}} P_{32}[r > r_0]_{CON} \tag{2-8}$$

2.4 Methodology used in the L1.2 geological DFN

The modelling methodology used by /Hermanson et al. 2005/ aims at deriving values of the location parameter r_0 for three regional steeply dipping fracture sets S_A, S_B and S_C in model domain A. The numerical procedure is iterative and treats one set at the time. The iterations are run until a simultaneous match is reached for the borehole fracture frequency $P_{10}[BH]$, the fracture length per unit area of outcrop $P_{21}[OC]$ and the deformation zone surface area per unit model volume $P_{32}[DZ]$. The 1.2 geological DFFN modelling procedure is based on several assumptions, out of which two of the more significant ones are:

1. The core-drilled boreholes are perfect scanlines.
2. All deformation zones with traces at ground surface greater than 1,000 m reaches the bottom of the model volume at –1,100.

2.4.1 Assumption 1

/Hermanson et al. 2005/ assume that core-drilled boreholes may be considered scanlines and that it is possible to infer a definite value of $P_{32}[r > r_0]$ from the measured fracture frequencies $P_{10}[BH]$ in such boreholes, where r_0 is the unknown location parameter of the power-law size population.

In our opinion also a slim borehole has a finite radius (cf Figure 2-3), which means that not all fractures seen on the surface of the borehole wall in a core-drilled borehole also cut the centre line of the cored rock cylinder. This creates some an uncertainty in the definition of fracture frequency and, consequently, in the derivation of the desired intensity value $P_{32}[r > r_0]$.

2.4.2 Assumption 2

/Hermanson et al. 2005/ assume that all deformation zones within the local model domain greater than 1,000 m in length reaches at least –1,100, which is the elevation of the bottom of the local model domain. The equivalent minimum radius r_1 of a circular fracture of the same area as a rectangular deformation zone is:

$$r_1 = \sqrt{\frac{1{,}000 \cdot 1{,}100}{\pi}} = 591.73 \text{ m} \qquad (2\text{-}9)$$

Figure 2-8 shows the lineaments longer than 1,000 m that intersect the local model domain. There are 71 or 80 deformation zones depending on if some of the lineaments (having name extensions A and B) are interpreted as one deformation zone or as two. Figure 2-9 shows the deformation zones in perspective view as modelled in SKB's Rock Visualisation System (RVS). The value of $P_{32}[r > r1] = 0.0047$ m^2/m^3 was calculated by /Hermanson et al. 2005/ by dividing the sum of the deformation zone areas by the model volume. According to /SKB 2005a/ many deformation zones are formed by linking short lineaments into longer lineaments. The lineaments themselves may be of different kinds, e.g. fracture data, geophysical anomalies and topographic lineaments. In our opinion the linking of short lineaments of different nature into long deformation zones is in parts a subjective process that may affect the evaluation of the shape parameter. Other uncertainties in the lineament/deformation transformation process are for example:

- Most lineaments/deformation zones are very old, almost as old as the bedrock itself, which means that the traces the lineaments/deformation zones make with ground surface are merely what remain to be seen on the present-day erosion surface. That is, portions of the visible lineaments/deformation zones have vanished due to weathering and erosion just as the bedrock itself. On the other hand, it is possible that there exist deformation zones at depth that do not intersect ground surface.
- Uncertainties are introduced when it is assumed that all lineaments that are used to form the deformation zones must at least reach the bottom of the model domain regardless of the length of the individual lineament segments.

Figure 2-10 demonstrate the approach used by /Hermanson et al. 2005/ together with an alternative approach discussed in the work reported here.

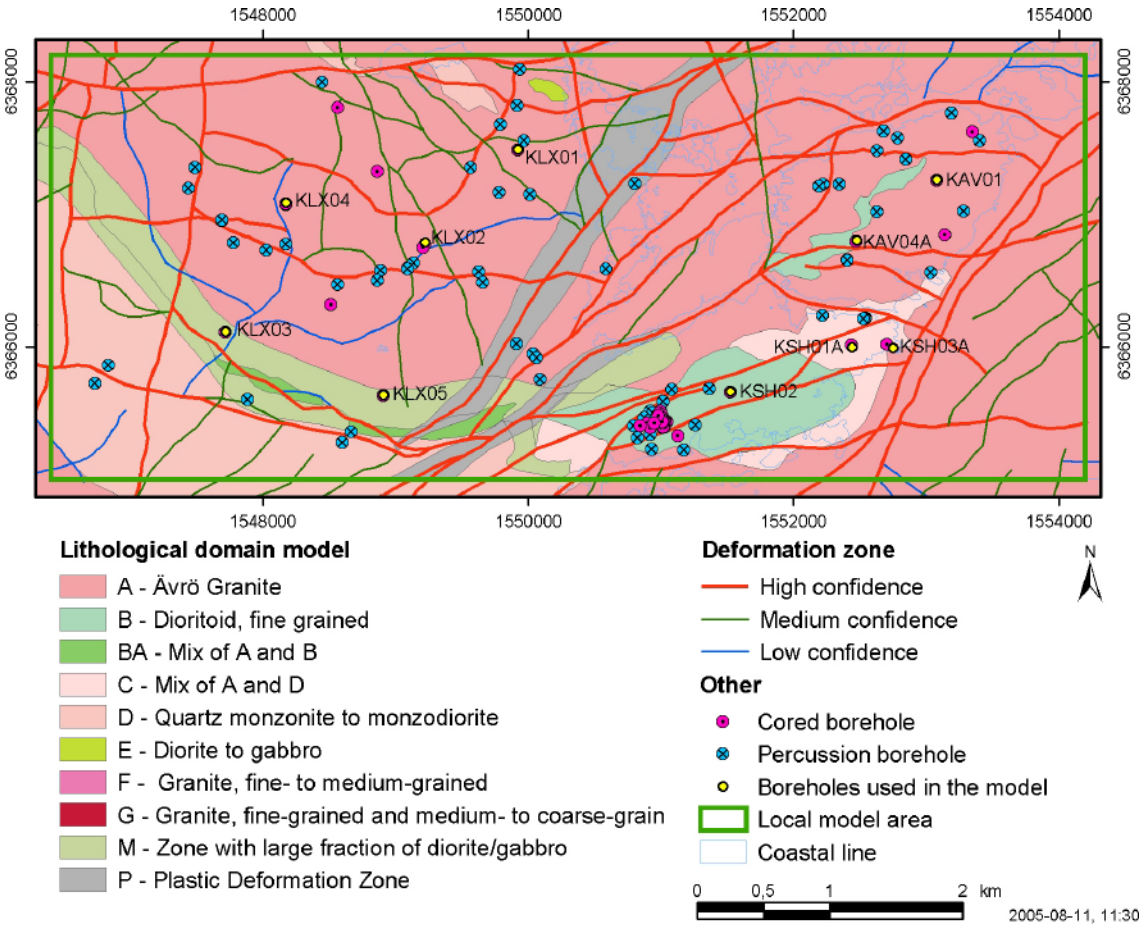

Figure 2-8. *Lineaments longer than 1,000 m that intersect the local model domain. Rock domain A is the dominating domain /Hermanson et al. 2005/.*

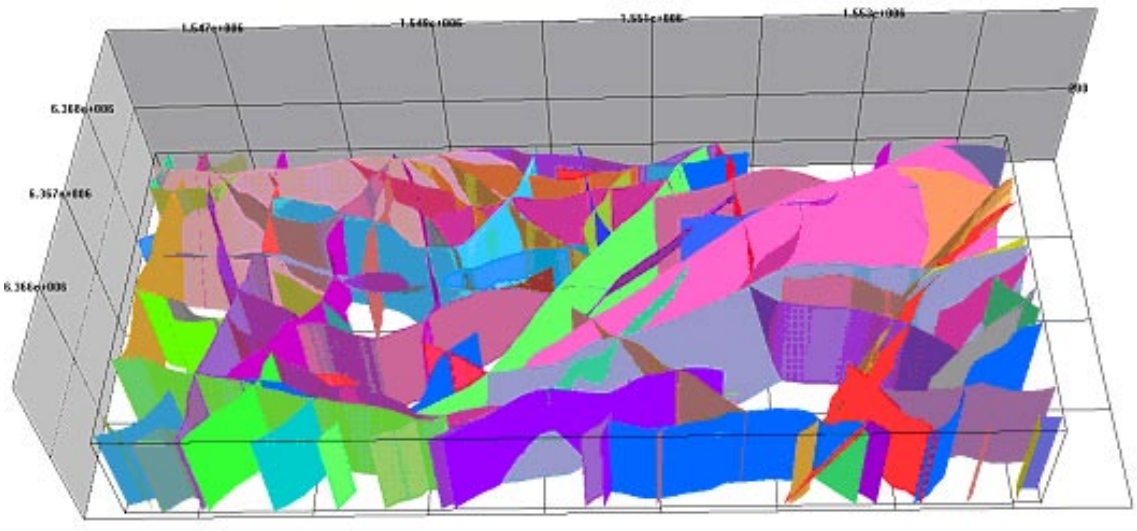

Figure 2-9. *All deformation zones within the local model domain for version L1.2 are assumed to reach at least –1,100 in the geological DFN model by /Hermanson et al. 2005/.*

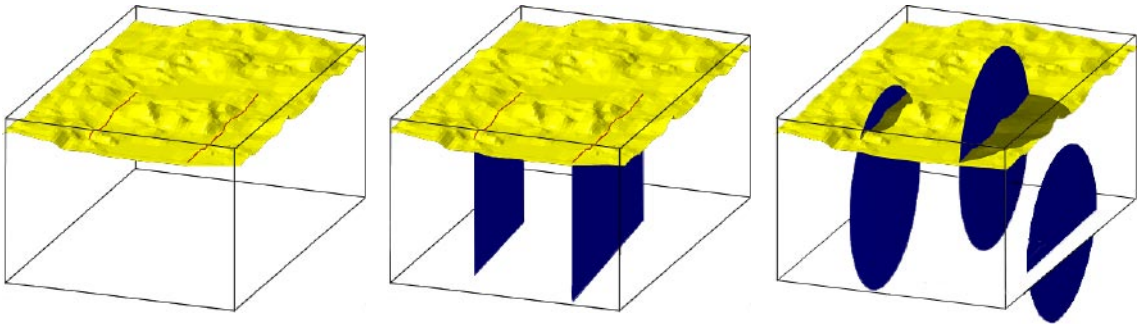

Figure 2-10. *Left: Lineaments (red lines) are often interpreted as deformation zone traces. Centre: The approach used in /Hermanson et al. 2005/. Right: Illustration showing a thought where portions of the lineaments/deformation zones have vanished due to weathering and erosion (just as the host bedrock). The illustration also contains an unseen deformation zone, i.e. the present-day surface is not an unbiased "trace plane".*

2.4.3 Reported results

Table 2-2 summarises the parameter values that characterise the geological DFN in the rock mass in rock domain A. The variability in the $P_{32}[r > r_0]$ intensities for the S_A, S_B and S_C sets reflects the uncertainty in the methodology used in the geological DFN modelling. For a detailed description of the use of these intensities, see /Hermanson et al. 2005/. It is noted that the data presented in Table 2-2 are based on a value of $P_{32}[r > 591.73\ \text{m}] = 0.0047\ \text{m}^2/\text{m}^3$ for sets S_A, S_B and S_C.

Table 2-2. Compilation of parameter values for the distributions used in the final geological DFN model. The $P_{32}[r > r_0]$ total fracture intensity varies between 7.03–8.36 m^2/m^3 and the $P_{32}[r > r_0]$ Open fracture intensity 2.87–3.40 m^2/m^3 depending the method used in the geological DFN modelling, see /Hermanson et al. 2005/. The $P_{32}[r > r_0]$ total fracture intensity for sets S_A, S_B and S_C varies between 3.31–4.64 m^2/m^3.

Laxemar subarea, Domain A Set ID	Orientation[1] Trend	Plunge	κ	Intensity[2] $P_{32}[r > r_0]$	% Open	Size Distribution[3]	λ or k_r	r_0
S_A	338.1	4.5	13.06	1.31–1.43	42.5	Power-law	2.85	0.328
S_B	100.4	0.2	19.62	1.03–1.69	37.9	Power-law	3.04	0.977
S_C	212.9	0.9	10.46	0.97–1.52	41.3	Power-law	3.01	0.858
S_d	3.3	62.1	10.13	2.32	40.1	Exponential	4	–
S_f	243	24.4	23.52	1.40	42.1	Power-law	3.6	0.4

[1] Fisher distribution

[2] Uniformly and randomly distributed.

[3] The parameter λ of the exponential distribution is given as $\lambda = \text{mean}^{-1}$. The parameters of the power-law distrbution are the shape parameter k_r and the location parameter r_0.

3 Assessment of structural and hydraulic data

3.1 Overview of data

Figure 3-1 shows the hydraulic testing conducted in KLX04. Measurements are made with PFL-f, PSS 5 m, PSS 20 m and PSS 100 m. The results are reported in /Rouhiainen and Sokolnicki 2005/ and /Rahm and Enachescu 2004/. The total length of KLX04 below the casing shoe is 882.71 m. The total thickness of the deformation zones is 119.5 m leaving 763.21 m to the rock masses outside the deformation zones.

Six intervals in the KLX04 borehole are interpreted to have different structural properties than the rock mass in general and are interpreted as deformation zones in the single-hole geological interpretation. The six intervals and are denoted by DZ1–DZ6. Two of the intervals, DZ5 and DZ6, are deterministically treated in the geological deformation zone model and modelled in the Rock Visualisation System (RVS) as ZSMEW007A (DZ5) and ZSMNW929A (DZ6). The remaining four intervals with deformation zone like properties are judged more uncertain geologically with regard to their orientation and size. DZ1–DZ44 have not been associated to interpreted lineaments in the geological deformation zone modelling.

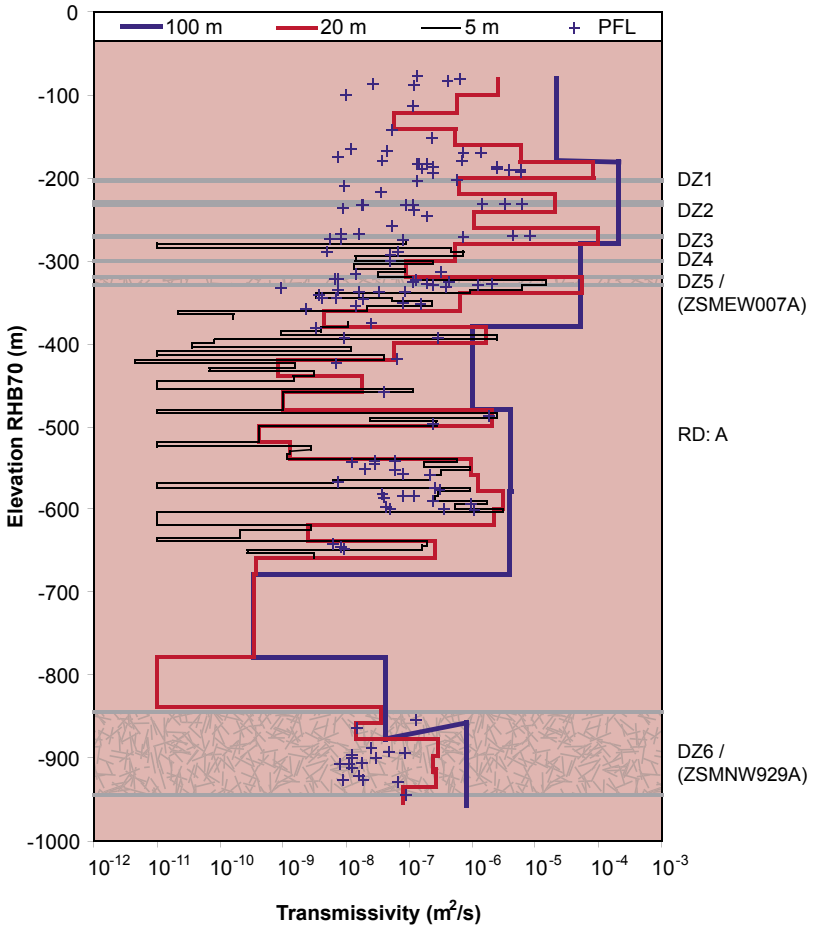

Figure 3-1. *Hydraulic testing conducted in KLX04; PSS = Pipe String System data: 100 m, 20 m, 5 m and PFL = Posiva Flow Log data. DZ5 and DZ6 are deterministically modelled in the geological deformation zone modelling.*

There are in total 5,551 mapped fractures in the KLX04 borehole including 53 so called Crush zones. Table 3-1 provides some additional figures of the statistics. Of particular interest is the number of Open fractures of different geological confidence with regard to their aperture – Certain, Probable and Possible. In our view a surprisingly large number of the Open and Partly open fractures are mapped as Possible regarding their aperture rather than Certain or Probable. The reason for this is not clear to us.

/Forssman et al. 2005/ and /Rhén et al. 2005/ analysed the correlation between PFL-f anomalies and mapped fractures. The analysis showed that each PFL-f anomaly, which in turn can be Certain or Uncertain, can be associated with one or several mapped fractures. Based on the results reported by /Forssman et al. 2005/ the following correlation scheme was used in the work reported here:

Couple first all Certain PFL-f flow anomalies to available mapped fractures with the following order of preference: 1) Certain, 2) Probable and 3) Possible. Secondly, repeat the procedure for the Uncertain PFL-f flow anomalies. If there is a choice between two or more mapped fractures pick the fracture closest to the PFL-f anomaly.

Table 3-2 shows the outcome of the correlation scheme. There is a greater number of PFL-f anomalies interpreted as Possible rather than Certain or Probable.

Table 3-1. Fracture statistics in the KLX04 borehole.

Object	Count	Object	Count
No. of fractures	5,551	No. of fractures inside the intervals with DZ type properties (= DZ1–DZ6)	1,222
No. of Crush zones	53	No. of fractures inside the intervals with RVS-DZ type properties (= DZ5–DZ6)	1,149
No. of Broken fractures	2,753	No. of fractures outside the intervals with RVS-DZ type properties (= DZ1–DZ6)	73
No. of Unbroken fractures	2,745		
No. of intervals with DZ type properties (= DZ1–DZ6)	6	No. of fractures in the Rock mass outside the Crush zones and the intervals with DZ type properties	4,276
No. of RVS-DZ (= DZ5 and DZ6)	2	No. of Open fractures in the Rock mass outside both the Crush zones and the intervals with DZ type properties	1,195
No. of Crush zones inside the intervals with DZ type properties	33	No. of Partly open fractures in the Rock mass outside both the Crush zones and the intervals with DZ type properties	13
No. of Crush zones outside the intervals with DZ type properties	20	No. of Sealed fractures in the Rock mass outside both the Crush zones and the intervals with DZ type properties	3,068
		No. of Open and Partly open fractures with a Certain aperture outside both the Crush zones and the intervals with DZ type properties	62
		No. of Open and Partly open fractures with a Probable aperture outside both the Crush zones and the intervals with DZ type properties	113
		No. of Open and Partly open fractures with a Possible aperture outside both the Crush zones and the intervals with DZ type properties	1,033

Table 3-2. Distribution PFL-f data outside the deformation zones DZ1–DZ6.

Object	Count	Object	Count
Total no. of PFL-f anomalies	129	No. of PFL-anomalies outside DZ1–DZ6	96
Certain PFL-f mapped as Certain Open or Partly open	21	*Uncertain PFL-f* mapped as Certain Open or Partly open	2
Certain PFL-f mapped as Probable Open or Partly open	11	*Uncertain PFL-f* mapped as Probable Open or Partly open	1
Certain PFL-f mapped as Possible Open or Partly open	32	*Uncertain PFL-f* mapped as Possible Open or Partly open	14
Certain PFL-f mapped as Crush Zone	11	*Uncertain PFL-f* mapped as Crush Zone	1
Certain PFL-f mapped as Certain Sealed (though Broken)	2	*Uncertain PFL-f* mapped as Certain Sealed (though Broken)	1

3.2 Modelling methodology

The hydrogeological DFN modelling carried out in the work presented here comprises four main steps:

1. Assessment of structural data.
2. Assessment of hydraulic data.
3. Modelling of connected fracture intensity.
4. Modelling of parameter values for a correlated transmissivity model.

Step 1 covers an examination of the geological DFN and the geological single-hole interpretations followed by an analysis of the fracture properties and intensities as well as orientations within each deformation zone and each rock domain in the boreholes.

Step 2 includes an analysis of hydraulic data to obtain a representative value for each uncertain (stochastic) deformation zone treated as a part of the hydrological DFN model. The certain (deterministic) deformation zones are excluded from the analysis. A second component is to define the transmissivity distribution.

Step 3 is accomplished by the use of stochastic fracture models (realisations) that compare with the mapped orientations and borehole fracture frequencies of Open and Partly open fractures in KLX04. Once the measured geological intensity of intercepts is matched, the connected fracture surface area per unit volume of rock mass is determined by a connectivity analysis.

Step 4 aims at deriving parameter values for a correlated transmissivity to size model. A correlated transmissivity model is invoked in the work presented here by assuming that it is the largest connected fractures intercepting the borehole in each stochastic DFN realisation that correspond to the measured fracture transmissivities.

This execution of step 3 and 4 with data from KLX04 is presented in Chapter 5. The work flow is described in Appendix A. It is noted that the fourth step is a working hypothesis. Indeed, any transmissivity to size model can be brought into play, but a correlated model is considered the most intuitive from a hydraulic point of view.

3.3 Assessment of stuctural data

3.3.1 Fracture intensity versus depth

The four insets in Figure 3-2 demonstrate the initial intensity analysis carried out. Inset A shows the measured cumulative frequency of all Open fractures. Inset B shows the Terzaghi corrected fracture frequency $P_{10,corr}$ /Terzaghi 1965/. Inset C shows the definition of the ordinate axis used for producing the intensity plot shown in inset D. The plotting approach eases the visual demarcation of intervals of constant intensities. Three intervals, denoted by Volumes I, II and III, of different, intensities $P_{10,corr}$ are identified in the plot shown in inset D, see Table 3-3.

Table 3-3. Preliminary estimations of $P_{32}[r > r_0] \approx P_{10,corr}$ in Volumes I–III in the KLX04 borehole, see Figure 3-2.

Volume	Borehole length interval [m]	$P_{32}[r > r_0] \approx P_{10,corr}$ [m²/m³]
I	102–442	~ 3.25
II	502–675	~ 5.40
III	749–982	~ 0.91

It is noted that the Terzaghi method is an approximation, e.g. it does not take fracture size into account. This is discussed by /Davy et al. *in press*, Darcel et al. 2004/. The general experience, however, is that the computed $P_{10,corr}$ values provide a good first guess of the desired three dimensional fracture intensity $P_{32}[r > r_0]$. This is demonstrated below.

Terzaghi correction

The Terzaghi method weights each fracture by:

$$W = 1/\cos(\vartheta) \qquad (3\text{-}1)$$

where ϑ is the angle between the pole to the fracture plane and the borehole trajectory at the point of intersection. A maximum weight of $W = 7$ is used in the work reported here based on previous modelling experiences. The chosen value means that the number of intercepted fractures is increased by a factor of seven for $\vartheta \geq \cos^{-1}(1/7) \approx 82°$. For angles below 82° the weighting factor for each fracture is determined by Equation (3-1).

Figure 3-3 shows the relationship between the angle ϑ and the Terzaghi correction factor together with the trace length that a fracture of angle ϑ makes with the borehole.

Figure 3-4 demonstrates how the relative proportions in $P_{10,corr}$ between the five fractures sets vary by the magnitude of the weighting factor W in Volume I. It is noted that the correction alters the relative proportions of sets S_A and S_d primarily. For a range of the weighting factor between 7–15 the changes in relative proportions between the five fractures sets are small.

Figure 3-5 shows the magnitudes of the set specific $P_{10,corr}$ values as well as the magnitude of the total $P_{10,corr}$ value as a function of the angle ϑ (or the Terzaghi correction factor). For a range in ϑ between 60–84° (W = 2–10) the value of the total $P_{10,corr}$ varies between 2.7 and 3.4 m^{-1}.

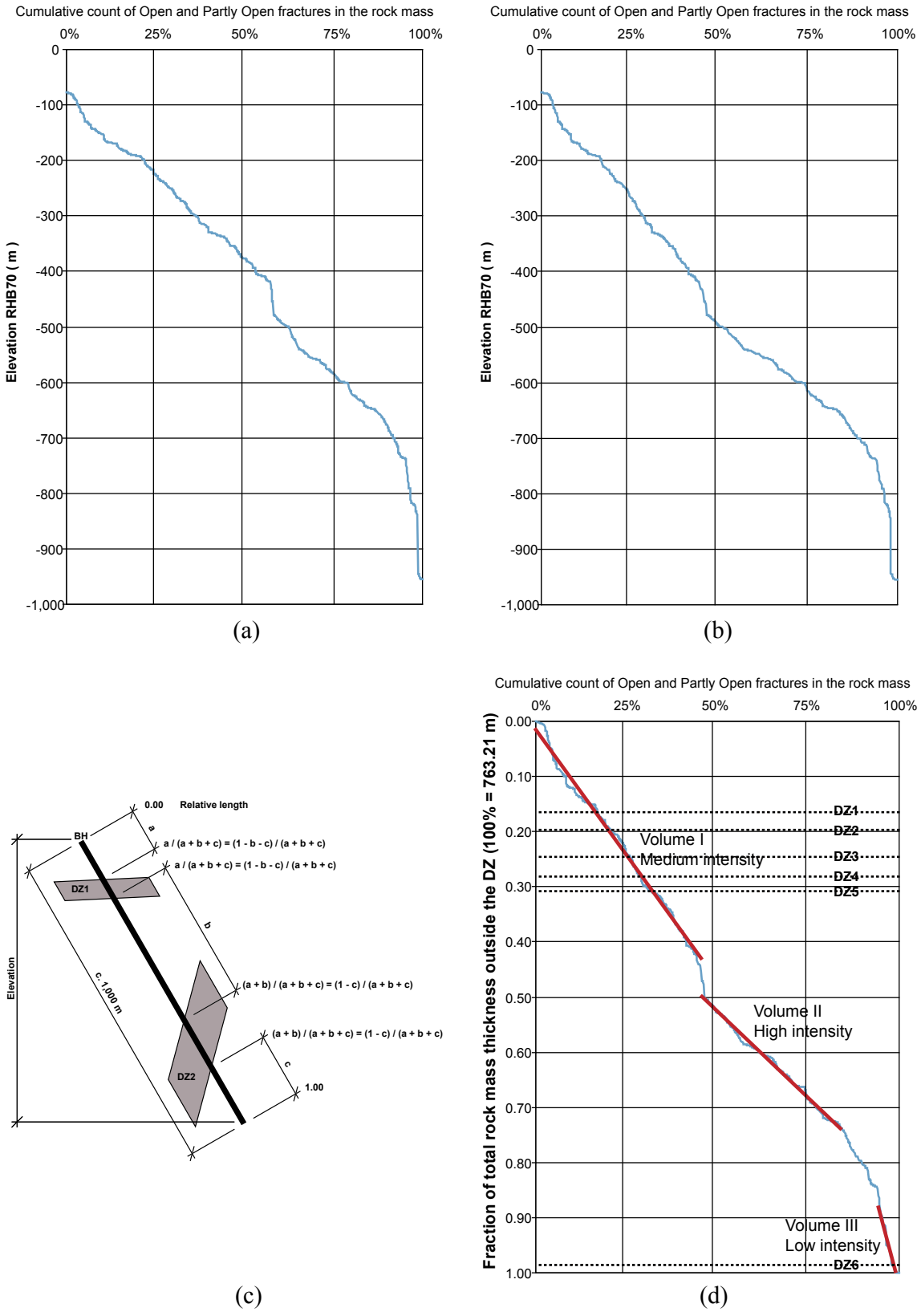

Figure 3-2. *Cumulative count of Open and Partly open fractures outside DZ1–DZ6 and Crush zones: (a) before Terzaghi correction (b) after Terzaghi correction. (c) Definition of rock mass thickness outside DZ1–DZ6 and Crush zones. (d) Plot used to delineate possible "intensity volumes" in the rock mass. The straight lines indicate three segments of constant, yet different, intensities. The segments are denotes Volumes I, II and III in the work reported here.*

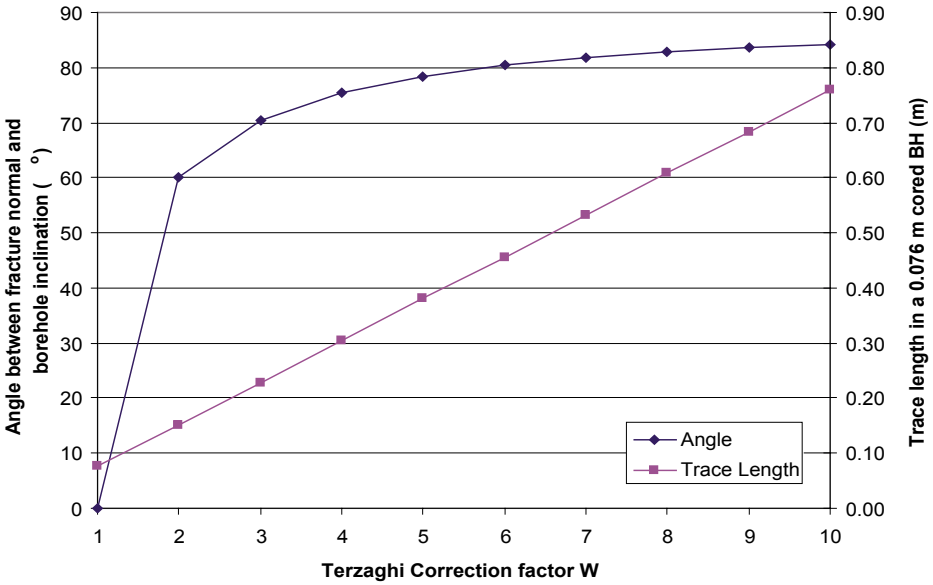

Figure 3-3. *Relationships between the angle ϑ and the Terzaghi correction factor (blue graph) and the trace length that a fracture of angle ϑ makes with the borehole and the Terzaghi correction factor (pink graph).*

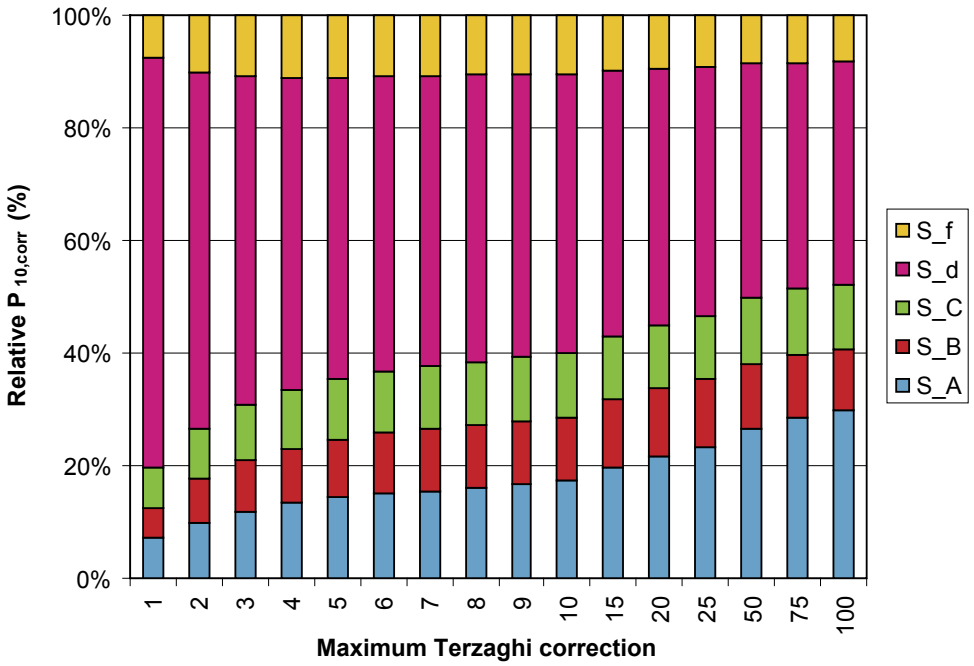

Figure 3-4. *Variation in relative proportions between the five fracture sets as a function of the Terzaghi correction.*

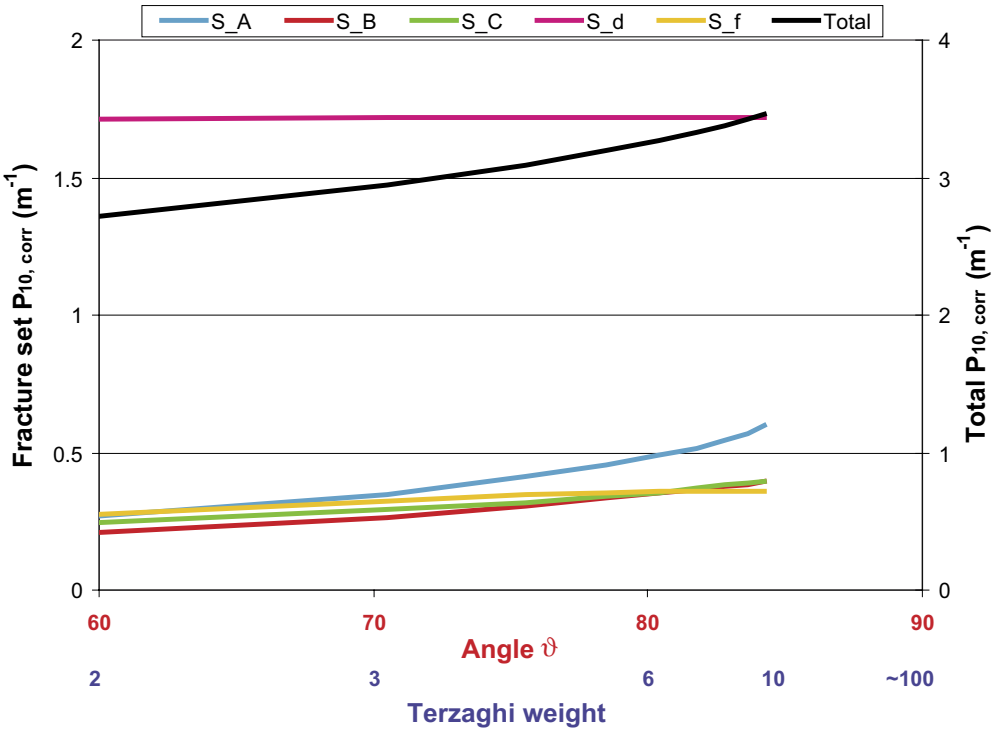

Figure 3-5. *Values of "Fracture set $P_{10,corr}$" and "Total $P_{10,corr}$" as a function of the angle ϑ (or the Terzaghi correction factor).*

The estimated range in the total $P_{10,corr}$ for Volume I in Figure 3-5, 3.25, compares well with the matched values of $P_{32}[r > r_0]$ for the Open and Partly open fractures in the geological DFN modelling. In Table 2-2, $P_{32}[r > r_0]$ for the Open and Partly open fractures varies between 2.87 m^2/m^3 and 3.40 m^2/m^3. This suggests that the Terzaghi corrected fracture frequency may be a reasonable first order estimator of the desired fracture surface area per unit volume of rock provided that the intensity estimation does not vary by depth. However, the Terzaghi corrected fracture frequencies are quite different in Volume II and Volume III, 5.40 and 0.91, respectively. This suggests that the fracture intensity on outcrops, which was used as calibration target for $P_{32}[r > r_0]$ in the geological DFN modelling, can be misleading as a calibration target for the rock mass conditions at depth.

3.3.2 Fracture orientation versus depth

Figure 3-6 shows a hard sector plot of the five fracture sets suggested by /Hermanson et al. 2005/, cf Table 2-2. The hard sector algorithm is used in the work reported here to determine the fracture set belonging of mapped fractures in the KLX04 borehole. The algorithm is explained in Appendix B.

Figure 3-7 shows the outcome of applying the hard sector algorithm to the fractures mapped in the rock mass in KLX04. As already mentioned there are 3,088 sealed fractures, 1,195 Open fractures and 13 Partly open fractures in the rock mass outside the deformation zones. The two plots in Figure 3-7 suggest that Open and Partly open fractures have the same principal orientations as the Sealed. However, it is noted that Set_B is quite weak in KLX04 and in practice absent for the Open and Partly open fractures. Further, the dominating sets appear to be Set_C and Set_d. The mean pole trend and plunge for Set_d suggested by the geological DFN modelling is not supported by data in the KLX04 boreholes.

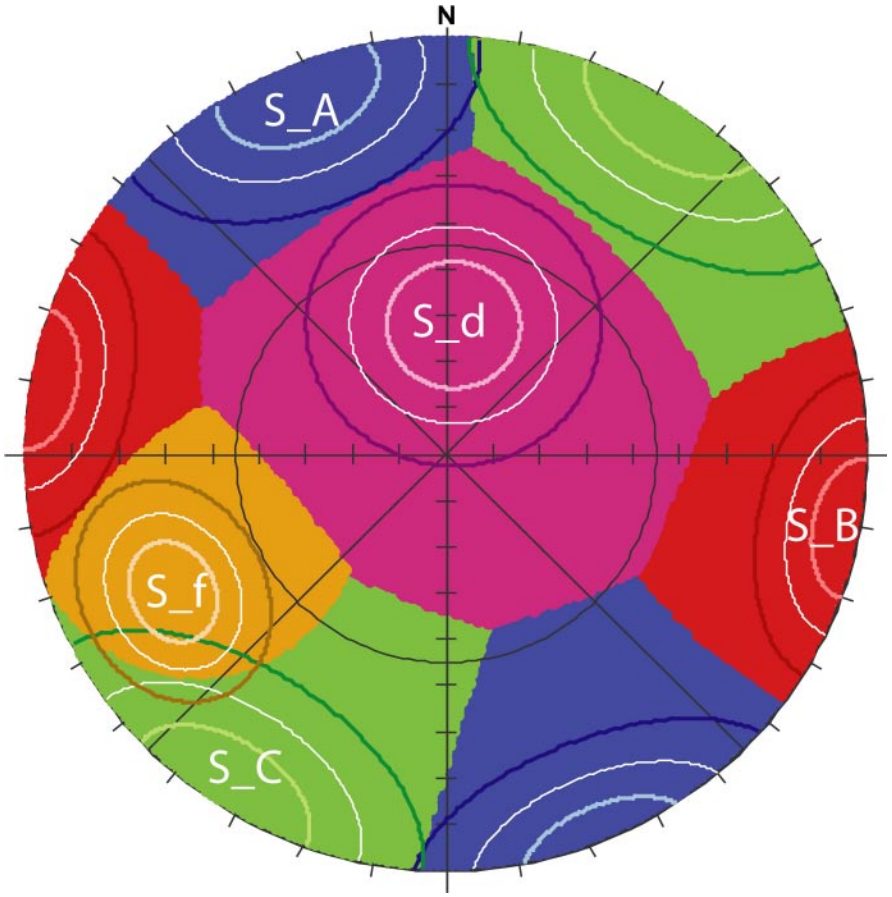

Figure 3-6. *Hard sector division of the five fracture sets shown in Table 2-2. The mean trend and plunge of each Fisher distribution is close to the position of its label. The contours show the 25%, 50% and 75% probability percentiles for each set, e.g. 25% of the fractures of fracture set S_C are found inside the innermost contour, 50% inside the next contour and 75% inside the outermost contour.*

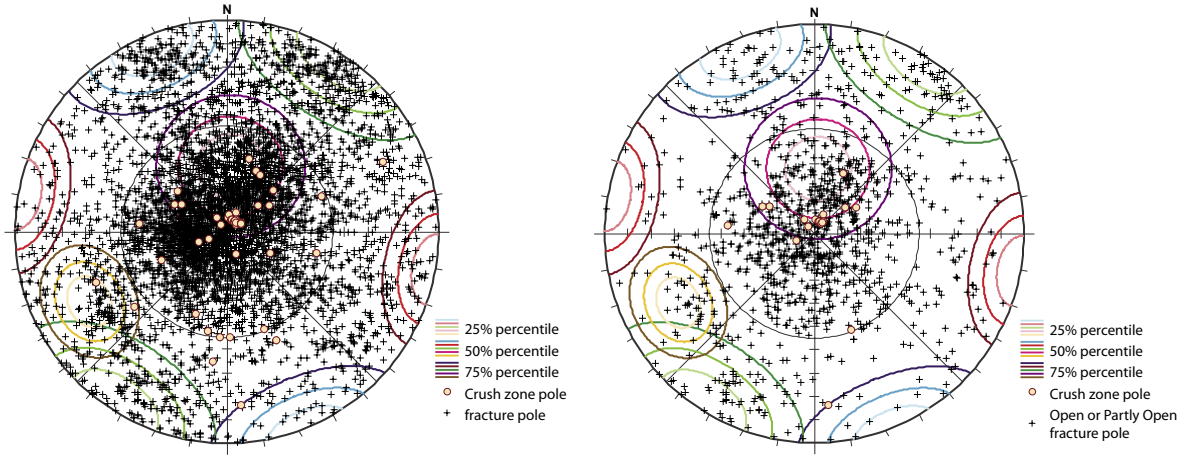

Figure 3-7. *Outcome of applying the hard sector algorithm to fractures mapped in the rock mass in KLX04. There are 3,088 sealed fractures, 1,195 Open fractures and 13 Partly open fractures in the rock mass outside the deformation zones. Left: All fractures. Right: Open and Partly open fractures.*

Table 3-4 shows the relative Terzaghi corrected intensities Rel. $P_{32}[BH]$ between the five fracture sets in the three intervals denoted by Volumes I, II and III. There is a clear geometrical anisotropy between the intervals. In Volume I the gently dipping fractures of Set_d dominate, whereas the NW striking fractures of Set_C dominate in Volume II and the NE striking fractures of Set_A dominate in Volume III. Set_B and Set_f are weak fracture sets in all three intervals.

Figure 3-8 shows the orientations of the Open and Partly open fractures outside the deformation zones versus depth. Each fracture is assigned a colour according to the hard sector division. The yellow line in the left plot in Figure 3-8 shows the inclination of the KLX04 borehole.

Table 3-4. Relative Terzaghi corrected intensities between the five fracture sets in the three intervals denoted by Volumes I, II and III.

Fracture set	Volume I *Rel. $P_{32}[BH]$* [%]	Volume II *Rel. $P_{32}[BH]$* [%]	Volume III *Rel. $P_{32}[BH]$* [%]
S_A	14.9	12.0	**55.4**
S_B	10.9	3.0	14.7
S_C	11.7	**57.0**	11.5
S_d	**52.2**	23.0	17.2
S_f	10.3	5.0	1.2

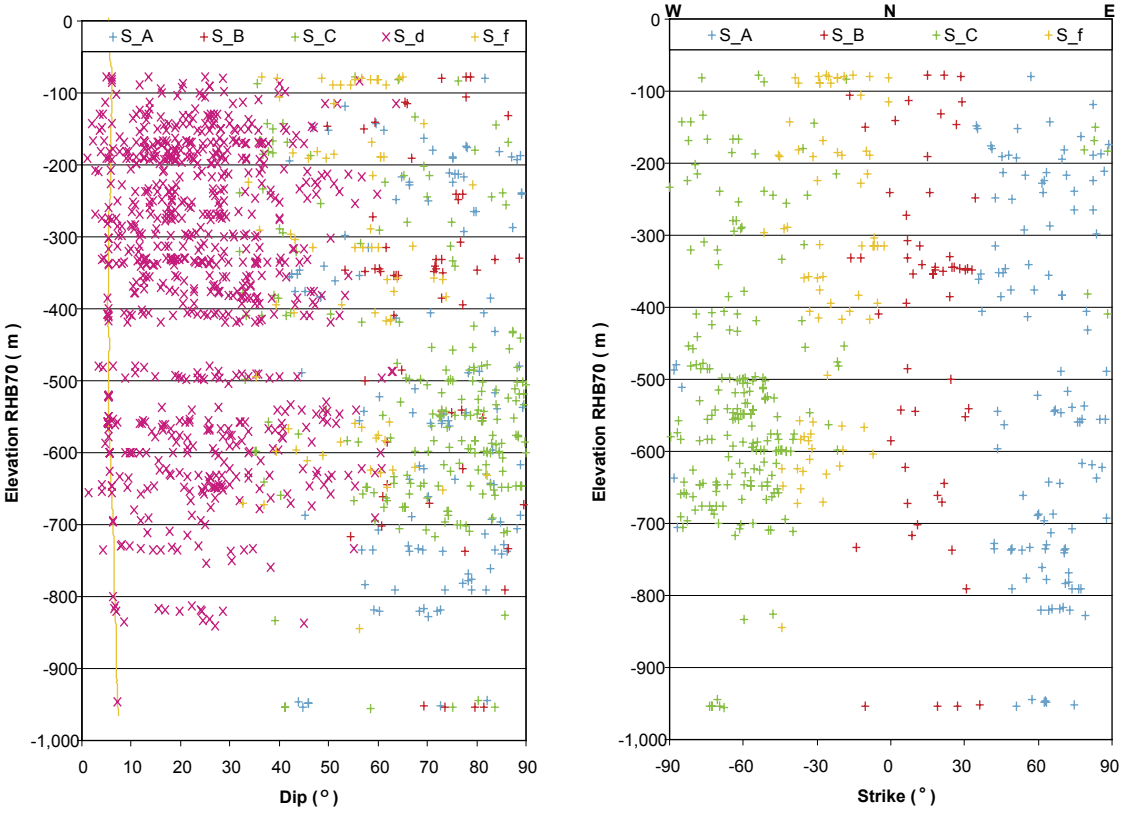

Figure 3-8. *Orientation of Open and Partly open fractures outside the deformation zones versus depth. Each fracture is assigned a colour according to the hard sector division. The yellow line in the left plot shows the inclination of KLX04.*

3.4 Assessment of hydraulic data

As previously mentioned all naturally Open and Partly open fracture are assumed to be potential candidates for flow. Sealed fractures, on the other hand, are by definition assumed to be impervious.

Table 3-5 shows the distribution of Open, Partly open and Sealed fractures in the deformation zones (DZ) and in the rock mass outside the deformation zones. Table 3-5 shows also the number of Crush zones and the number of PFL-f anomalies associated with each object

Table 3-5. Distribution of Open, Partly open and Sealed fractures as well as Crush and PFL-f anomalies.

Object	Open (Cert/Prob/Poss)	Partly open (Cert/Prob/Poss)	Sealed (Cert/Prob/Poss)	Crush	PFL-f (Features)
DZ1	10 (1/0/9)	0	3 (3/0/0)	1	2 (2)
DZ2	19 (0/0/19)	0	17 (17/0/0)	1	4 (1)
DZ3	10 (3/0/7)	0	12 (12/0/0)	2	3 (2)
DZ4	2 (0/1/1)	0	0	1	1 (1)
DZ5/ZSMEW007A	16 (0/1/15)	0	9 (9/0/0)	1	7 (2)
DZ6/ZSMNW929A	757 (19/287/451)	0	367 (364/0/3)	27	16 (16)
Rock mass	1,195 (54/112/1,029)	13 (8/1/4)	3,068 (3,056/5/6)†	20	96 (96)

† 1 fracture is missing a confidence tag.

3.4.1 Comparison between PSS and Σ PFL-f

The PFL-f transmissivities in the rock mass were lumped together according to the packer positions of the corresponding PSS test sections (5, 20 and 100 m). Figure 3-9 and Figure 3-10 show cross plots of the lumped transmissivities versus transmissivity data from PSS 5 m, 20m and 100 m tests. Three of the plots refer to KLX04 data and one plot to KLX03 data.

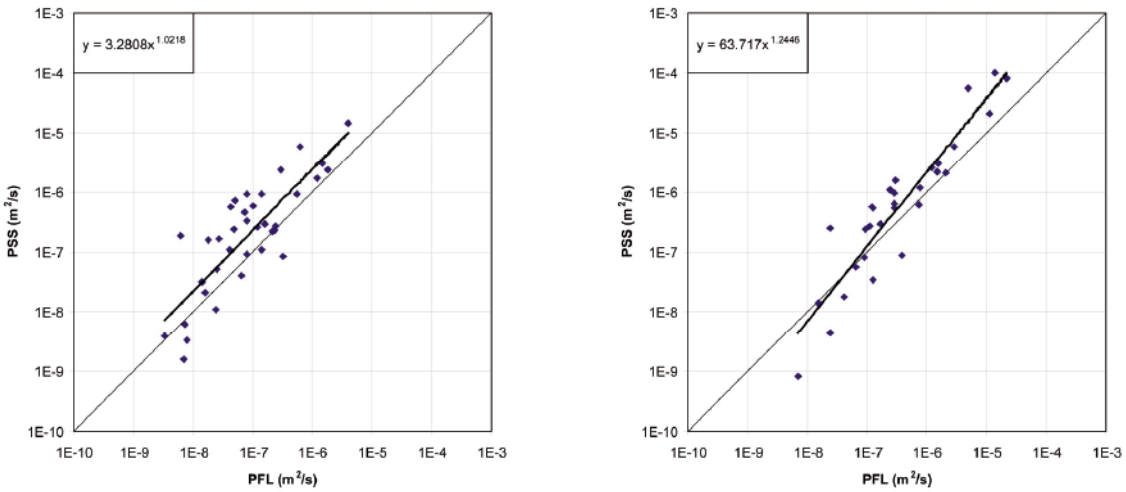

Figure 3-9. *Posiva Flow Log transmissivities versus transmissivity data from PSS 5 m and 20 m tests in KLX04. The straight lines are least-squares fits.*

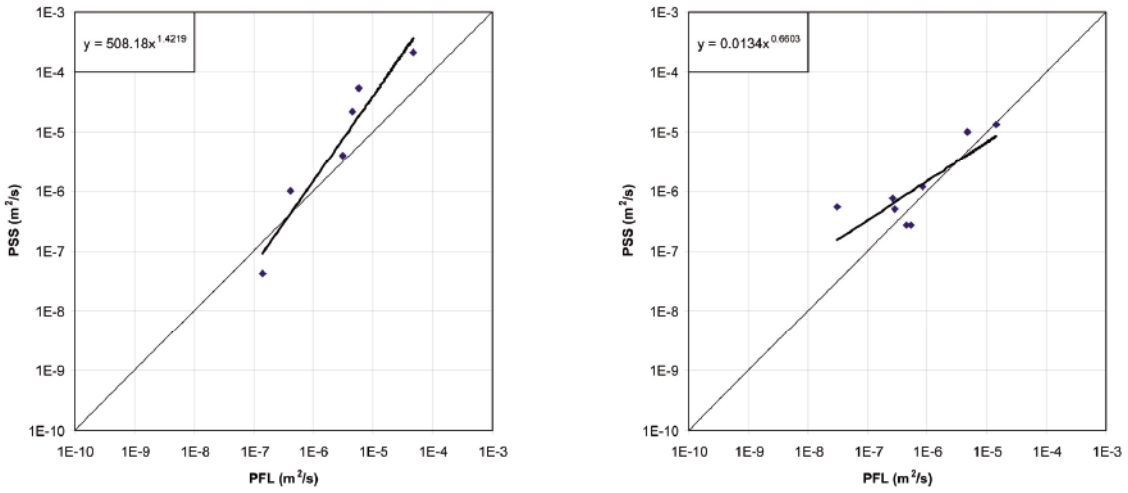

Figure 3-10. *Posiva Flow Log transmissivities versus transmissivity data from PSS 100 m tests in KLX04 and KLX03, respectively. The straight lines are least-squares fits.*

The cumulative values of the PFL-f transmissivities in KLX04 seem to underestimate the test section transmissivity, or, alternatively, the PSS measurements overestimate the test section transmissivity. However, the situation changes at higher magnitudes. The situation in KLX03, in turn, differs from the situation in KLX04. There are several possible reasons for the uncertain matches. Some of the more obvious ones are:

- Difference in flow regime; the borehole acts as a line sink during the PFL-f pumping measurements, whereas the PSS injection tests may be considered more spherical. If the flow regime is spherical and one uses a radial flow model the interpretation will overestimate the transmissivity.
- The PSS measurements may cause a shortcut back to the borehole above or below the packers.
- The interpretation of PFL-f measurements assumes steady state flow, which imply that the interpreted values are sensitive to skin effects. Skin effects may arise from using a nitrogen pulse to clean the borehole after the drilling is completed. That is, pockets of gas may reside in the fracture system close to the borehole for some period of time. This would effect the PFL-f measurements more since this method is used pretty soon after the borehole is cleaned. Also, the PFL-f measurements are known to be sensitive to "degassing". In contrast, PSS measurements are made several weeks-months after the drilling is completed depending on the extent of the hydrogeochemical programme.
- The PFL-f method misses small transmissivity values due to somewhat greater measurement limit.

3.4.2 Fracture transmissivity distribution

Figure 3-11 shows a complementary cumulative density function (CCDF) plot of the PFL-f transmissivity data in the rock mass and the six deformation zones DZ1–DZ6 in KLX04. The transmissivity data in each deformation zones were lumped together into a single value using Equation (4-2) in Section 4.1.3. The deterministically treated deformation zones DZ5–DZ6 are included in the deformation zone model. Thus, the deformation zones DZ1–DZ4 represent four data points in the hydrogeological DFN modelling reported here.

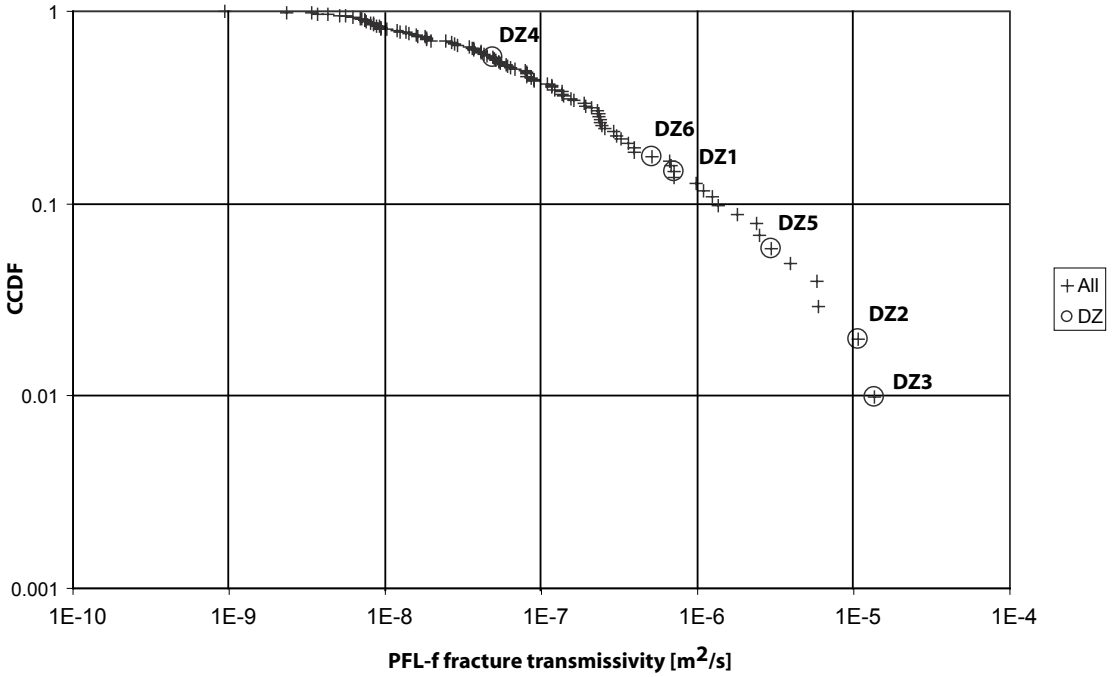

Figure 3-11. *CCDF plot of the PFL-f transmissivity data in the rock mass and the six deformation zones DZ1–DZ6 (33 data points) in KLX04.*

Figure 3-12 shows a CCDF plot of the rock mass fractures coloured according to their set belonging. The deterministically treated deformation zones DZ5–DZ6 are left out. Hence, Figure 3-12 constitutes the primary hydraulic data set for a hydrogeological DFN model of the rock mass outside the deformation zones.

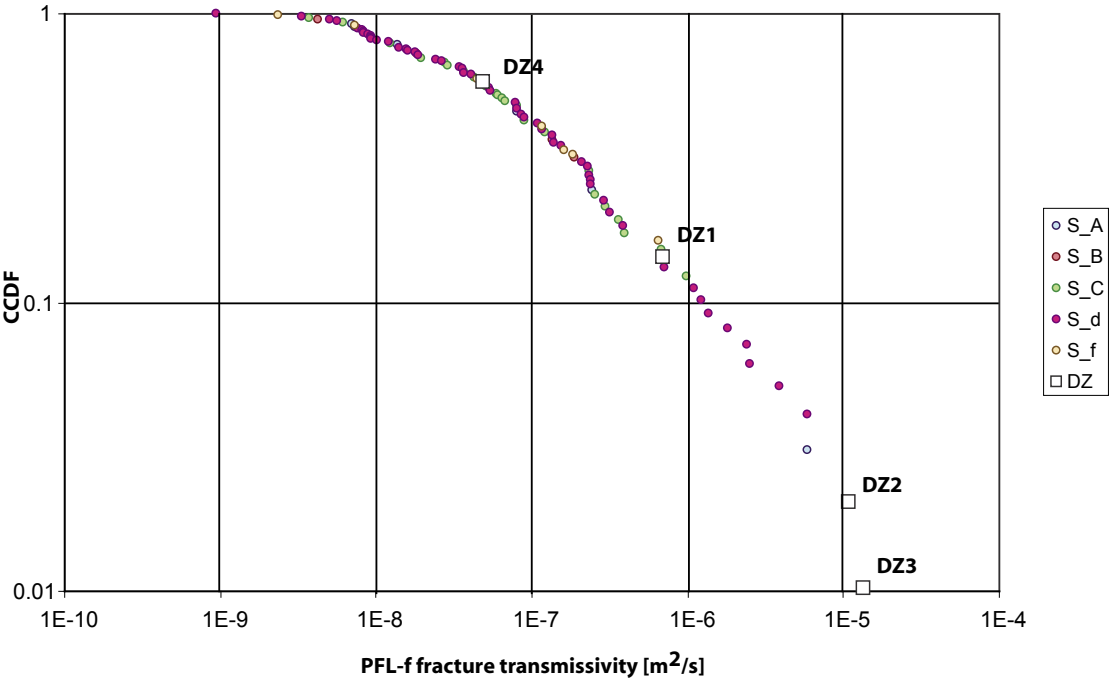

Figure 3-12. *CCDF plot the of hydraulic data outside the deterministically treated deformation zones. The data points are coloured according to their set belonging.*

By fitting a straight line to data shown in Figure 3-12 the shape parameter and the location parameter of a power-law transmissivity distribution may be calculated from:

$$G[T' > T] = (1 - P[T' \leq T]) = \left(\frac{m_T}{T} \right)^{k_T} \qquad (3\text{-}2)$$

where the slope $k_{T,1D}$ is the shape parameter and the intercept $m_{T,1D}$ is the location parameter. How these values are used to define a correlated transmissivity to size model is described in Chapter 4.

Figure 3-13 contains six stereo nets showing different aspects of the deduced PFL-f orientations. The right-hand column in Figure 3-13 reveal that there is a significant hydraulic anisotropy associated with the proposed division of KLX04 into subvolumes. However, it is vital to note that the hydraulic anisotropy is primarily due to the coupling to the geometrical anisotropy. That is, the univariate statistics of the transmissivities in each fracture set reveal no great differences between the sets in terms of the mean and standard deviation of log (T) in Volumes II and III, see Table 3-6 and Table 3-7, respectively. The rock mass in Volume III is considered to be sparsely connected in the work reported here. The PFL-f anomaly associated with this interval is located in the immediate proximity to the steeply dipping deformation zone ZSMNW929A (DZ6), cf Figure 3-1.

Table 3-6 and Table 3-7 suggest that the hydraulic anisotropy is primarily due to the coupling to the geometrical anisotropy. The geometric means and the standard deviations of the log transmissivities are similar regardless of orientation. Moreover, there is no obvious depth trend indicated by the statistics.

Table 3-6. Univariate statistics of PFL-f transmissivities [m²/s] for the different fracture sets in Volume I. The interval is dominated by the gently dipping fracture set S_d, see Figure 3-9.

Set	No. of PFL-f		*Tg*	$\log_{10} T_g$	$\log_{10} s_T$
S_A	6	8%	6.60E–08	–7.180	1.136
S_B	4	6%	3.79E–08	–7.422	0.774
S_C	6	8%	7.77E–08	–7.109	0.796
S_d	45	63%	6.26E–08	–7.203	0.891
S_f	6	8%	7.88E–08	–7.103	0.837
DZ	4	6%	1.49E–06	–5.826	1.149
All	71	100%	7.59E–08	–7.120	0.935

Table 3-7. Univariate statistics of PFL-f transmissivities [m²/s] for the different fracture sets in Volume II. The interval is dominated by the NW steeply dipping fracture set S_C and gently dipping fracture set S_d, see Figure 3-9.

Set	No. of PFL-f		*Tg*	$\log_{10} T_g$	$\log_{10} s_T$
S_A	0	0%	N/A	N/A	N/A
S_B	0	0%	N/A	N/A	N/A
S_C	16	62%	7.09E–08	–7.149	0.595
S_d	9	35%	1.03E–07	–6.989	0.820
S_f	1	3%	7.36E–09	–8.133	N/A
DZ	0	0%	N/A	N/A	N/A
All	26	100%	7.39E–08	–7.132	0.689

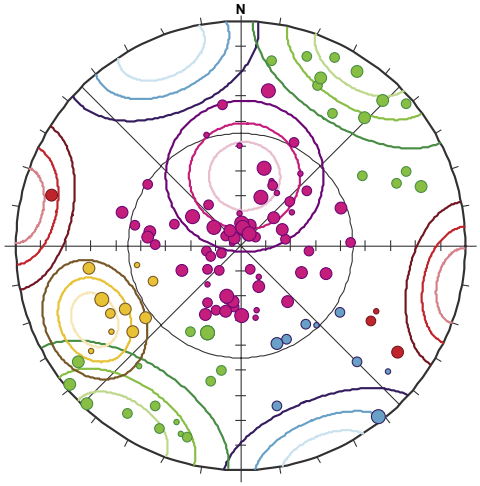

All PFL-f data (129); All Volumes

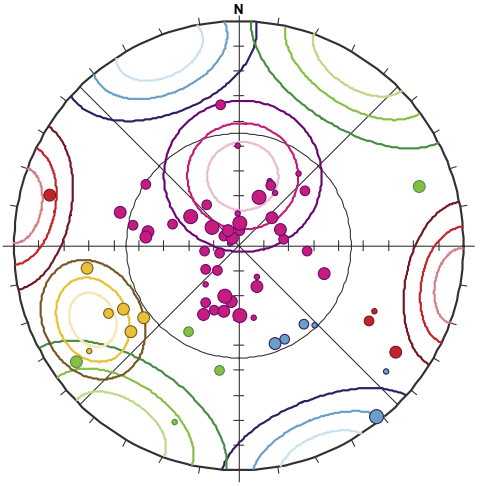

Rock mass PFL-f data; Volume I (71)

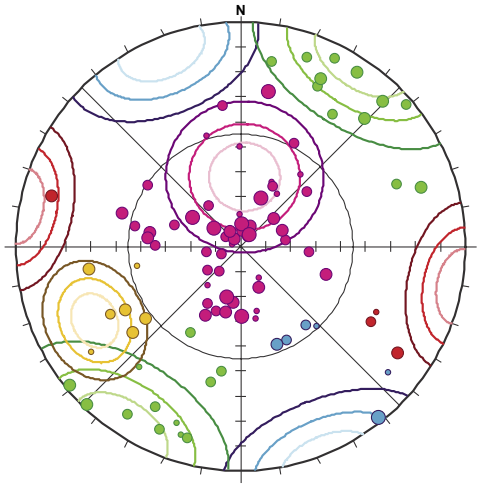

Rock mass PFL-f data (96); All Volumes

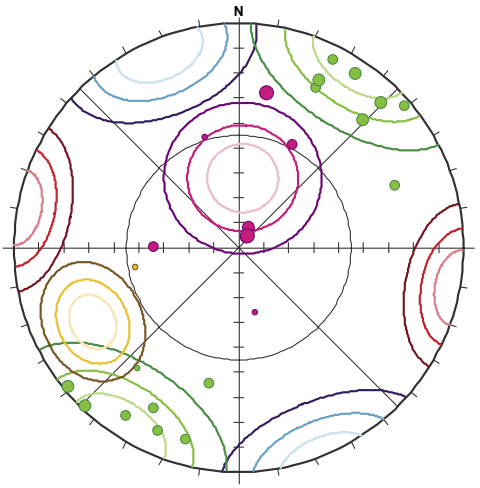

Rock mass PFL-f data; Volume II (26)

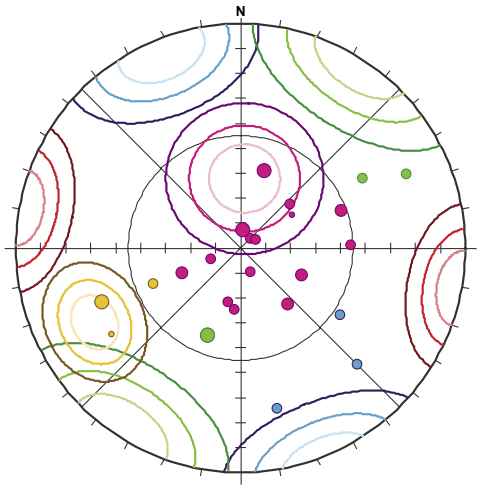

DZ PFL-f data (33); All Volumes

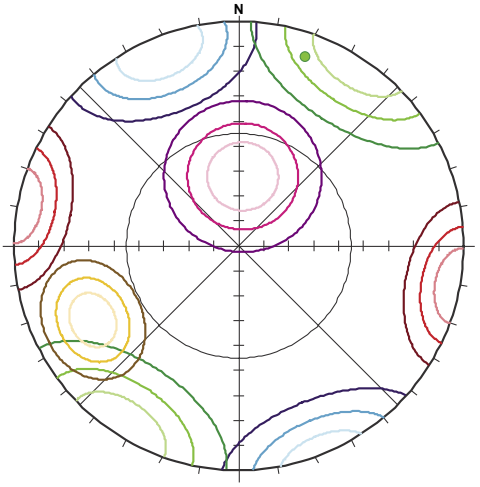

Rock mass PFL-f data; Volume III (1)

Figure 3-13. *Orientations of the transmissive fractures observed in KLX04. The plots suggest a hydraulic anisotropy in Volumes I and II. Volume III has one flowing feature in the immediate proximity to the deformation zone ZSMNW929A (DZ6).*

Figure 3-14 and Figure 3-15 show the final CCDF plots of the PFL-f transmissivity data for the rock mass in Volume I and Volume II, respectively. The power-law slope $k_{T,1D}$ and the power-law intercept $m_{T,1D}$ values evaluated from these plots are reported in Chapter 5.

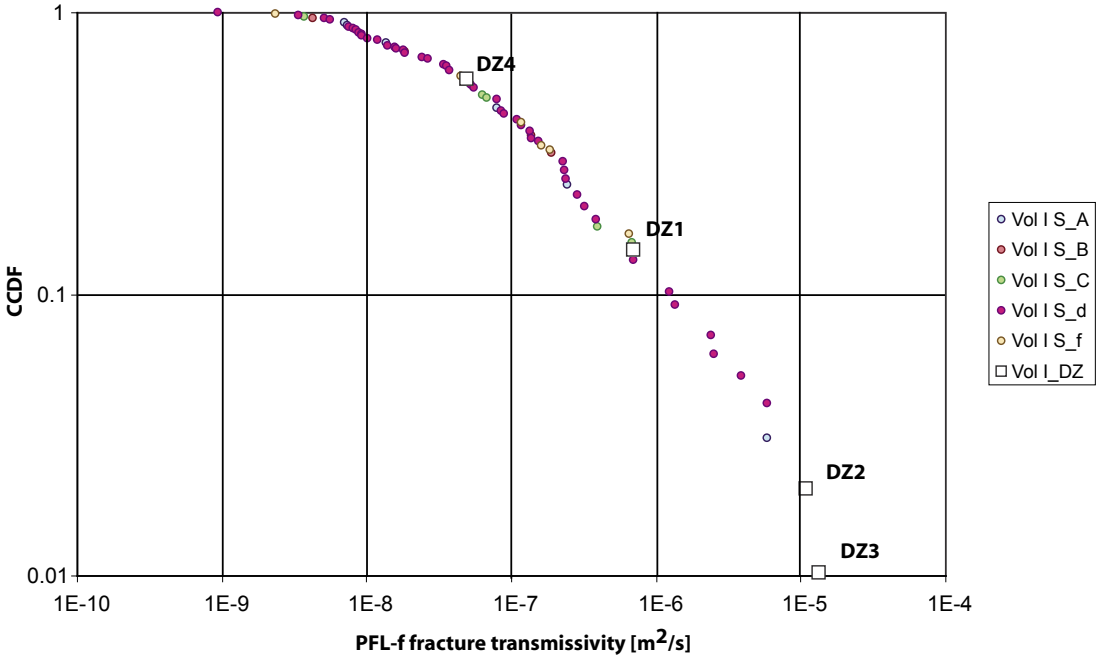

Figure 3-14. *CCDF plot of the hydraulic data in Volume I. The data points are coloured according to their set belonging.*

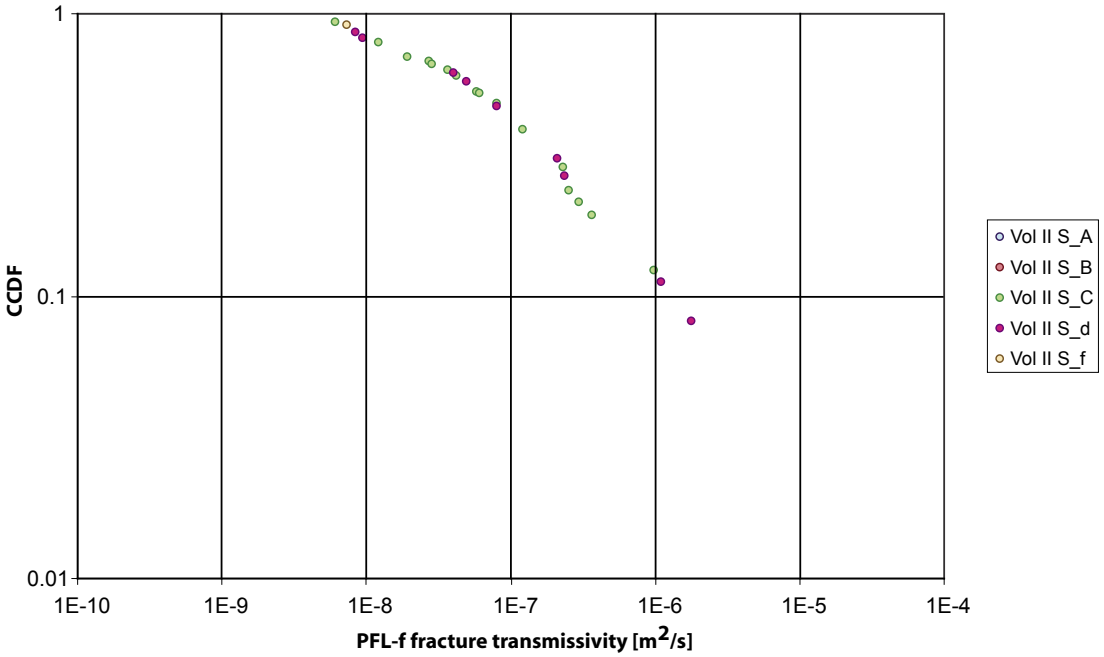

Figure 3-15. *CCDF plot of the hydraulic data in Volume II. The data points are coloured according to their set belonging.*

4 Hydrogeological DFN model set-up

4.1 Hydrogeological assumptions

The numerical DFN modelling conducted with DarcyTools during the 1.2 modelling stage is based on several conceptual simplifications. Three of the more important assumptions constraining the validity of the results in the work reported here are commented on below.

4.1.1 Conductive fractures

An Open fracture is by definition associated with a naturally broken core, i.e. the natural fracture is as large as or larger than the core diameter. A Partly open fracture is by definition a fracture that does not break the core, but still have some kind of aperture associated to it. All Partly open fractures are mapped to greatest detail possible from a practical point of view, which means that there is threshold defined. Partly open and Open fractures are treated like in SICADA database as they both contribute to the concept of borehole fracture frequency, P_{10}.

All naturally Open and Partly open fractures, regardless of their aperture confidence (Certain, Probable and Possible), are assumed to be potential candidates for flow from the onset in the connectivity analysis. Sealed fractures, on the other hand, are assumed to be impervious. This simplification is recognised to be incorrect on a detailed scale.

4.1.2 Flow in conductive fractures

Conductive fractures are assumed to be completely flat surfaces with homogenous macroscopic hydraulic properties, i.e. transmissivity T and storativity S. In case of heterogeneous fracture properties, equivalent homogeneous (effective) values are considered. In reality, the flow is distributed through channels across the fracture plane. Possibly, also intersections between fractures can be considered as potential channels. The channels are formed by the undulating fracture surfaces (spatial distribution of the fracture asperity) that do not exactly match, thus creating channels. The distribution of flow is, however, governed by the acting boundary conditions and processes such as barometric pressure changes, tidal effects, precipitation, etc, all of which may be transient. The flow channels within a fracture plane occupy only a minor part of the fracture surface, because parts of the fracture surface are closed due to its undulating nature. In conclusion, most fractures are probably Partly open although they are mapped as Open or Sealed in the borehole.

4.1.3 Stochastic deformation zones as single conductive fractures

A number of intervals with fracture swarms are generally observed in the core-drilled boreholes. Some of the swarms are treated (modelled) as deterministic deformation zones, other as non deterministic, i.e. stochastic. Hence, it is useful to characterise these fractures to get some indication of the width and fracture intensities within these zones. However, at this regional modelling stage, fracture swarms interpreted as deterministic or stochastic deformation zones will be approximated as large fracture planes in a continuous range of fracture sizes, as shown in Figure 4-1. It is important that data, such as fracture intensity and the PFL-f flow anomalies, are handled in a manner consistent with this concept.

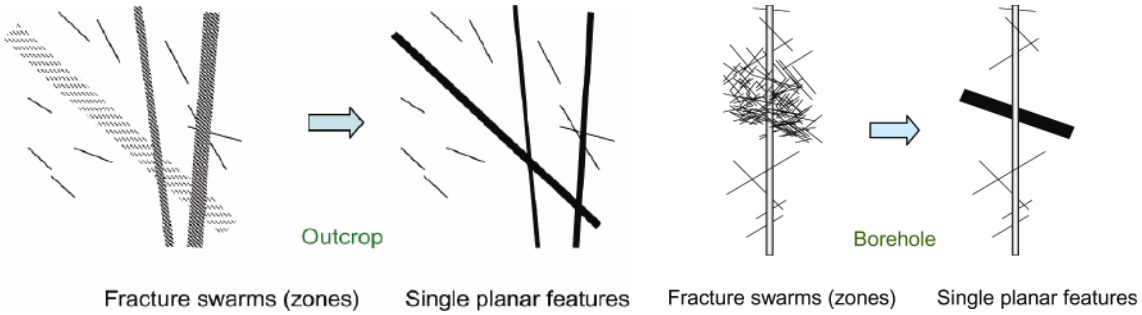

Figure 4-1. *An important assumption in the hydrogeological DFN analysis is the representation of fracture swarms (zones) as single planar fractures.*

Figure 4-1 implies that the fracturing within a deformation zone is not studied in terms of its components, but treated as a single object. Both stochastic and deterministic deformation zones are treated in this way.

If N_{TOT} is the total number of Open and Partly open fractures in a borehole and N_{DZ} is the number of Open and Partly open fractures in an intercepted stochastic deformation zone, the remaining number of potentially flowing Open and Partly open fractures in the borehole to be matched in the modelling process N_{CAL} may be written as:

$$N_{CAL} = N_{TOT} - \sum (N_{DZ} - 1) \qquad (4\text{-}1)$$

The summation in Equation (4-1) is made over all intercepted stochastic deformation zones. The subtraction by 1 is made as the zone itself is one fracture to be included in the modelling process. This is found to be important in cases where the rock is sparsely fractured. So called Crush and Sealed networks are generally associated with deformation zone intervals and are treated accordingly, i.e. no particular attention. Crush and Sealed Networks rarely occur in the rock mass.

In analogy with Equation (4-1) the transmissivity of a potentially flowing stochastic deformation zone is considered equal to its geological thickness-hydraulic conductivity product and the storativity is equal to its geological thickness-specific storativity product. This implies that the transmissivity of a stochastic deformation zone, as determined at its intersection with a borehole, is equal to the sum of the transmissivities of the flowing fractures:

$$T_{DZ} = \sum (T_f) \qquad (4\text{-}2)$$

The summation in Equation (4-2) is made over all PFL-f anomalies belonging to the intercepted stochastic deformation zone. In case of heterogeneous deformation zone properties, equivalent homogeneous values are considered.

It is noted that Equation (4-2) may overestimate the deformation zone transmissivity T_{DZ} if the flowing fractures intersecting the borehole merge at some distance away from the borehole. This problem was discussed in Section 3.4.1 where the results from the difference flow logging (PFL-f) is cross-plotted against the results from the 5 m long double-packer injection tests (PSS 5 m)

4.2 Generation of DFN with DarcyTools

The discrete fracture network generator in DarcyTools is based on the following key geometric assumptions/limitations:

- Univariate Fisher distributed fracture orientations.
- Power-law distributed fracture sizes.
- Poisson distributed fracture centres.

These basic assumptions are used to define geometry of the stochastically modelled fracturing. The assumptions/limitations imply that the number of discrete fractures per unit volume P_{30} in the size interval $[r_{\min}, r_{\max}]$ in an infinite model domain may be written as /cf Hedin 2005/:

$$P_{30}[r_{\min}, r_{\max}] = P_{32}[r > r_0] r_0^{(k_r-2)} \frac{(k_r-2)}{\pi\, k_r} \left((r_{\min})^{-k_r} - (r_{\max})^{-k_r} \right) \quad (4\text{-}3)$$

Appendix C presents a technical note on the geometrical properties of DFNs generated with DarcyTools. The investigations presented do not motivate any firm statements. However, the comment made in Appendix C is that the connected fractures show fractal properties (D < 3 in three-dimensions) even if the generation process behind the DFN realisations is Poissonian in DarcyTools (D = 3 in three-dimensions).

The hydraulic properties are either specified deterministically or generated from probability distribution functions (PDFs). The stochastic properties may be generated independently or correlated. For model version L1.2 site-specific fracture data available for modelling consist of fracture transmissivities T solely. General formulae are suggested for assigning equivalent parameter values of the fracture storativity S and the transport aperture e_t:

$$S = 7\times10^{-4}\, T^{0.5} \quad (4\text{-}4)$$

$$e_t = 0.5\, T^{0.5} \quad (4\text{-}5)$$

These formulae are taken from the findings reported in /Rhén et al. 1997, Rhén and Forsmark 2001, Andersson et al. 1998, 2000, Dershowitz et al. 2003/. It is noted that the fracture storativity and the transport aperture are both modelled as power-law functions of the fracture transmissivity. The experimental basis for assuming that fracture transmissivity is a power-law function of the fracture size is discussed in /Dershowitz et al. 2003/. From a hydraulic point of view one can advocate that a correlated model is logical. This comes from the evidence that hydraulic tests have different scales of support, i.e. radius of influence, r_e, /Jacob 1950/. The radius of influence for transient radial flow in an infinite and homogeneous fracture may be written as:

$$r_e = \sqrt{\frac{2.25\, T\, t}{S}} \quad (4\text{-}6)$$

Equation (4-6) is illustrated in Figure 4-2.

Hence, a hydraulic test in an infinite and homogeneous fracture of high transmissivity implies a greater radius of influence than for an infinite and homogeneous fracture of low transmissivity. If the size (radius) of the high transmissive and homogeneous fracture is less than its theoretical hydraulic radius of influence, the hydraulic test should sensor this limitation as a flow boundary.

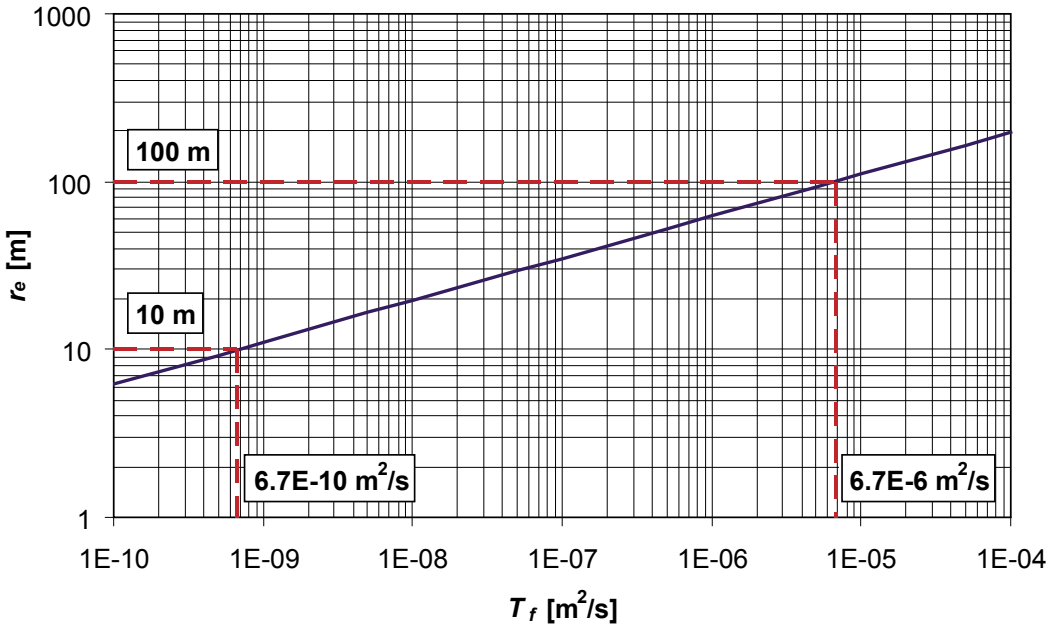

Figure 4-2. *Illustration of the radius of influence of a 20 minute long injection test in an infinite and homogenous fracture, see Equation (4-6). In this plot the fracture storativity is related to the fracture transmissivity as specified by Equation (4-4).*

Another argument for a correlated transmissivity model is that, at least for deformation zones, the zone thickness often increases with size, and thus generally so does the number of individual conductive fractures associated with a zone. If the transmissivity distribution for individual fractures is the same, then based on the above assumption it follows that the effective transmissivity for the deformation zone should increase with the size of the fracture zone.

These arguments are the primary motives in the work reported here for assuming that it is the largest connected fractures intercepting the borehole in each stochastic DFN realisation that correspond to the measured fracture transmissivities (cf Section 3-2). The correlated transmissivity-size model may be written as:

$$T = a\, r^{b} \qquad (4\text{-}7)$$

where a and be b are deduced by means of numerical simulations. The simulations couple realisations of the geological DFN model to the hydraulic testing with the PFL-f method. The results derived are checked against the (PSS 5 m) data.

4.3 Sensitivity study

For the sake of understanding how the uncertainties in the geological DFN modelling propagate into the hydrogeological DFN modelling, two parameter combinations that are along the results of the geological DFN modelling are explored in the work reported here. The two combinations simplify the geological DFN modelling in Table 2-2:

A. $k_r = 2.90$ and $r_0 = 0.282$ m B. $k_r = 2.56$ and $r_0 = 0.038$ m

4.3.1 Motives for parameter combination A

Parameter combination A mimics the parameter values of the geological DFN modelling fairly well, cf Table 2-2. The motive for choosing $r_0 = 0.282$ m rather than a value in the range 0.328–0.977 m is that 0.282 m is used in the hydrogeological DFN modelling conducted with *ConnectFlow* code by /Hartley et al. 2006/. Hence, the conclusions drawn from the work reported here may perhaps be of use in a wider DFN context as the ConnectFlow code is also used for regional flow modelling.

4.3.2 Motives for parameter combination B

If we exclude the assumption made in the geological DFN that all deformation zones are rectangular and reach –1,100 m above sea level (i.e. we exclude the assumption the assumption that $P_{32}[r > 591.73\ \text{m}] = 0.0047\ \text{m}^2/\text{m}^3$, cf Section 2.4.3) and focus solely on the reported value of $P_{32}[r > r_0] = 3.31\ \text{m}^2/\text{m}^3$ for set S_A, S_B and S_C in Table 2-2, parameter combination A ($k_r = 2.90$ and $r_0 = 0.282$ m) in combination with Equation (4-3) render only "24" deformation zones with radii greater than 591.73 m within the local model domain. In comparison, the deformation zone model shown in Figure 2-9 have three times as many deformation zones, i.e. 71–80, cf Section 2.4.2.

In the hydrogeological DFN modelling conducted in support of the site descriptive modelling of Simpevarp and Forsmark /Follin et al. 2005ab/ suggested that $r_0 \approx r_w$, where r_w is the cored borehole radius 0.038 m in SKB's site investigations. If we insert $r_0 = 0.038$ m into Equation (4-3) we can match 71–80 deformation zones for $k_r \approx 2.56$. This appears to be an unrealistic low value of k_r with regard to the values shown in Table 2-2. Nevertheless, this is the motive for choosing parameter combination B. Figure 4-3 schematically illustrates the principle difference between parameter combinations A and B.

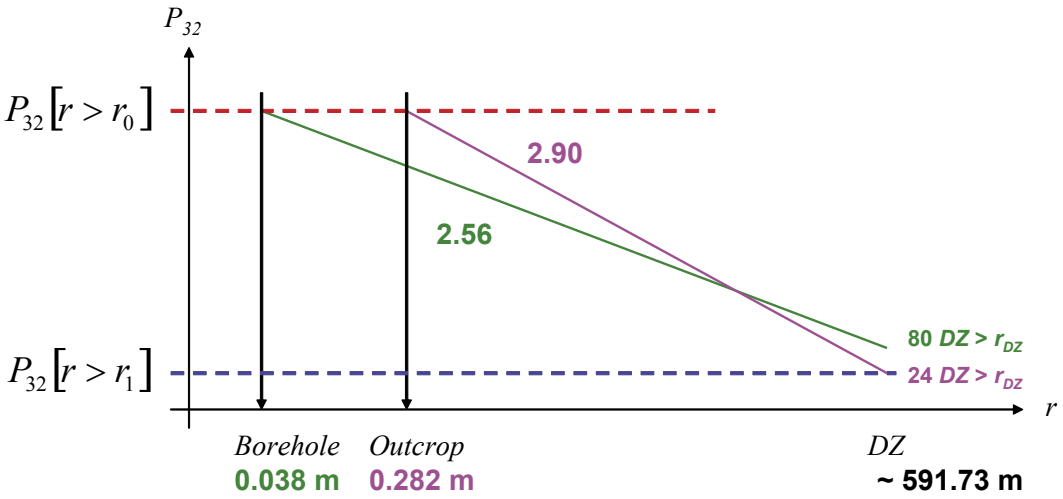

Figure 4-3. *Schematic illustration of the fracture surface area per unit volume as a function of k_r and r_0 for parameter combinations A ($k_r = 2.90$ and $r_0 = 0.282$ m) and B ($k_r = 2.56$ and $r_0 = 0.038$ m). $P_{32}[r > 591.73\ \text{m}]$ is slightly larger for parameter combination B compared to the value of parameter combination A.*

5 Hydrogeological DFN modelling

This chapter demonstrates modelling steps 3 and 4 in Section 3.2 using the parameter combinations A and B described in Section 4.3. Ten realisations are run for each parameter combination and volume. To simplify the reading not all intermediate steps of the analysis are shown for all parameter combinations and subvolumes.

5.1 Derivation of connected fracture frequency

The simulation domain consists of three concentric shells; one large (outer), one intermediate large (middle) and one small (inner). In the centre of the simulation domain there is a scanline mimicking a steeply dipping core-drilled borehole. The model set-up and dimensions of the shells are shown in Figure 5-1.

Within the outer shell stochastic fractures in the size range L = 20–1,000 m (r = 11.3–564 m) are generated, within the middle shell L = 1–20 m (r = 0.564–11.3), and within the inner shell $L = L_0$–1 m ($r = r_0$–0.564) m. The fractures are generated in order beginning with the outer shell. The approximate procedure of generating an connected network is done as follows:

- the connected stochastic fractures within the outer shell are retained while the stochastic fractures in the middle shell are generated, and
- the connected stochastic fractures within the outer and middle shells are retained while the stochastic fractures in the inner shell are generated.

The simulations are done twice for each seed. In the first run there is a scanline in the centre of the simulation domain. The scanline represents the borehole to be matched with regard to N_{CAL}, the measured number of Open and Partly open fractures. In the second run there is no scanline and the connected fractures, N_{CON}, are measured. That is, the scanline (borehole) used in the first run intersects not only the connected fractures but also the isolated fractures. In the second run the isolated fractures are sorted out by means of a connectivity analysis.

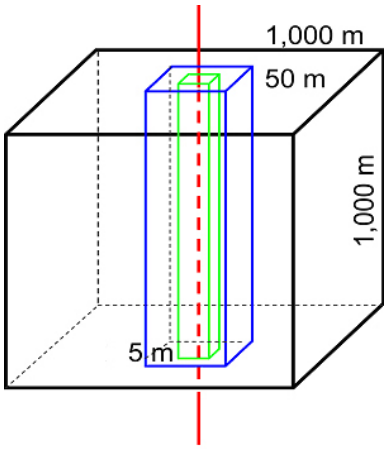

Figure 5-1. *Simulation model set-up and dimensions of the three fracture shells; outer (black), middle (blue) and inner (green).*

Table 5-1 presents the basic fracture frequency data outside the deformation zones that is used in the connectivity analysis. T_{PFLmin} is the smallest transmissivity value measured and may be considered as an estimate of the lower measurement limit. The lower measurement limit of the PFL-f tests is not a threshold with a fixed magnitude, but varies in space dependent on the in situ borehole conditions. The frequency of potentially flowing Open and Partly open fractures, P_{10CAL}, differs almost an order of magnitude between the Volumes I and III. The value of P_{10PFL} in each Volume is c one order of magnitude lower than the corresponding value of P_{10CAL}. For Volume III there is only one flow anomaly above the lower measurement limit.

Table 5-2 presents mean values of the simulation results on fracture connectivity of Volumes I–III for the two parameter combinations.

Table 5-1. Statistics of Open fractures and PFL-f data in the rock mass outside the deformation zone intervals in the KLX04 borehole.

Borehole	Volume	Interval	N_{CAL} [–]	P_{10CAL} [(100 m)$^{-1}$]	N_{PFL} [–]	P_{10PFL} [(100 m)$^{-1}$]	T_{PFLmin} [m^2/s]	T_{PFLmax} [m^2/s]
KLX04	I	102–442	704	206	71	21	9.43×10^{-10}	1.34×10^{-5}
KLX04	II	502–675	351	202	26	15	6.17×10^{-9}	1.80×10^{-6}
KLX04	III	749–982	84	36	1	0.4	9.00×10^{-8}	9.00×10^{-8}

Table 5-2 Results from the connectivity analyses in Volumes I–III. N_{CON} is the number of connected Open and Partly open fractures after calibration against N_{CAL}, which is the total number of Open and Partly open fractures. P_{10CON} is the frequency matching N_{CON}. $P_{32}[r > r_0]$ is the Terzaghi corrected P_{10corr}, which is first estimated from N_{CAL} and then adjusted to match the variability in k_r between the five fractures sets. P_{32CON}[%] is N_{CON} /N_{CAL}. All values represent mean values of ten realisations.

Case	k_r [–]	r_0 [m]	N_{CON} [–]	P_{10CON} [100m]	$P_{32}[r > r_0]$† [m^2/m^3]	P_{32CON} [%]	P_{32CON} [m^2/m^3]	$P_{32CON} < T_{min}$ [% of P_{32CON}]	$P_{32CON} > T_{min}$ [% of P_{32CON}]
Volume I: N_{CAL} = 704									
A	2.90	0.28	702	205	3.73	99.8	3.86	90	10
B	2.56	0.038	638	187	3.79	90.6	3.55	89	11
Volume II: N_{CAL} = 351									
A	2.90	0.282	351	202	5.38	100	5.38	93	7
B	2.56	0.038	344	198	5.53	98.1	5.43	92	8
Volume III: N_{CAL} = 84									
A	2.90	0.282	68	29	0.98	81.2	0.79	99	1
B	2.56	0.038	10	4	1.10	12.3	0.14	90	10

† The values shown are the arithmetic averages of ten realisations and should be equal within each volume regardless of the values of k_r and r_0. The differences are caused by too few simulations.

Parameter combination A renders a well connected DFN, where c 100% of all Open and Partly open fractures are connected in Volumes I and II and c 81% in Volume III. Parameter combination B leads to a somewhat less connected DFN, where c 91% of all Open and Partly open fractures in Volume I are connected, c 98% in Volume II, and c 12% in Volume III. In conclusion, both parameter combinations render fairly well connected DFNs in the Volumes I and II. For Volume III the difference between the two parameter combination is much greater because of the lower value of $P_{32}[r > r_0]$, which suggests that the magnitude of $P_{32}[r > r_0]$ affects the role of r_0 on the connectivity.

5.2 Properties for a correlated transmissivity-size model

Figure 5-2 shows a schematic illustration of a complementary cumulative density function (CCDF) plot of ordered fracture transmissivity measurements in a borehole. The CCDF equation for the fracture transmissivity may be written as:

$$G[T' > T] = (1 - P[T' \le T]) = \left(\frac{m_T}{T}\right)^{k_T} \qquad (5\text{-}1)$$

where m_T is the transmissivity value where the power-law regression intersects $G[T' > T_0]$ and k_T is the slope of the power-law regression:

$$m_T = T \quad \sqrt[\{1/k_T\}]{G[T' \ge T]} = T_{PFL\,\min} \left(\frac{N_{PFL}}{N_{CON}}\right)^{(k_T)^{-1}} \qquad (5\text{-}2)$$

In order to compute the value of the transmissivity m_T we make use of T_{PFLmin} and N_{PFL} in Table 5-1 and the previous simulated values of N_{CON} in Table 5-2.

Figure 5-3 shows the inferred shape parameter values k_T of the fracture transmissivity data observed in Volumes I–II. For Volume III there is only one fracture transmissivity value above the measurement limit. In the work reported here it is assumed that the shape parameter for Volume III is identical to that of Volume II.

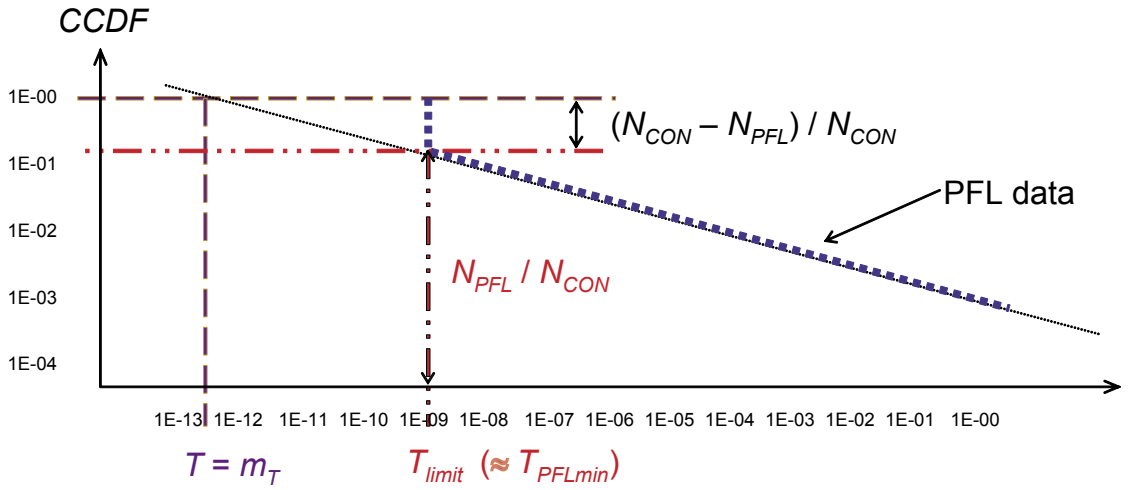

Figure 5-2. *Illustration showing the evaluation of a CCDF plot of ordered fracture transmissivity measurements in a borehole.*

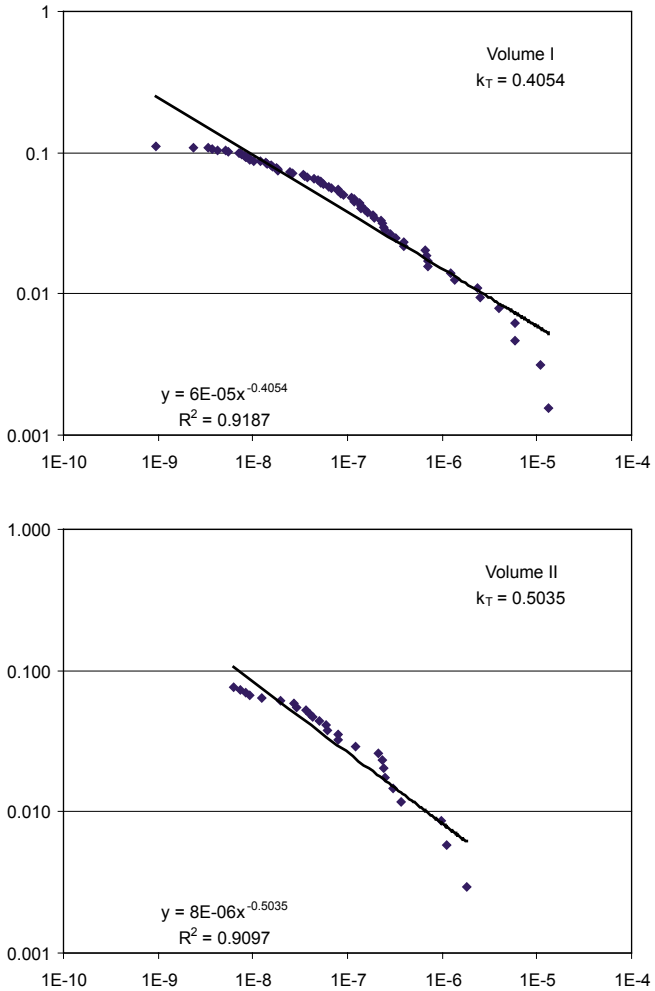

Figure 5-3. *Inferred shape parameters k_T of the fracture transmissivity data in Volumes I and II. In the work reported here it is assumed that the shape parameter for Volume III is identical to that of Volume II.*

Table 5-3 presents the simulated values of m_T in Volumes I using Equation (5-1). The input values of T_{PFLmin} and N_{PFL} are shown in Table 5-1 and the input values of N_{CON} in Table 5-2.

Table 5-3. Estimated values of m_T [m²/s] for parameter combinations A and B in Volumes I using Equation (5-7).

Parameter combination A Volume; m_T	#1	#2	#3	#4	#5	#6	#7	#8	#9	#10
I; $m_T = N\times10^{-10}$	0.285	0.214	0.245	0.226	0.243	0.248	0.297	0.258	0.270	0.241
II; $m_T = N\times10^{-10}$	0.769	0.638	0.697	0.679	0.635	0.655	0.728	0.697	0.748	0.787
III; $m_T = N\times10^{-10}$	0.175	0.146	0.256	0.121	0.165	0.189	0.111	0.219	0.136	0.175
Parameter combination B										
I; $m_T = N\times10^{-10}$	0.317	0.313	0.301	0.336	0.385	0.277	0.325	0.285	0.329	0.337
II; $m_T = N\times10^{-10}$	0.776	0.642	0.731	0.845	0.678	0.744	0.785	0.718	0.731	0.663
III; $m_T = N\times10^{-10}$	4.76	18.9	3.24	25.6	7.69	18.9	11.5	9.29	14.5	18.9

In the work presented here it is assumed that the largest fractures among the N_{CON} connected fractures that intersect the borehole in the simulation model correspond to the flow in the N_{PFL} flow anomalies. Since the borehole is a one dimensional object the slope of the power-law regression $k_{r,BH}$ of the CCDF plots is:

$$k_{r,1D} = k_r - 2 \tag{5-3}$$

where k_r is the three-dimensional scaling exponent of the parent fracture size distribution. The magnitude of m_r, i.e. the fracture size where the power-law regression intersects $G[r' \geq r] = 1$ is evaluated as:

$$m_{r,1D} = r^{\left\{1/k_{r,BH}\right\}}\sqrt{G[r' \geq r]} = r_{N_{PFL}} \left(\frac{N_{PFL}}{N_{CON}} \right)^{(k_{r,BH})^{-1}} \tag{5-4}$$

where $r_{N_{PFL}}$ denotes the size of the smallest fracture among the N_{PFL} largest connected fractures.

Ten realisations are run for each volume. Table 5-4 presents the minimum and maximum values of the N_{PFL} largest fracture sizes of each realisation. For Volume III there is one flow anomaly above the measurement limit only.

Figure 5-4 demonstrates the outcome of the first realisation for both parameter combinations in Volume I.

Table 5-4. Minimum and maximum fracture sizes of each parameter combination realisation and Volume I.

Parameter combination A										
Volume	**#1**	**#2**	**#3**	**#4**	**#5**	**#6**	**#7**	**#8**	**#9**	**#10**
I min r	4.8	2.7	3.8	3.4	3.4	3.4	3.1	4.2	3.1	3.4
I max r	298.9	397.5	256.2	529.2	307.4	139.1	130.4	271.6	201.1	176.5
II min r	3.8	6.6	6.3	5.0	6.7	6.1	5.9	7.1	4.6	4.4
II max r	81.0	121.2	221.0	137.2	131.4	291.8	382.5	418.2	130.1	518.7
III min r	556.2	371.7	25.9	244.2	92.8	107.3	214.4	115.8	67.2	167.1
III max r	556.2	371.7	25.9	244.2	92.8	107.3	214.4	115.8	67.2	167.1
Parameter combination B										
I min r	1.9	2.6	2.1	1.4	2.0	2.6	1.6	2.6	2.7	2.0
I max r	358.8	409.7	328.3	313.7	553.0	204.5	351.6	379.6	508.2	465.3
II min r	3.3	3.3	6.0	2.4	4.1	4.7	3.3	2.6	3.9	5.1
II max r	184.2	467.7	558.4	120.2	357.5	54.3	410.1	491.4	412.8	321.2
III min r	198.6	19.1	39.0	246.8	66.2	107.4	72.9	93.7	79.8	22.0
III max r	198.6	19.1	39.0	246.8	66.2	107.4	72.9	93.7	79.8	22.0

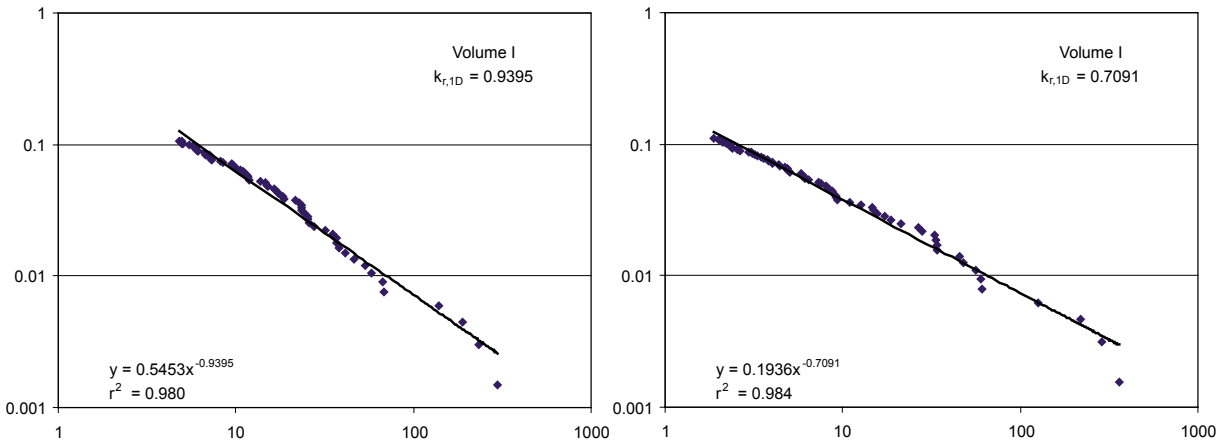

Figure 5-4. *Outcome of the first realisation of the N_{PFL} greatest fractures among the N_{CON} connected fractures that intersect the borehole in Volume I. Left: Parameter combination A. Right: Parameter combination B.*

Table 5-5 and Table 5-6 present the deduced values of $k_{r,1D}$ and $m_{r,1D}$ of Volumes I–III for the two parameter combinations A and B, respectively. The inferred values of the four variables $\{m_T, k_T\}$ and $\{m_{r,1D}, k_{r,1D}\}$ make it possible to derive the values of the coefficient a and the exponent b in Equation (4-7) by assuming that the complementary cumulative density functions are correlated. The derivation is explained in Appendix A.

Table 5-5. Simulated slopes $k_{r,1D}$ for the N_{PFL} greatest fractures.

Parameter combination A Volume	#1	#2	#3	#4	#5	#6	#7	#8	#9	#10
I	0.940	0.852	0.975	0.793	0.851	0.981	1.207	0.856	0.877	1.106
II	0.933	0.929	0.889	1.077	0.829	0.796	0.843	0.660	0.964	0.607
III	0.558	0.599	0.853	0.580	0.640	0.640	0.650	0.652	0.721	0.603

Parameter combination B										
I	0.709	0.698	0.639	0.698	0.620	0.805	0.699	0.738	0.692	0.703
II	0.706	0.572	0.672	0.707	0.628	1.201	0.660	0.619	0.646	0.756
III	0.302	0.264	0.378	0.247	0.289	0.292	0.265	0.249	0.333	0.254

Table 5-6. Simulated intercepts $m_{r,1D}$ for the N_{PFL} greatest fractures.

Parameter combination A Volume	#1	#2	#3	#4	#5	#6	#7	#8	#9	#10
I	0.524	0.187	0.413	0.193	0.244	0.371	0.578	0.328	0.213	0.418
II	0.264	0.431	0.308	0.444	0.305	0.215	0.262	0.136	0.325	0.060
III	0.347	0.364	0.473	0.338	0.415	0.344	0.343	0.380	0.440	0.322

Parameter combination B										
I	0.099	0.122	0.076	0.071	0.070	0.150	0.085	0.111	0.135	0.092
II	0.080	0.028	0.142	0.069	0.081	0.597	0.081	0.039	0.083	0.172
III	0.055	0.133	0.072	0.105	0.117	0.220	0.145	0.032	0.235	0.096

Table 5-7 and Table 5-8 show the deduced values of *a* and *b* for ten realisations in each of the three volumes, respectively. The variability between the realisations means that there is an uncertainty in the exact shape of the correlation between the fracture transmissivity and the fracture size. Table 5-9 provides the geometric means of *a* and *b* for all simulations. Figure 5-5 and Figure 5-6 show the outcome of the ten realisations for parameter combinations A and B in Volumes I–III, respectively.

Table 5-7. Estimated values of *a* in Volumes I–III.

Parameter combination A Volume; *a*	#1	#2	#3	#4	#5	#6	#7	#8	#9	#10
I; $a = N\times10^{-10}$	1.27	7.29	2.06	5.66	4.69	2.72	1.52	2.71	7.68	2.59
II; $a = N\times10^{-10}$	9.06	3.02	5.58	3.86	4.48	7.46	6.83	9.53	6.43	23.3
III; $a = N\times10^{-10}$	0.565	0.486	0.910	0.421	0.505	0.735	0.441	0.767	0.439	0.679
Parameter combination B										
I; $a = N\times10^{-10}$	18.2	11.7	17.6	32.1	22.6	11.9	22.9	15.5	10.0	21.1
II; $a = N\times10^{-10}$	26.8	36.9	9.91	36.3	15.6	2.54	21.0	38.9	17.8	9.33
III; $a = N\times10^{-10}$	27.2	54.3	23.4	77.4	26.5	45.4	31.6	50.8	37.8	61.6

Table 5-8. Estimated values of *b* in Volumes I–III.

Parameter combination A Volume	#1	#2	#3	#4	#5	#6	#7	#8	#9	#10
I	2.318	2.101	2.406	1.957	2.098	2.420	2.979	2.111	2.164	2.318
II	1.854	1.844	1.765	2.139	1.647	1.581	1.673	1.311	1.915	1.854
III	1.109	1.189	1.694	1.152	1.271	1.271	1.292	1.295	1.431	1.198
Parameter combination B										
I	1.749	1.721	1.576	1.721	1.529	1.985	1.725	1.821	1.706	1.734
II	1.401	1.136	1.335	1.404	1.247	2.386	1.310	1.229	1.283	1.502
III	0.600	0.523	0.751	0.491	0.575	0.580	0.526	0.494	0.662	0.504

Table 5-9. Geometric means of *a* and *b* for all realisations in Volumes I–III shown in Table 5-7 and Table 5-8. Transmissivities for 1 m 10 m and 100 m radii are also shown.

Volume	Parameter combination	k_r [–]	r_0 [m]	*a* [=*T(1m)*]	*b*	*T(10 m)* [m²/s]	*T(100 m)* [m²/s]
I	A	2.90	0.282	3.20×10^{-10}	2.310	6.5×10^{-8}	1.3×10^{-5}
	B	2.56	0.038	1.73×10^{-9}	1.723	9.1×10^{-8}	4.8×10^{-6}
II	A	2.90	0.282	6.74×10^{-10}	1.672	3.2×10^{-8}	1.5×10^{-6}
	B	2.56	0.038	1.69×10^{-9}	1.393	4.2×10^{-8}	1.0×10^{-6}
III	A	2.90	0.282	5.75×10^{-11}	1.281	1.1×10^{-9}	2.1×10^{-8}
	B	2.56	0.038	4.05×10^{-9}	0.565	1.5×10^{-8}	5.5×10^{-8}

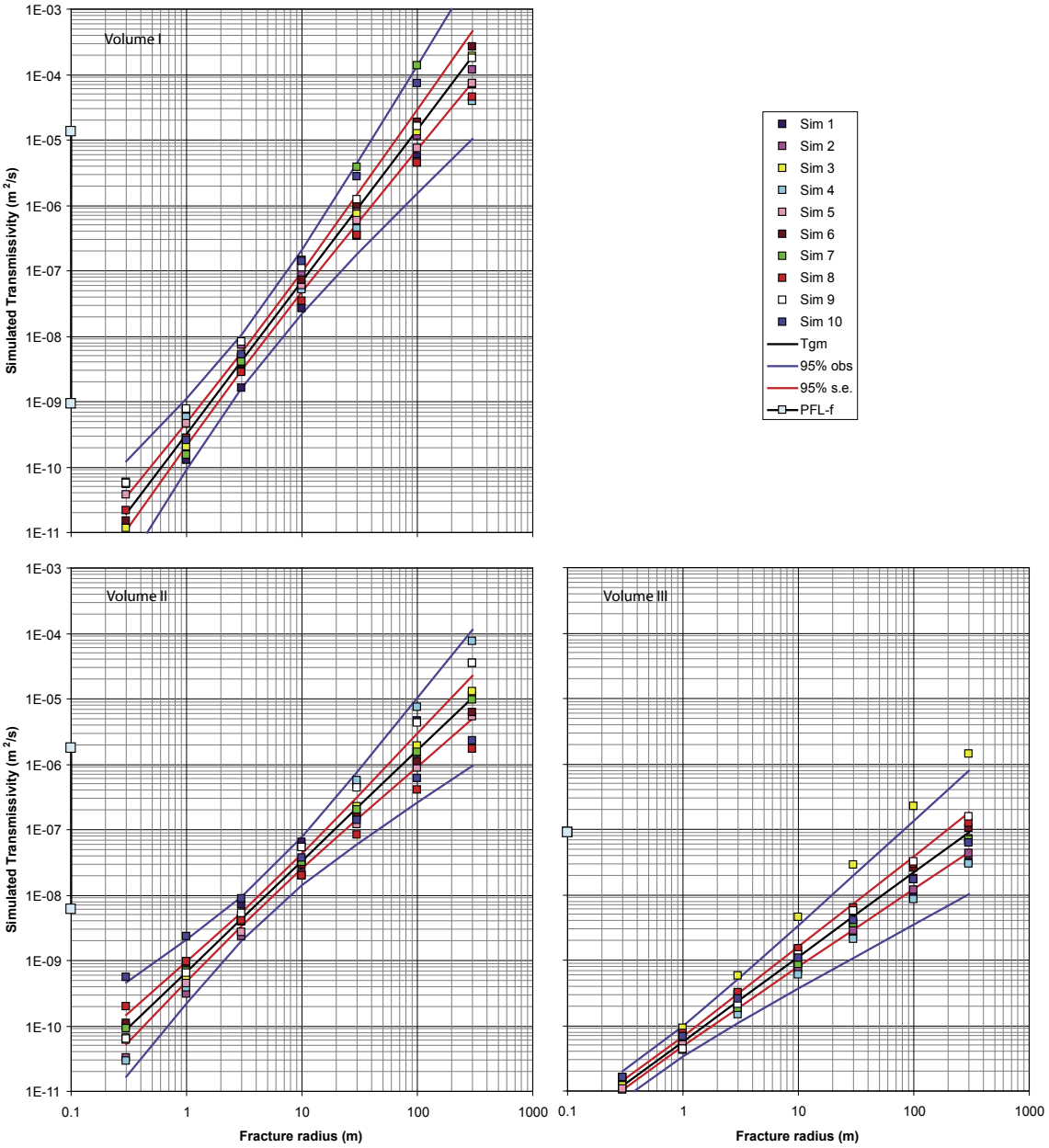

Figure 5-5. *Simulation results for parameter combination A.*

The magnitude of the coefficient a is generally greater for parameter combination B than for parameter combination A. That is, the transmissivity of a 1 m fracture radius in a somewhat more sparsely connected DFN (e.g. parameter combination B) must increase in order to keep the cumulative flow rate to the borehole constant. In contrast, the differences in transmissivity between the two parameter combinations are considerable less for 10 m and 100 m fracture radii. This is interpreted to be due to the postulated correlated transmissivity-size model. That is, in each simulation the largest fractures are associated with the N_{PFL} observed inflows (transmissivities). Hence, the major difference between different parameter combinations is in lower end of the size distribution where the number of connected fractures ($N_{PFL} - N_{PFL}$) differs depending on the assumed values of k_r and r_0. The contribution of flow from small fractures is difficult to appreciate hydraulically, however, because of the magnitude of lower measurement limit of the PFL-f method, which is c $(1–2)\times10^{-9}$ m^2/s.

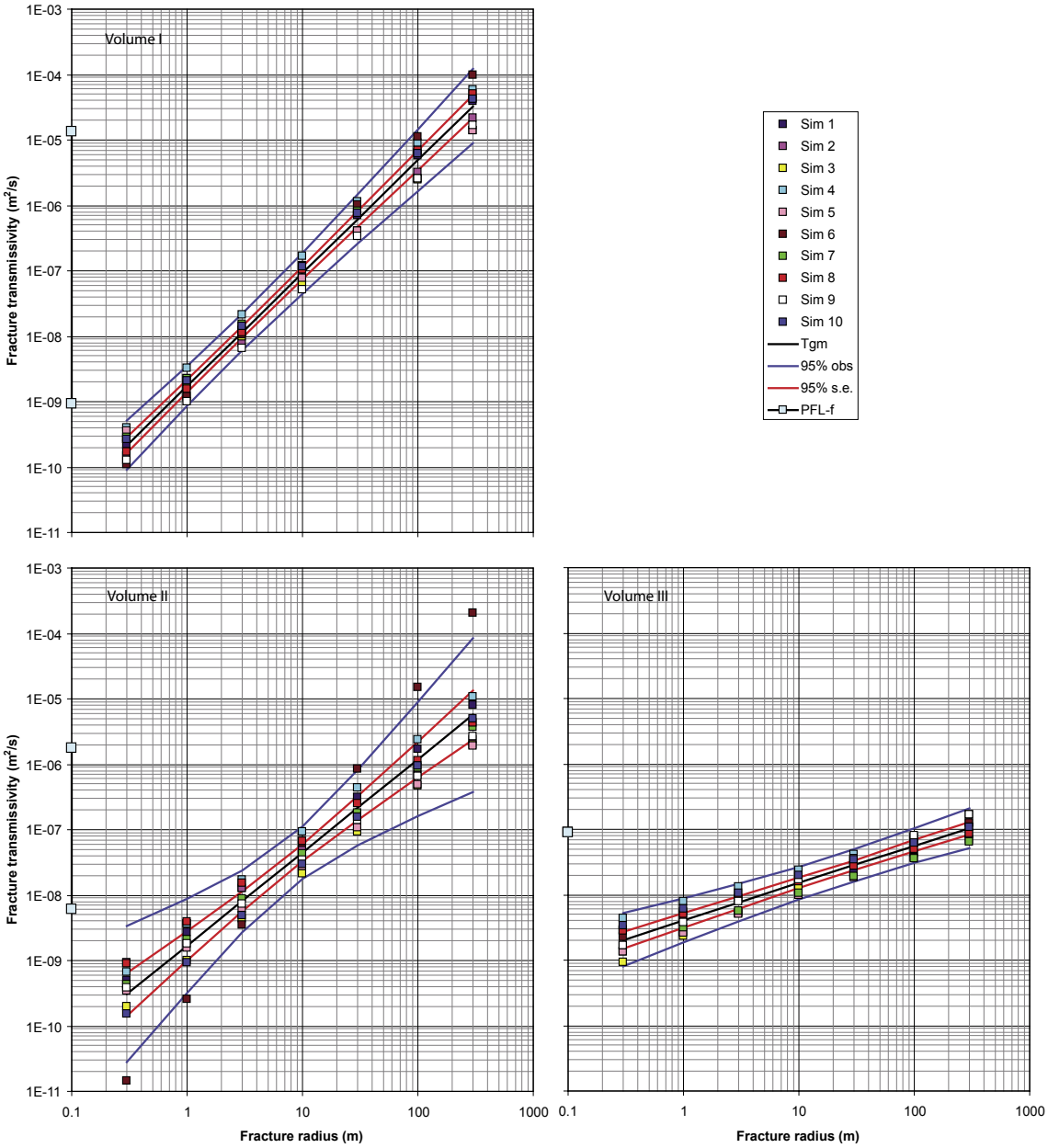

Figure 5-6. *Simulation results for parameter combination B.*

It is interesting to compare the aforementioned 100 m transmissivity values in Figure 4-2. It is vital to note, however, that this plot does not show fracture size but the radius of influence r_e of a 20 minute long injection test in an **infinite** fracture, i.e. $r \geq r_e$.

5.3 A validity test

Up till now the use of single-hole hydraulic test data from the core-drilled boreholes have been purposely limited to treat PFL-f. The reason for this is twofold. First, the methodology developed in the work presented here requires the detailed information about fracture transmissivities provided by PFL-f measurements. Secondly, we need a second data set to test the validity of the hydrogeological DFN models derived.

The validity test proposed here is to produce cross plots of simulated T_{5m}, using the correlated transmissivity-size models derived for parameter combinations A and B, versus measured T_{5m} of the PSS 5 m injection tests. The simulated T_{5m} are calculated by using an equation in analogy to Equation (4-8), i.e.

$$T_{5m} = \sum_{\sec up}^{\sec low} (T_f) \qquad (5\text{-}5)$$

where T_f is estimated from Equation (4-7) using the values of a and b shown in Table 5-9. The summation in Equation (5-5) is made over all simulated fractures belonging to the given positions of the PSS 5 m test sections as provided by the section bounds [secup, seclow]. The application of the test to Forsmark data is described in Section 4.3.3.

The outcome of the validity test is demonstrated for Volume I where there are 26 measurements of PSS 5 m tests out of which c 23% are at or below the lower measurement limit of the PSS equipment for 5 m injection tests, i.e. 6.75×10^{-10} m^2/s. Each model is run ten times and the results are shown in Figure 5-7 (parameter combination A) and Figure 5-8 (parameter combination B).

The results shown in Figure 5-7 and Figure 5-8 indicate that both parameter combinations render similar results, both in terms of explaining the transmissivity range seen in the PSS 5 m injection tests for Volume I, which spans four order of magnitude, and in terms of the percentage of simulated 5 m tests that are below the lower measurement limit. A "by eye estimation" perhaps put parameter combination B in front.

For Volume II both models render also similar fits, however, a wider spread around the unit slope. A possible explanation for this behaviour is that the simulations use five equally transmissive fracture sets despite the fact that two of the fracture sets carry the body of the measured flow, see Figure 3-9 in Volume II. For Volume III there are no PSS 5 m tests conducted and no comparison is made.

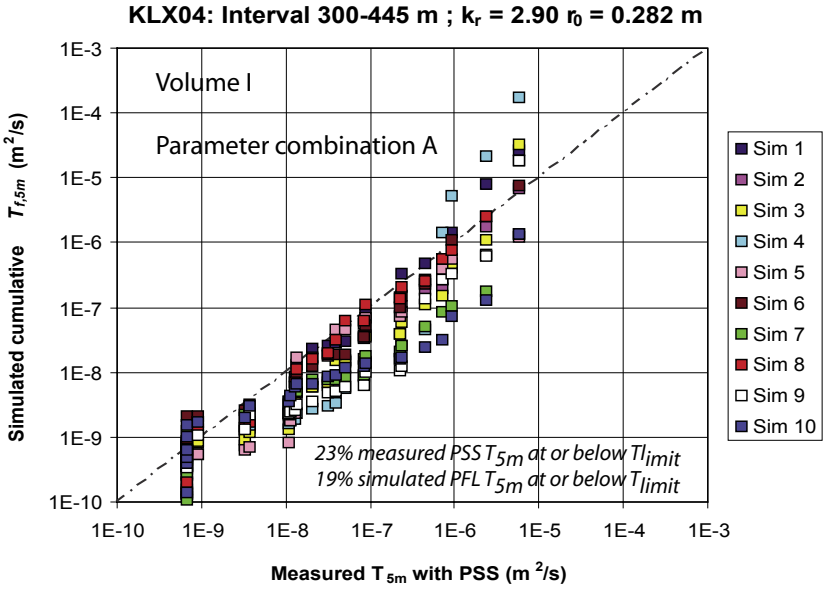

Figure 5-7. *Cross plot of simulated T_{5m} versus measured T_{5m} using parameter combination A in Volume I.*

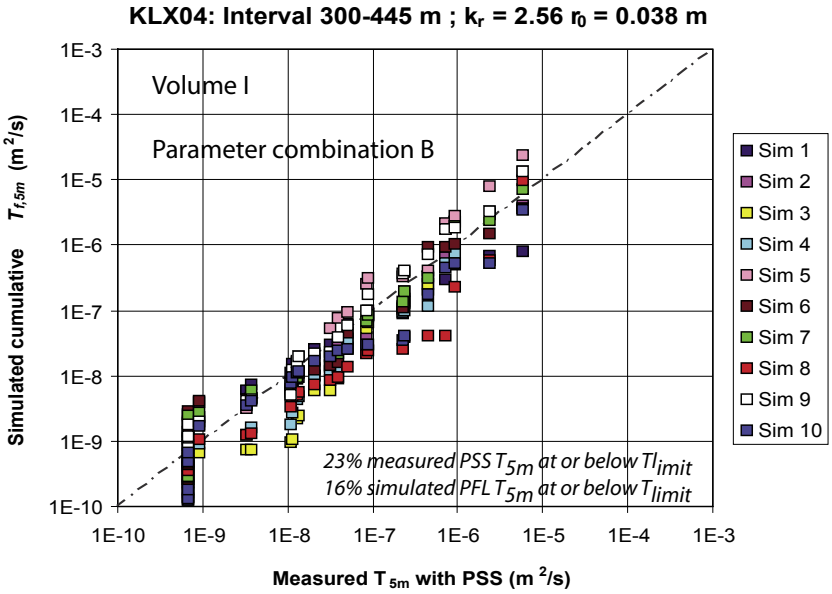

Figure 5-8. *Cross plot of simulated T_{5m} versus measured T_{5m} using parameter combination B in Volume I.*

6 Discussion and conclusions

The spatial variation of the fracture intensity is a key issue for the hydrogeological DFN modelling. Throughout the 1.2 modelling stage, the statistics of outcrop fractures have been used as input data as well as calibration targets in the geological DFN modelling. Based on the work reported form the geological DFN modelling and the work reported here we advocate that the usefulness of fracture intensity measures from outcrop data should be used with care. We consider the fracture frequency P_{10} in core-drilled boreholes a much more important entity. The Terzaghi correction, which is used in the work reported here, is a simplistic method to correct for borehole orientation bias, although it often proves to serve its purpose. We note that other methods exist but we have not explored them in the work reported here.

The modelling experiences gained from the hydrogeological DFN modelling in the Simpevarp subarea and in Forsmark area suggest that the value of the location parameter r_0 is important for the deduced fracture connectivity. However, it is observed in the modelling reported here that the role of r_0 for the fracture connectivity also depends highly on the magnitude of P_{10}. For a high value of P_{10} the fracture connectivity is less sensitive to the value of r_0.

The mean spacing between Open and Partly open in the KLX04 borehole, i.e. P_{10}^{-1}, is c 0.5 m above –650 m above sea level and c 2.8 m below. For the suggested range of the location parameter in the geological DFN modelling, i.e. 0.328–0.977 m, the hydrogeological DFN modelling conducted in the work report here renders a mean spacing between *connected* Open and Partly open fractures of c 0.5 m above –650 m above sea level and c 3.5 m below, hence implying a well connected DFN of Open and Partly open fractures. Using a value of the location parameter that is significantly lower than the value suggested by the geological DFN modelling, e.g. 0.038 m, renders a somewhat greater mean spacing, i.e. a somewhat less connected fracture network. However, the mean spacing between connected Open and Partly open fractures cannot exceed the observed spacing between the PFL-f anomalies if the latter are a subset of all connected Open and Partly open fractures. The PFL-f measurements conducted in the KLX04 borehole show that the maximum mean spacing between flowing fractures greater than the lower measurement limit, which is c $(1–2)\times10^{-9}$ m^2/s, is c 5–7 m above –650 m above sea level and c 250 m below. In conclusion, the frequency of PFL-f flow anomalies in the KLX04 borehole indicate already a fairly well connected network of flowing fractures in rock mass around this borehole down to c –650 m above sea level and a poorly connected network of flowing fractures in the rock mass below this elevation.

The observed range of the PFL-f transmissivities in the KLX04 borehole associated with the hydrogeological DFN modelling in the work reported here is c 10^{-9}–10^{-5} m^2/s. Together with the aforementioned spacing of the PFL-f flow anomalies this implies a fairly permeable rock mass above –650 m above sea level In conclusion, if the observations in the KLX04 borehole are considered representative for the rock mass in general in rock domain A, the bedrock at repositiory depth in the Laxemar subarea is fairly permeable. However, we question if the KLX04 borehole is representative for rock domain A given the outcome of the hydraulic testing in the KLX01–KLX03 boreholes. It is suggested that more borehole data at other locations in rock domain A are acquired before the generality of the KLX04 borehole data is concluded or used in a regional flow model.

The postulated correlated transmissivity-size model used in the work reported here is demonstrated to render results that compare well with measured PSS 5 m (Pipe String System) transmissivity data including the number of 5 m sections below transmissivity threshold of the PSS 5 m tests, which is c 6.5×10^{-10} m^2/s. It is noted that the choice of parameter values of the power-law size distribution model does not seem to have a crucial impact on the fit if a correlated transmissivity-size model is postulated. This is interpreted to be due to the high fracture intensity and the postulated correlated transmissivity-size model. That is, in each simulation the largest fractures are associated with the N_{PFL} observed inflows (transmissivities). Hence, the difference between the different power-law parameter combinations studied here (denoted by A and B in the report) is predominantly in the lower end of the size distribution. It is in this segment of the power-law size distribution the number of connected fractures differs depending on the assumed values of k_r and r_0. The contribution of flow from low-transmissivity fractures is difficult to appreciate, however, because of the magnitude of the lower measurement limit of the PFL-f method.

In conclusion, if the magnitude of the lower measurement limit of the PFL-f method is sufficient, e.g. from a Safety Assessment point of view, the spacing of the PFL-f anomalies is already a good indicator of the hydrogeological DFN connectivity. If the magnitude of the lower measurement limit of the PFL-f method is too large, however, e.g. an order of magnitude or so, the spacing between the hydrogeologically connected fractures is smaller than the spacing between the PFL-f anomalies, which means that the connectivity of important features increases. In such case the spacing between the features of interest is probably better represented by $P_{10,CON}^{-1}$, which is the mean spacing of the *connected* Open and Partly open fractures. However, $P_{10,CON}^{-1}$ depends on the values of r_0, hence an uncertain model parameter.

7 References

Andersson P, Ludvigson J-E, Wass E, 1998. Äspö Hard Rock Laboratory, True Block Scale Project, Preliminary characterisation – Combined interference tests and tracer tests, SKB IPR-01-44, Svensk Kärnbränslehantering AB.

Andersson P, Ludvigson J-E, Wass E, Holmqvist M, 2000. Äspö Hard Rock Laboratory. TRUE Block Scale Project. Tracer test stage. Interference tests, dilution tests and tracer tests. SKB IPR-00-28, Svensk Kärnbränslehantering AB.

Darcel C, Davy P, Bour O, de Dreuzy J-R, 2004. Alternative DFN model based on initial site investigations at Simpevarp. SKB R-04-76, Svensk Kärnbränslehantering AB.

Davy P, Darcel C, Bour O, Munier R, de Dreuzy J R, 2005. Note on the Terzaghi angular correction applied to fracture intensity profile along core, in press.

Dershowitz W, Winberg A, Hermanson J, Byegård J, Tullborg E-L, Andersson P, Mazurek M, 2003. Äspö Task Force on modelling of groundwater flow and transport of solutes, Task 6C, A semi-synthetic model of block scale conductive structures at the Äspö HRL, SKB IPR-03-13, Svensk Kärnbränslehantering AB.

Follin S, Stigsson M, Svensson U, 2005a. Variable-density groundwater flow simulations and particle tracking – Numerical modelling using DarcyTools. Preliminary site description Forsmark area – version 1.2. SKB R-05-11, Svensk Kärnbränslehantering AB.

Follin S, Stigsson M, Svensson U, 2005b. Regional hydrogeological simulations for Forsmark – Numerical modelling using DarcyTools. Preliminary site description Forsmark area – version 1.2. SKB R-05-60, Svensk Kärnbränslehantering AB.

Forssman I, Zetterlund M, Forsmark T, Rhén I, 2005. Oskarshamn site investigation. Correlation of Posiva Flow Log anomalies to core mapped features in KLX02, KLX03, KLX04, KAV04A and KAV04b. SKB P-05-241, Svensk Kärnbränslehantering AB.

Hartley L, Hoch A, Hunter F, Jackson P, Marsic N, 2005a. Regional hydrogeological simulations – Numerical modelling using ConnectFlow. Preliminary site description Simpevarp subarea – version 1.2. SKB R-05-12, Svensk Kärnbränslehantering AB.

Hartley L, Cox I, Hunter F, Jackson P, Joyce S, Swift B, Gylling B, Marsic N, 2005b. Regional hydrogeological simulations for Forsmark – Numerical modelling using ConnectFlow. Preliminary site description of the Forsmark area – version 1.2. SKB R-05-32, Svensk Kärnbränslehantering AB.

Hartley L, Jackson P, Hunter F, McCarthy M, Gylling B, Marsic N, 2006. Regional hydrogeological simulations – numerical modelling using CONNECTFLOW. Preliminary site description Laxemar subarea – version 1.2. SKB R-06-23. Svensk Kärnbränslehantering AB.

Hedin A, 2005. An analytical method for estimating the probability of canister/fracture intersections in a KBS-3 respository, SKB R-05-29, Svensk Kärnbränslehantering AB.

Hermanson J, Forssberg O, Fox A, La Pointe P R, 2005. Statistical model of fractures and deformation zones. Preliminary site description Laxemar subarea – version 1.2. SKB R-05-45, Svensk Kärnbränslehantering AB.

La Pointe P R, Hermanson J, 2005. Statistical model of fractures and deformation zones. Preliminary site description Simpevarp subarea – version 1.2. SKB R-05-28, Svensk Kärnbränslehantering AB.

La Pointe P R, Olofsson I, Hermanson J, 2005. Statistical model of fractures and deformation zones in Forsmark. Preliminary site description Forsmark area – version 1.2. SKB R-05-26, Svensk Kärnbränslehantering AB.

Jacob C E, 1950. Flow of groundwater. In: Rouse H (ed.) *Enginering Hydraulics*, Wiley.

Rahm N, Enachescu C, 2004. Oskarshamn site investigation. Hydraulic injection tests in borehole KLX04, 2004. Subarea Laxemar. SKB P-04-292. Svensk Kärnbränslehantering AB.

Rhén I, Gustafson G, Stanfors R, Wikberg, P, 1997. Äspö HRL – Geoscientific evaluation 1997/5. Models based on site characterization 1986–1995, SKB TR-97-06, Svensk Kärnbränslehantering AB.

Rhén I, Forsmark T, 2001. Äspö Hard Rock Laboratory. Prototype repository, Hydrogeology, Summary report of investigations before the operation phase, SKB IPR-01-65, Svensk Kärnbränslehantering AB.

Rhén I, Forsmark T, Forssman I, Zetterlund M, 2005. Oskarshamn site investigation. Hydrogeological single-hole interpretation of KLX02, KLX03, KLX04, KAV04A and KAV04b. SKB R-06-21, Svensk Kärnbränslehantering AB.

Rouhiainen P, Sokolnicki M, 2005. Oskarshamn site investigation. Difference flow logging of borehole KLX04. Subarea Laxemar. SKB P-05-68. Svensk Kärnbränslehantering AB.

SKB, 2004a. Preliminary site description. Forsmark area – version 1.1. SKB R-04-15, Svensk Kärnbränslehantering AB.

SKB, 2004b. Preliminary site description. Simpevarp area – version 1.1. SKB R-04-25, Svensk Kärnbränslehantering AB.

SKB, 2005a. Preliminary site description. Simpevarp subarea – version 1.2. SKB R-05-08, Svensk Kärnbränslehantering AB.

SKB, 2005b. Preliminary site description. Forsmark area – version 1.2. SKB R-05-18, Svensk Kärnbränslehantering AB.

Svensson U, 2004. DarcyTools, Version 2.1. Verification and validation. SKB R-04-21, Svensk Kärnbränslehantering AB.

Svensson U, Ferry M, 2004. DarcyTools, Version 2.1. User's guide. SKB R-04-20, Svensk Kärnbränslehantering AB.

Svensson U, Kuylenstierna H-O, Ferry M, 2004. DarcyTools, Version 2.1. Concepts, methods, equations and demo simulations. SKB R-04-19, Svensk Kärnbränslehantering AB.

Terzaghi R D, 1965. Sources of error in joint surveys, *Geotechnique*, V.15, 287-304.

Appendix A

Work flow of hydrogeological DFN modelling with DarcyTools during modelling stage 1.2

Below follows a brief description of the work flow used by Team DarcyTools during modelling stage 1.2. The methodology presented was initiated by /Follin et al. 2005a/ for SDM S1.2, and elaborated by /Follin et al. 2005b/ for SDM F1.2. The application to Laxemar data (KLX04) is demonstrated in Chapter 3 and Chapter 5.

Work flow

1. List the Fisher distribution properties (trend, plunge, concentration (κ)) for each fracture set as reported for the geological DFN modelling. If a different kind of distribution than Fisher is suggested use the best equivalent Fisher properties.

2. Analyse the frequency of Open and Partly open fractures in each borehole with regard to rock domains, deformation zones and PFL-f anomalies. Compute the Terzaghi corrected fracture frequency $P_{10,CORR}$ for each set by weighting each fracture by $1/\cos(\vartheta)$, where ϑ is the angle between the pole to the fracture plane and the borehole trajectory.

3. Decide the values of the shape parameter k_r and the location parameter r_0, that will be used in the analysis.

4. Assume that:

   $$P_{32}[r > r_0] \approx P_{10,corr} \qquad \text{(A-1)}$$

   and compute α_{DT} from Equation (2-5).

5. Define a simulation domain with three shells and insert a borehole, see Figure A-1. The borehole will act as a boundary meaning that fractures that touch the borehole are not sorted out in the filtering process if they are disconnected from the rest of the DFN.

6. Generate fractures (squares) throughout each shell with the following size ranges:

   outer shell: (20–1,000) m
   middle shell: (1–20) m
   inner shell: (r_0–1) m

7. Compute the number of fractures that intersect the borehole and check if the number meets the measured number N_{CAL}. If necessary adjust α_{DT} and repeat step 5 and 6 until a good match is obtained. Compute the resulting value of $P_{32}[r > r_0]$.

8. Exclude the borehole and generate the same DFN a second time. As there is no borehole in the centre in the second run all isolated fractures that survived in the first run because they touched the borehole are now sorted out. The remaining number represents the desired number of connected fractures N_{CON}. N_{CON} can be inferred by inserting a borehole into the simulation domain posterior to the second run.

9. Repeat step 6, 7 and 8 for all together ten realisations.

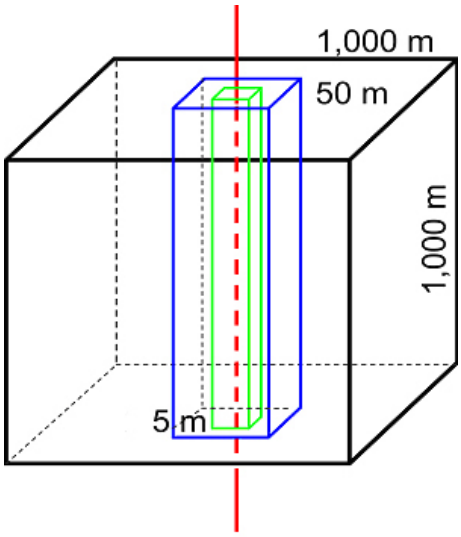

Figure A-1. *Simulation model set-up. Three different shells are used for the DFN simulations.*

10. Assume that the largest fractures among the N_{CON} connected fractures that intersect the borehole in the simulation model correspond to the N_{PFL} flow anomalies.

11. Order the intercepted connected fractures with regard to size and plot the data in a complementary cumulative density plot (CCDF). Evaluate the slope $k_{r,BH}$ and the intercept m_r of the straight line corresponding to:

$$G[r' \geq r] = \left(\frac{m_r}{r} \right)^{k_{r,BH}} \tag{A-2}$$

12. Order the PFL-f anomalies with regard to transmissivity and plot the data in a complementary cumulative density plot (CCDF). Evaluate the slope k_T and the intercept m_T of the straight line corresponding to:

$$G[T' \geq T] = \left(\frac{m_T}{T} \right)^{k_T} \tag{A-3}$$

13. Assume that:

$$\left(\frac{m_T}{T} \right)^{k_T} = \left(\frac{m_r}{r} \right)^{k_{r,BH}} \tag{A-4}$$

which may be written as

$$T = m_T \left(m_r^{-1} \, r \right)^{\left(\frac{k_{r,BH}}{k_T} \right)} \tag{A-5}$$

or

$$T = a \, r^{\,b} \tag{A-6}$$

where

$$b = \frac{k_{r,BH}}{k_T} \tag{A-7}$$

and

$$a = \frac{m_T}{(m_r)^b} \tag{A-8}$$

14. Transform the intersecting fractures in the aforementioned ten realisations (those without boreholes) to transmissivities using Equation (A-6).

15. Lump the fractures into 5 m intervals and compute $\sum_{5m} (T_{PFL})_i$

16. Order the lumped transmissivities and plot against the ordered PSS 5 m transmissivities.

Appendix B

Hard sector division

The hard sector division algorithm is used in the work reported here to determine the fracture set belonging of a mapped fracture given a series of predefined Fisher distributed fracture sets *i*. The algorithm computes the angles θ_i between the fracture pole and the different set poles. Secondly, the probability for fractures at angles greater than θ_i is computed for each set based on the sets' Fisher concentration factors (kappa, κ). A given fracture is associated to the fracture set that has the greatest probability for having fractures at angles greater than θ_i. The drawback of this method is that it focuses on the concentration factor solely, i.e. there is no overlap between fracture sets.

Example

Figure B-1 shows a fracture pole (ж) with trend/plunge 220/60 together with the poles of the three sets that are closest to the fracture, S_C (green), S_d (purple) and S_f (yellow), cf Table 2-2. The different contours show the 25%, 50% and 75% probability percentiles for each set, e.g. 25% of the fractures of fracture set S_C are found inside the innermost green contour, 50% inside the next contour etc.

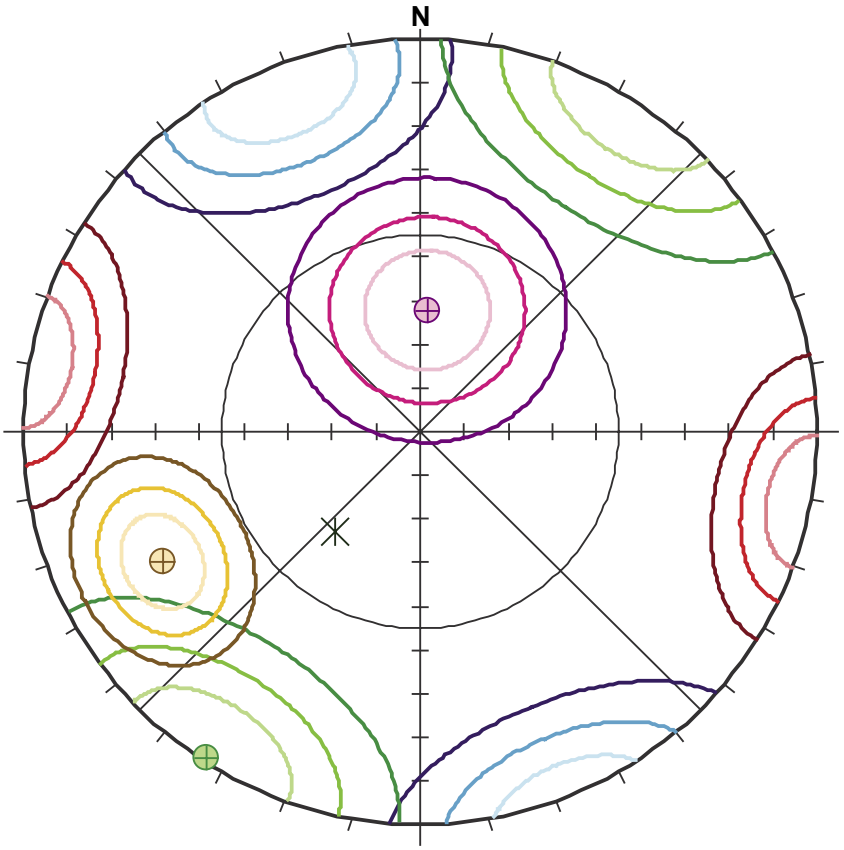

Figure B-1. *Mean pole trend and plunge for set S_C (green), S_d (purple) and S_f (yellow) together with a fracture (ж) with pole orientation 220/60.*

The angles between the example fracture pole and the mean poles of the three nearest sets are shown in Table B-1. The smallest angle is obtained for set S_f, 39°. However, due to the high Fisher concentration the probability of set S_f for having fractures with angles greater than 39° is only 0.53%. For set S_d the angle between the mean pole and the fracture is 55°. The probability of set S_d for having fractures with angles greater than 55° is 1.39%. Finally, the probability of set S_C for having fractures with angles greater than 59° is 0.59%. Hence the example fracture will be associated with set S_d.

Figure B-2 shows the cumulative density function for the univariate Fisher distribution for Set_C, Set_d and Set_f. The straight lines show the portion of fractures having a angle smaller than the angle between the fracture and the mean pole of the three sets. Figure B-3 shows a close up of Figure B-2.

Table B-1. Hard sector results for the example fracture shown in Figure B-1. Fracture set S_d has the greatest probability for having fractures with angles greater than the angle between the fracture pole and the set pole.

Set name	Pole trend	Pole plunge	Kappa	Angle between fracture pole and set pole	Probability
S_C	212.9	0.9	10.46	59.36	0.593%
S_d	3.3	62.1	10.13	54.71	1.388%
S_f	243.0	24.4	23.52	39.02	0.526%

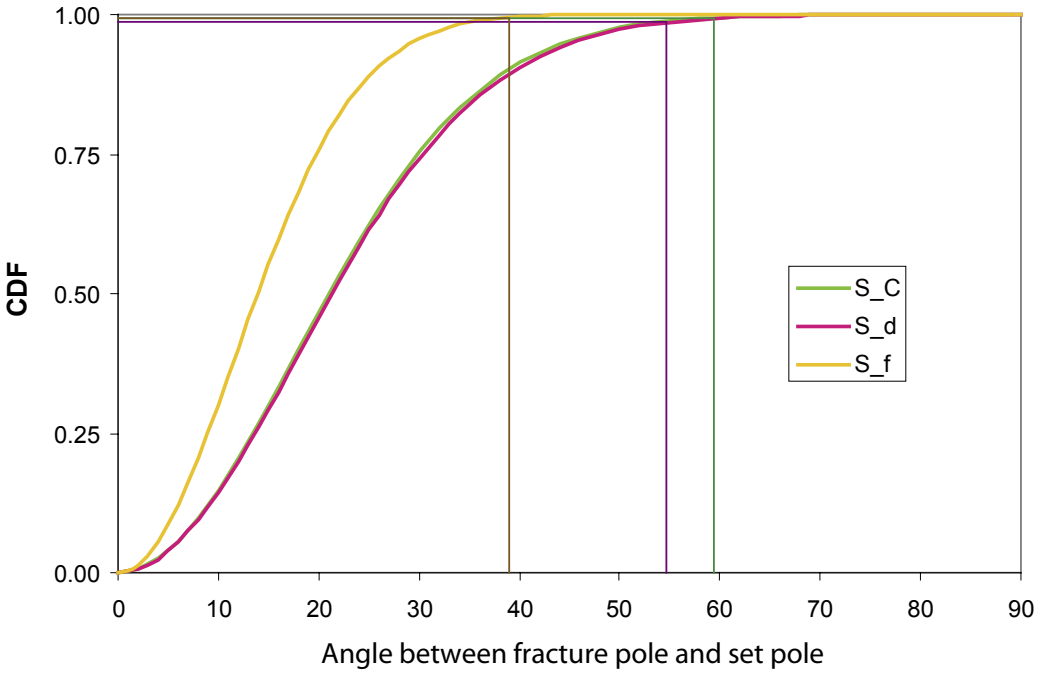

Figure B-2. *The cumulative density function for P[angle<X], i.e. the density of fracture poles that is within a given angle X from the set pole. An univariate Fisher distribution is assumed.*

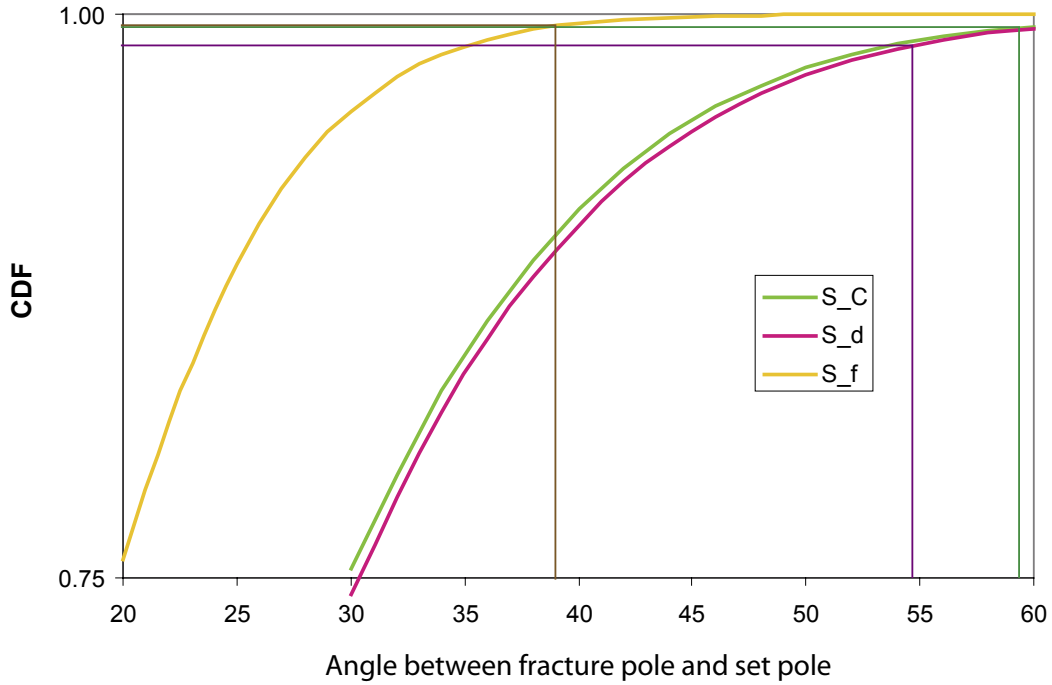

Figure B-3. *Close-up of the plot in Figure B-2.*

Appendix C

Technical note

Generation of fracture networks as governed by power laws and a spatial fractal dimension

Urban Svensson
Computer-aided Fluid Engineering AB

Preface

This technical note is intentionally brief and does not provide any background to the topics discussed. A reader who is not familiar with the subject is recommended to consult the report by /Darcel 2003/ or the paper by /Bonnet et al. 2001/ see references.

Introduction

In a recent report /Darcel 2003/ it is demonstrated that the variability in fracture size at the Äspö Site is best described by a power-law distribution and that the spatial distribution of fracture centres is Poissonian or fractal. It is further suggested that the fracture network is self-similar, which indicates that the network is scale invariant. Similar findings have been reported earlier; for the Äspö site see /La Pointe et al. 1999/ and, more generally, /Sahimi 1995/ and /Bonnet et al. 2001/.

In this report it will be assumed that the fracture size distribution follows a power law and that the spatial distribution is fractal (the Poissonian distribution may be regarded as a limiting case of the fractal distribution). For such a system /Bour and Davy 1997/ and /Bour et al. 2002/ give the following expression for the number of fractures $N(L)$, in a system of size L:

$$N(L) = \frac{\alpha L^D}{a-1}\left(l_{\min}^{-a+1} - l_{\max}^{-a+1}\right) \qquad \text{(C-1)}$$

where l_{min} and l_{max} are the smallest and largest fractures, respectively, contained in the system. The fractal dimension is denoted by D, a is the exponent of the power-law size frequency distribution and α is a fracture intensity term.

The code DarcyTools /Svensson et al. 2004/ is used in this study. The generation of fracture networks by DarcyTools has been governed by the needs from real world applications and the question of fractal dimension has not been in focus. Instead the inclusion of deterministic fracture zones, property specification (transmissivity, porosity, etc), have been regarded as more important. For the present task we need to briefly review how DarcyTools generates a fracture network:

- A set of deterministic structures normally form the “backbone” of the network. These structures are regarded as known in every respect.
- Random fractures, normally smaller than the deterministic structures, are then generated. These are Poissonian in space, use a Fisher distribution for orientation and a power-law size distribution.

- A sorting procedure determines which of the random fractures, or groups of fractures, that are isolated and removes these. Fractures in contact with domain boundaries are kept in this procedure, as we can not determine if these are isolated or not.

These are the main steps; for further details see /Svensson et al. 2004/.

Objetives

After the sorting procedure described above is carried out the retained network of connected fractures will not be Poissonian in terms of the fractal dimension D. The main objective of this study is to determine if the resulting network has fractal properties and, if so, what the fractal dimension is. It will further be the ambition to find out how a network with specified fractal dimension can be generated.

The focus will be on the power law exponent a and the fractal dimension D. It is expected, however, that the study will continue by considering also the fracture properties, in particular the transmissivity.

Simulations

Introduction

A number of methods to calculate the fractal dimension are available; the most common one is perhaps the box-counting method. According to /Bonnet et al. 2001/, the most accurate method is based on the two-point correlation function, which is defined as:

$$C_2(r) = 2N_p(r)/(N(N-1)) \qquad \text{(C-2)}$$

where $N\,p$ (r) is the number of pairs of points whose distance is less than r and N is the total number of points in the system. For a fractal population of points, $C_2(r)$ is expected to scale with r as r^D, where D is the fractal dimension. This method will be used, with the points representing the fracture centres, when analysing the fractal dimension of the generated networks.

The fracture network in DarcyTools is generated by:

$$N_{DT}(L) = \frac{\alpha_{DT} L^3}{a-1}\left(l_{\min}^{-a+1} - l_{\max}^{-a+1}\right) \qquad \text{(C-3)}$$

where the index DT stands for DarcyTools; other notations as for Equation (C-1). Note that this notation is specific for this report (and motivated by the reference to Equation (C-1) and differs somewhat from the notation in /Svensson et al. 2004/. The key point to note is, as already mentioned, that DarcyTools generates the random fractures with a Poissonian spatial distribution. Hence, N_{DT} is proportional to L^3 and not L^D, as in Equation (C-1). Further, α_{DT} is the specified intensity before the sorting procedure and hence not directly comparable to α in Equation (C-1).

Generic cases

As an introductory exercise, the two-point correlation method and its implementation were tested; random points were generated in two- and three- dimensional systems of length L. It was found, as expected, that the fractal dimension is 2.0 for the plane and 3.0 for the volume. Another outcome of the exercise was that the evaluation of D was best done in the interval $0.01 < r / L < 0.1$, following /Bour et al. 2002/ (their Figure 5).

In order to understand the properties of the network generated by DarcyTools, a reference case and a number of variations were studied. All cases studied are summarised in Table C-1. The common feature of all cases is the domain (L = 100 m) and the fracture size interval ($1 \leq l \leq 200$ m). The input to DarcyTools is α_{DT}, a and fracture orientation as specified by a Fisher distribution; these are the three properties that will be varied and the resulting network, in particular its D, will be studied.

The reference case is specified as $\alpha_{DT} = 0.35$, $\alpha = 0.35$ and random orientation. In fact, α_{DT} was calibrated to 0.35 as this value give a $D = 2.65$ and the reference case is hence self-similar, as $\alpha = D+1$, see /Darcel 2003/. This network can be studied in Figure C-1, where both the 3D box (with 69 531 fractures) and the intersections with a plane are shown. Figure C-2 shows the intersections with a scan line and Figure C-3 the relation between C_2 (r) and r. It is the slope of this curve that gives the fractal dimension of the network. The intersection with a scanline gives directly the commonly used measure P_{10}, which is defined as the number of intersections per metre. P_{10} will be further discussed below.

Variants of the reference case can be studied in Figures C-4 through C-6 and Table C-1. A few things to note:

- A higher intensity, Figure C-4, gives a higher D.
- Changing a affects the distribution of fracture sizes; increasing a gives fewer large fractures, see Figure C-5.
- Fracture orientation is specified by Fisher's κ; 5 and 15 are used for the illustrations in Figure C-6. The mean orientation of the fractures is vertical and 22.5° counter clockwise from the y-coordinate, as shown in Figure C-6. As can be seen in Table C-1, the orientation of the fractures will affect D.

Table C-1. Summary of reference case and variations. Box size is 100 m and fracture length interval $1 \leq l \leq 200$ m.

Case	Specified			Calculated	
	α_{DT}	a	κ	N_{BOX}	D
Reference Case	0.35	3.65	0	69,531	2.65
alfa02	0.2	3.65	0	20,738	2.40
alfa05	0.5	3.65	0	142,846	2.82
*a*35	0.35	3.5	0	97,184	2.78
*a*38	0.35	3.8	0	51,439	2.54
kappa 5	0.35	3.65	5.0	62,865	2.61
kappa 15	0.35	3.65	15.0	37,022	2.46

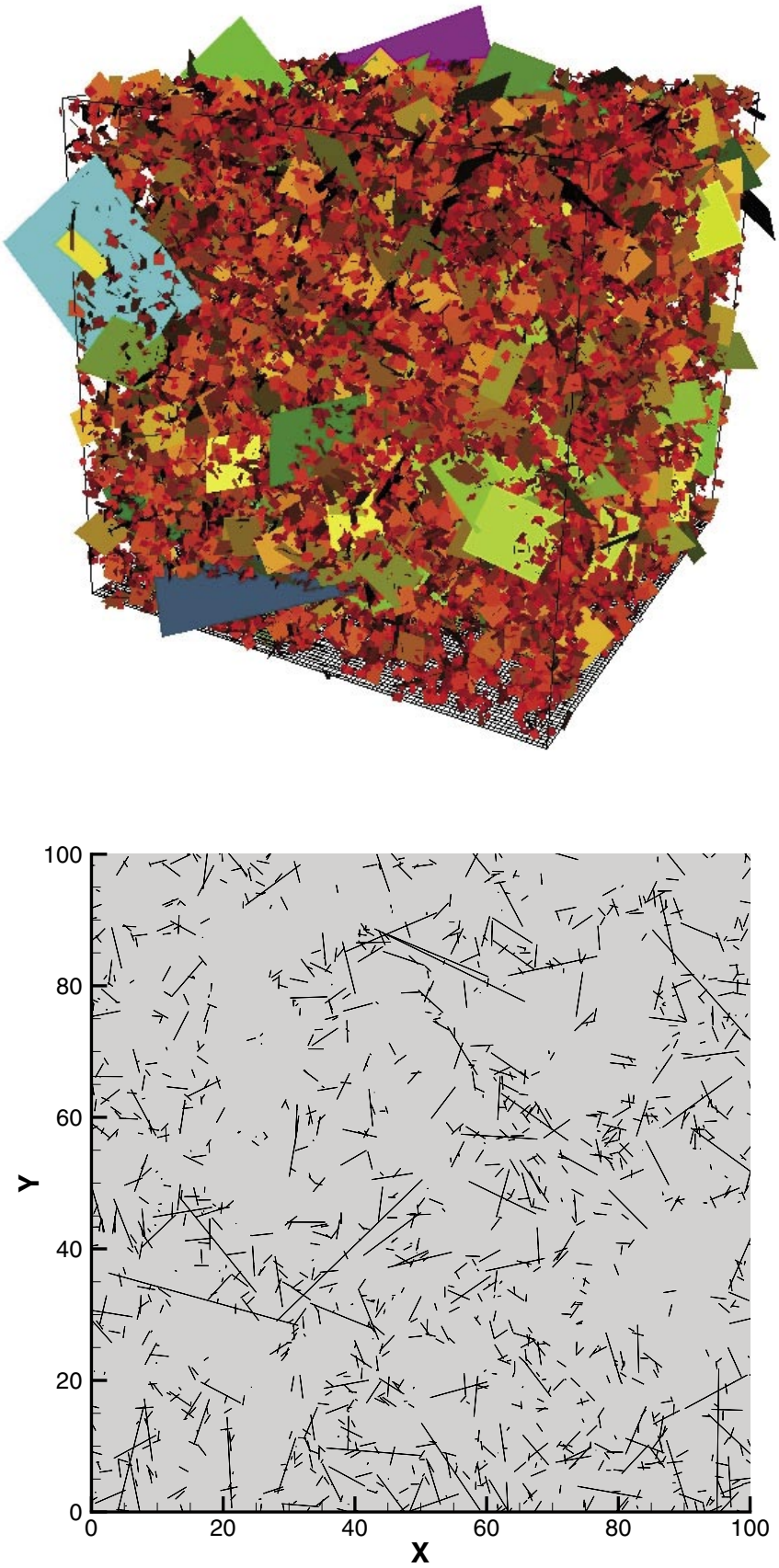

Figure C-1. *Reference case. The box with fractures (top) and fracture intersections with a plane (bottom).*

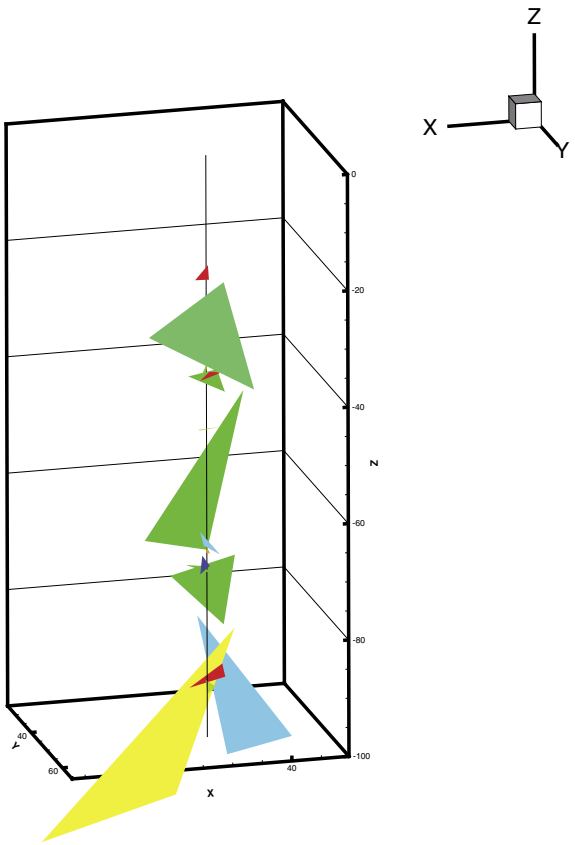

Figure C-2. *Reference case. Intersections with a scan line. Each square fracture consist of two triangles. Only the intersected triangle is shown*

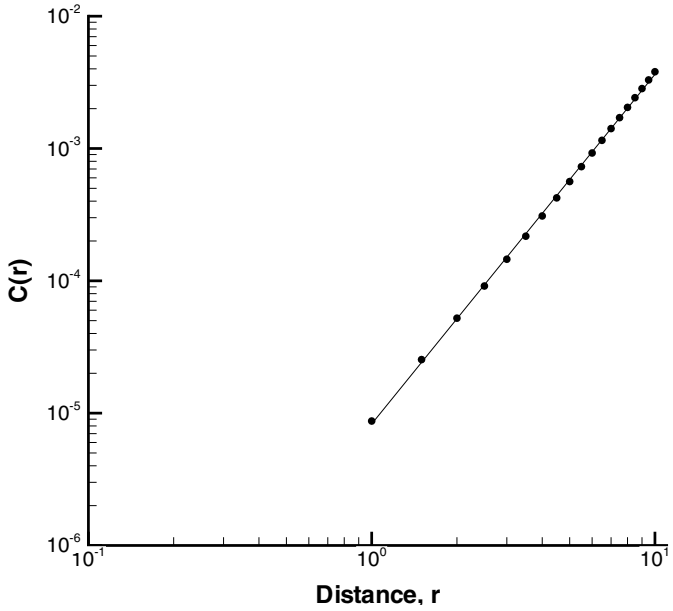

Figure C-3. *Reference case. Determination of the fractal dimension D. The slope of the curve is 2.65.*

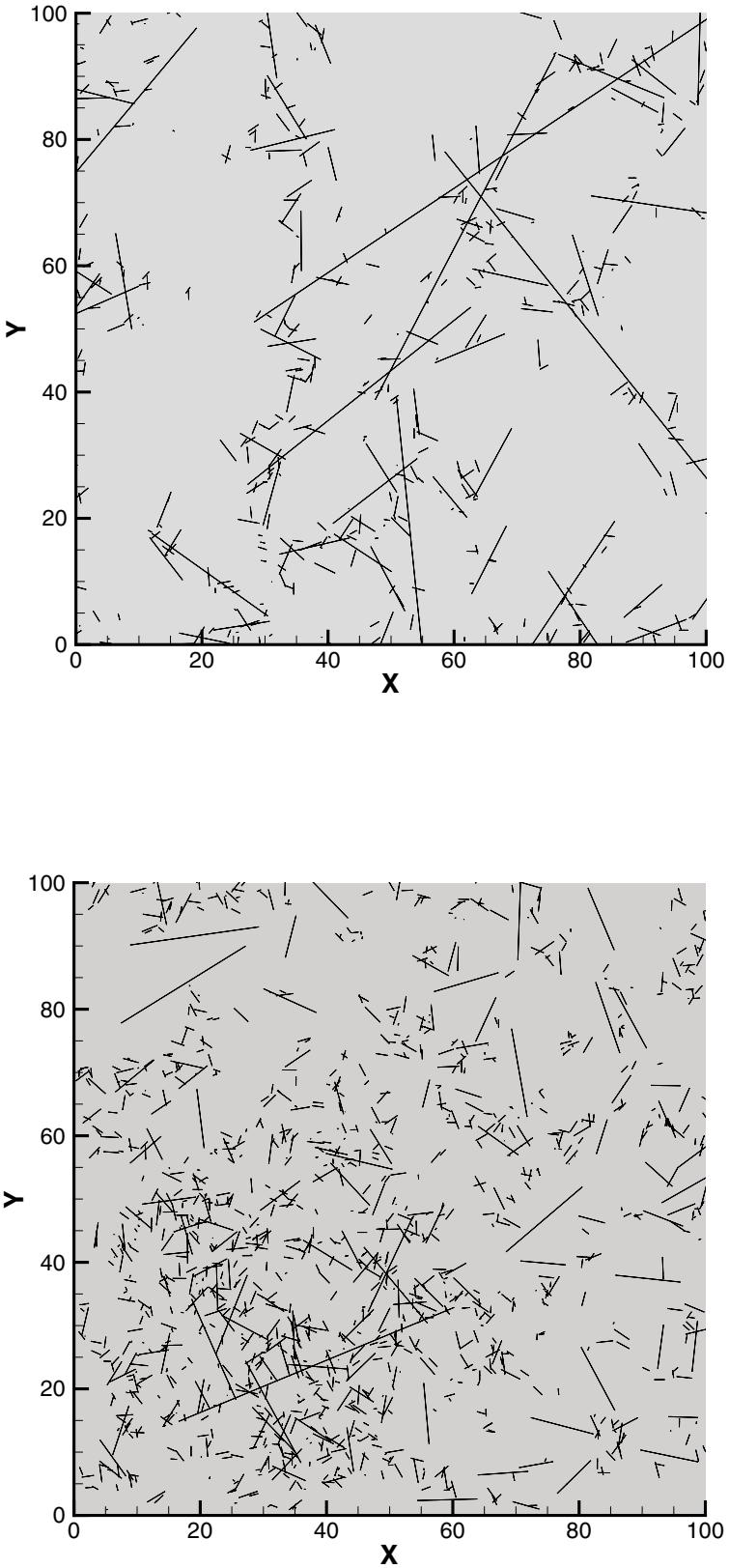

Figure C-4. *Varying the intensity;* $\alpha_{DT} = 0.2$ *(top) and* $\alpha_{DT} = 0.5$ *(bottom).*

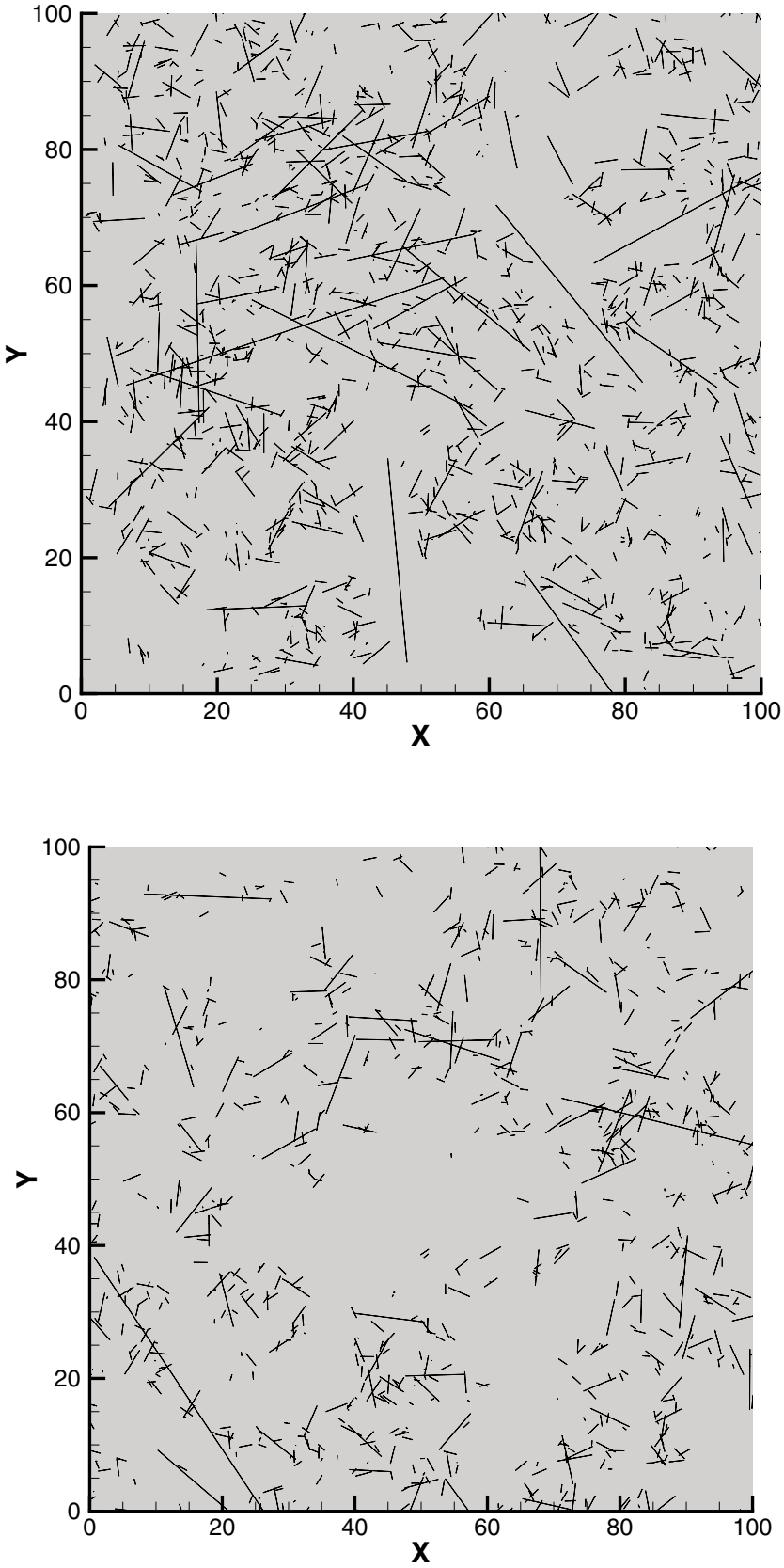

Figure C-5. *Varying the size exponent; α = 3.5 (top) and α = 3.8 (bottom).*

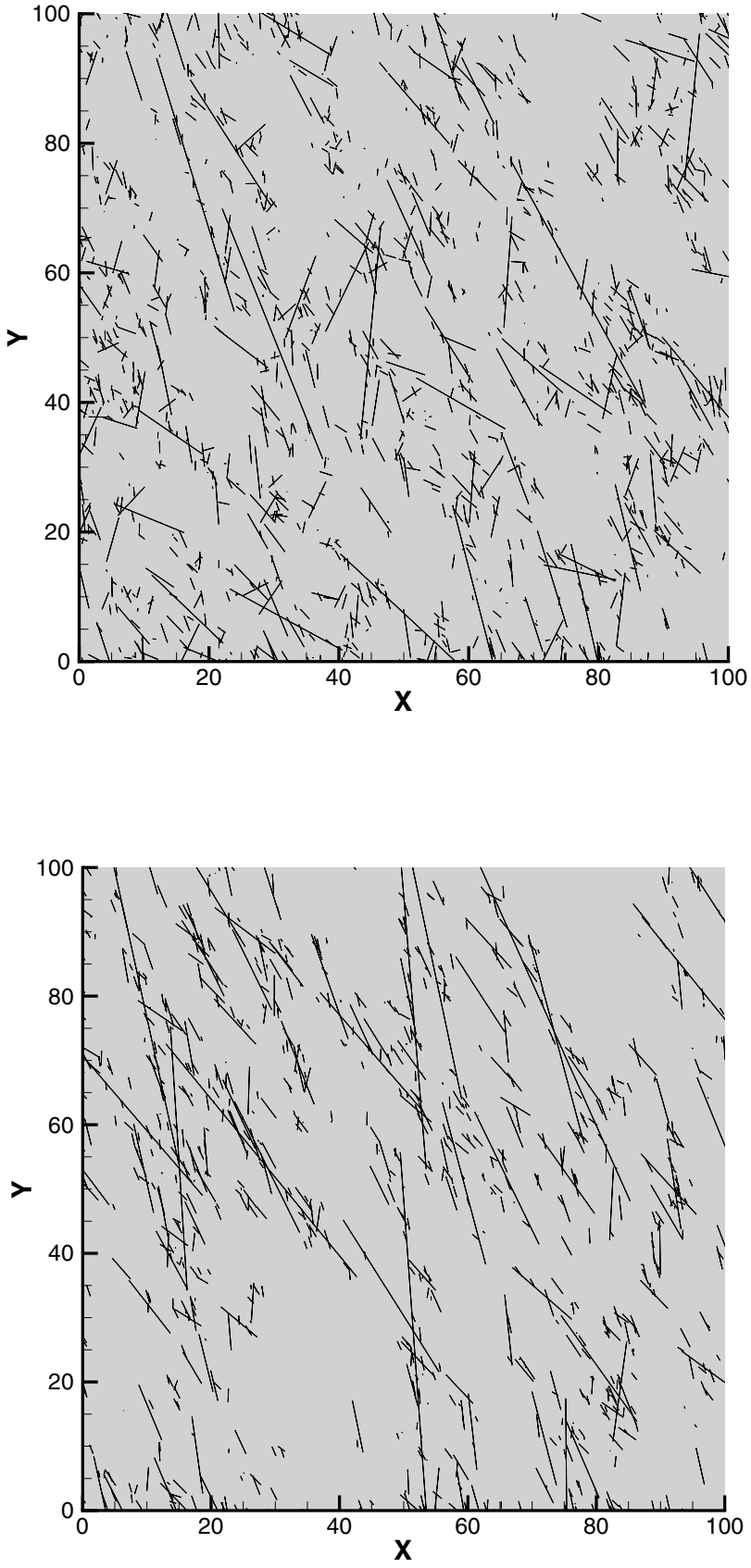

Figure C-6. *Varying orientation; κ = 5 (top) and κ = 15 (bottom).*

The TRUE Block

Next the TRUE Block at the Äspö site will be considered. One reason for choosing this domain is that /Darcel 2003/ analysed data and determined the fractal dimension of this volume. Another reason is that the TRUE Block is extensively examined and a comprehensive data base is readily available.

The objective of this task is to evaluate if we can generate a fracture network which is constrained by a large number of conditions. The following conditions are set up:

- A set of deterministic fractures should be part of the network. These structures are considered to be larger than 50 m.
- Following /Darcel 2003/ a self-similar network, with $\alpha = 3.8$ and $D = 2.8$, is realistic for the TRUE Block.
- The stochastic fractures should have a length scale ≤ 50 m, as the deterministic fractures should be regarded as a seamless continuation of the stochastic field.
- Fracture intensity. The intensity should be such that if the stochastic field is enlarged to include $50 \leq l \leq 200$ m, the number of fractures should match the number of deterministic structures, i.e. around 30 (Deterministic and Synthetic structures, see Task 6C report). Further P_{10} and P_{32} values should be in the range observed.
- Fracture orientation. Two sets of background fractures need to be considered.

Further details of these conditions are given in Table 2. It is clear from this list of conditions that the generation of a fracture network for a well examined site can be quite demanding.

As a is specified, the first thing to investigate is if an α_{DT} that gives $D = 2.8$ can be found. $\alpha_{DT} = 0.5$ was found to produce a network with $D = 2.8$. In fact, α_{DT} is the only input parameter left to tune as both a and the orientation are given as input parameters. The minimum fracture size, l_{min}, was set to 2 m. Sensitivity studies showed that D is not very sensitive to l_{min}. The general recommendation when generating a fracture network in DarcyTools is that l_{min} should be set to the cell size which in turn is set to 1% of the domain size see /Svensson et al. 2004/ for motives. As The TRUE Block has $L = 200$ m, l_{min} was fixed to 2 m. The choice of l_{min} is of course also due to practical considerations, as only a limited number of fractures (of the order 10^6) can be handled efficiently on the computer. Thus, $\alpha_{DT} = 0.5$, $l_{min} = 2$ m and the data given in Table C-2 completes the specification.

Results from simulations are shown in Figures C-7 to C-10 and Table C-3. Two realisations, using the same input specification, are discussed. From Table C-3 we see that D is close to 2.8 for both realisations. As part of the simulations P_{10}, P_{21} and P_{32} were also calculated; the resulting values shown in Table C-3 are considered to be in fair agreement with field data, although these values are strongly affected by l_{min}. Fracture traces in a horizontal cut at z = –450 m above sea level are shown in Figure C-7, where also the traces of the deterministic structures are included. Fractures crossing a vertical scan line are illustrated in Figure C-8; typically 20 fractures (giving $P_{10} \approx 0.1$) are intersecting the line. As we keep track of all fractures individually it is possible to specify the properties of the intersecting fractures. In Figure C-9, the length and transmissivity is given as a function of the vertical coordinate. Finally, in Figure C-10, the diagram determining D is shown. The symbols are well fitted to a straight line.

Table C-2. TRUE Block. Summary of input specification.

Domain:	East–West: 1,800 → 2,000
	North–South: 7,070 → 7,270
	Vertical: –530 → –350
	(In the Äspö co-ordinates)
Deterministic structures:	11 structures as specified in the Task 6C-report (Table 4-6), see /Dershowitz et al. 2003/
Stochastic fractures:	$2 \le l \le 50$
	Power-law exponent for length = 3.8
	Two sets, see the Task 6C report (page 48) with respect to trend, plunge, intensity and κ.

Table C-3. TRUE Block. Summary of results for two realisations.

Realisation	D	P_{10}	P_{21}	P_{32}	N_{50-200}
1	2.78	0.13	0.28	0.32	29
2	2.79	0.10	0.29	0.33	33

Discussion

The previous section showed that a network that is subject to a number of constraints can be generated. From a pragmatic point of view one may claim that all requirements have been fulfilled and there is nothing more to add. However, the method used needs to be clearly stated and scrutinized. The key elements of the procedure can be stated as:

- Produce a Poissonian stochastic network, eliminate isolated fractures, or groups of fractures, and obtain a network that has a clear fractal signature.

It is not surprising that the resulting network has fractal properties as small fractures are always connected to larger fractures, which in turn are connected to even larger fractures; this is a characteristic feature of a fractal system. It is however an open question if the network is realistic considering, for example, the fragmentation process.

If the pragmatic view "all specified requirements have been met" is adopted, we need to discuss how a network with specified properties is generated. As the fractal dimension is not an input parameter some trial and error procedure may be needed. However, some guidelines can be given. In Figure C-11, the number of fractures discarded in the sorting process versus the fractal dimension is shown. Fractures in the size range $0.01L \le l \le 0.05L$ are studied as larger fractures contribute very little to the total number. Obviously, if 0% are discarded we are back to the Poissonian distribution and $D = 3.0$. The symbols in Figure C-11 represent the cases studied in this work and the straight line is fitted by eye to these points. If a self-similar network is required, the diagram in Figure C-12 can be of assistance. The line gives the relation $\alpha = D+1$ and this line also separates regions where $\alpha > D+1$ and $\alpha < D+1$, respectively. From this diagram it is clear that once one of the parameter α_{DT} or a is specified, all three parameters α_{DT}, a and D are specified for the self-similar case.

These guidelines should be considered as tentative as they are based only on the generic simulations presented in this report. However, similar diagrams can be constructed for a specific site under study and reveal the properties specific for that site.

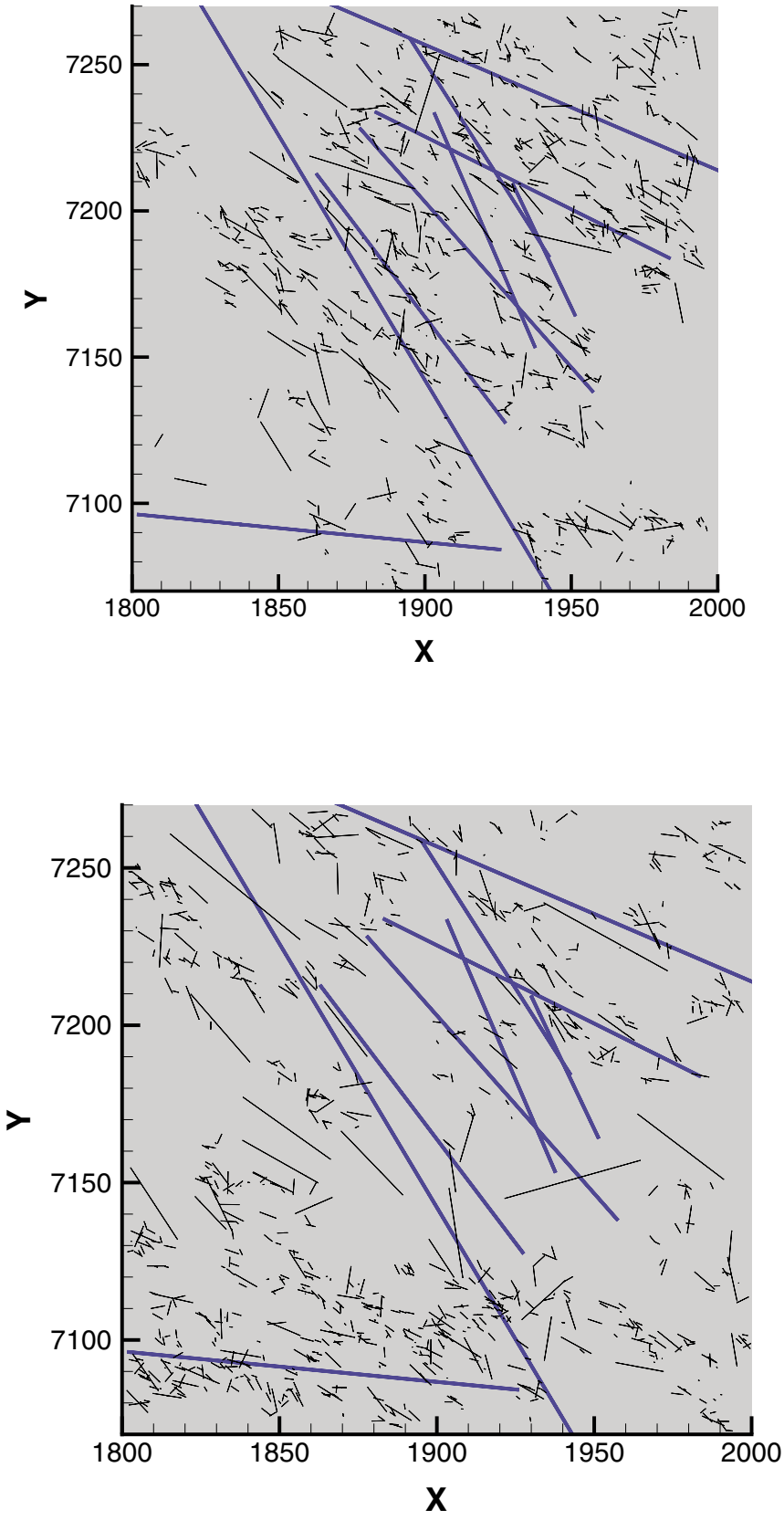

Figure C-7. *The TRUE Block. Fracture intersections with a horizontal plane for two realisations. Thick blue lines indicate deterministic structures.*

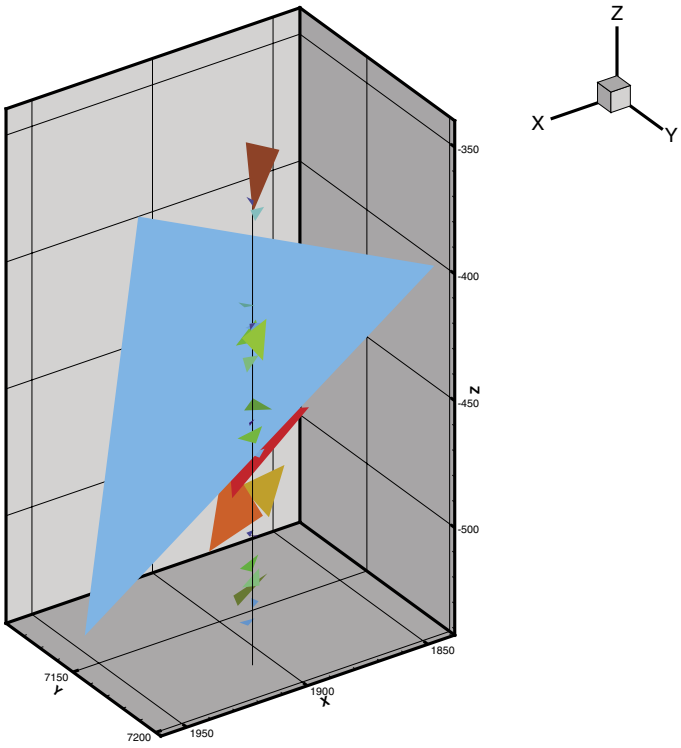

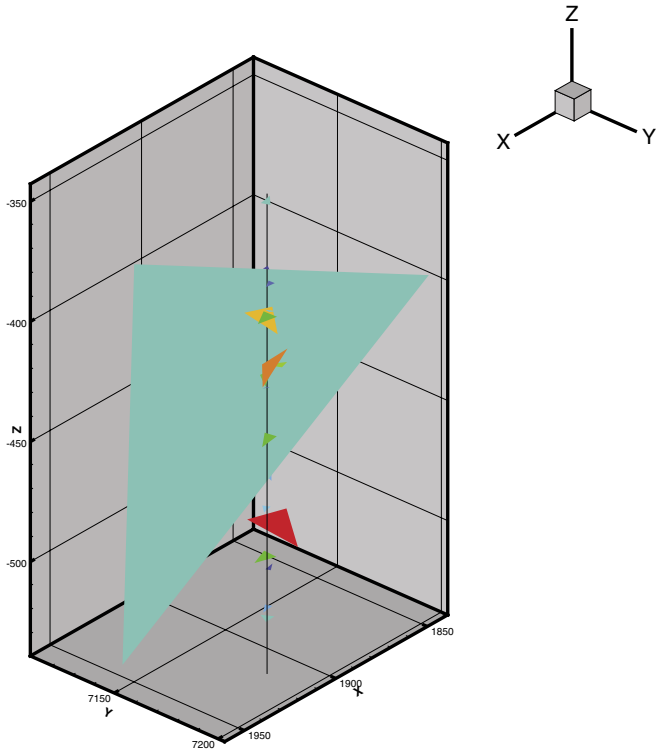

Figure C-8. *The TRUE Block. Fracture intersections with a vertical scan line for two realisations.*

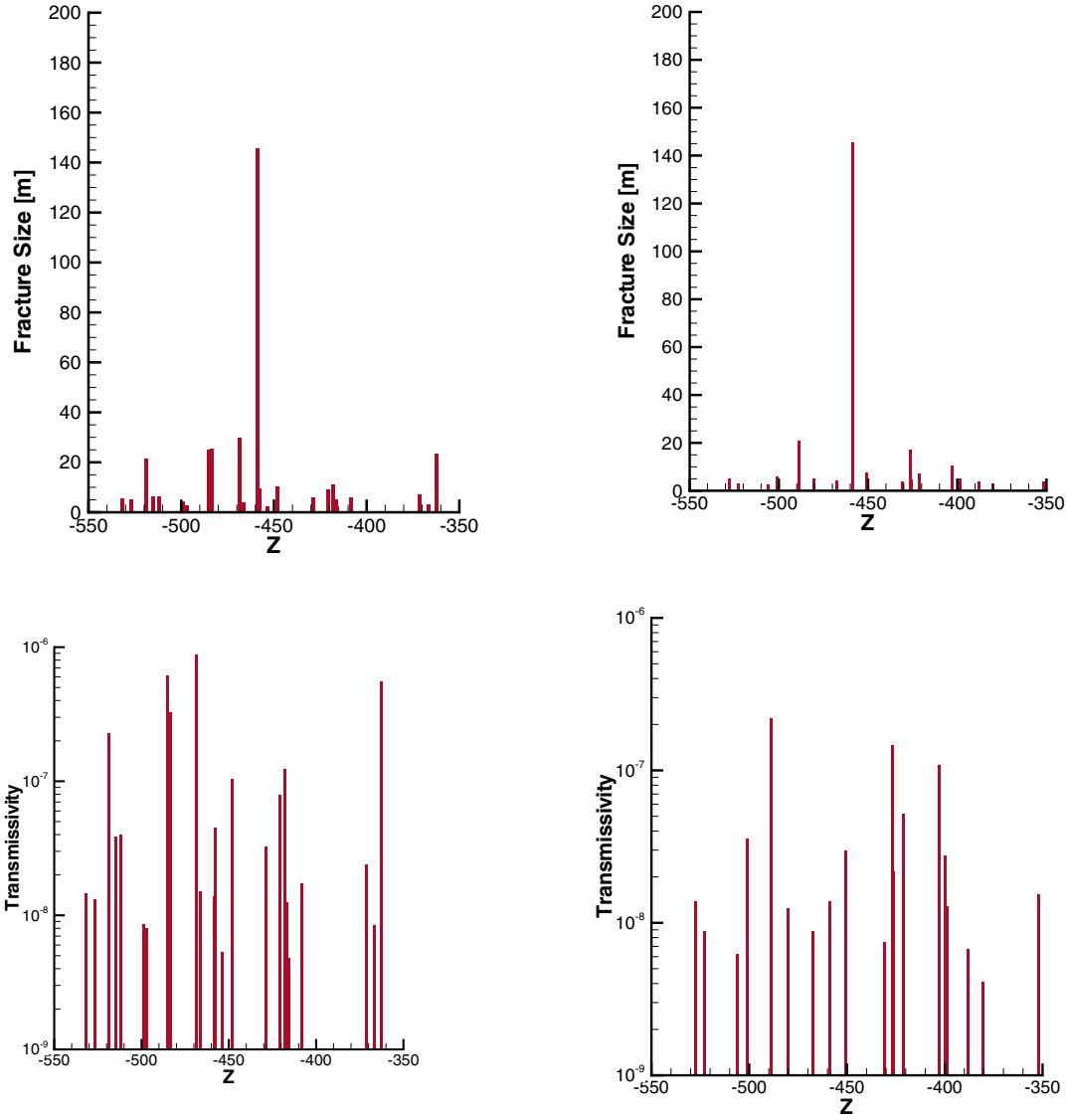

Figure C-9. *The TRUE Block. Fracture transmissivity and length versus depth for two realisations. Left column: realisation 1. Right column: realisation 2.*

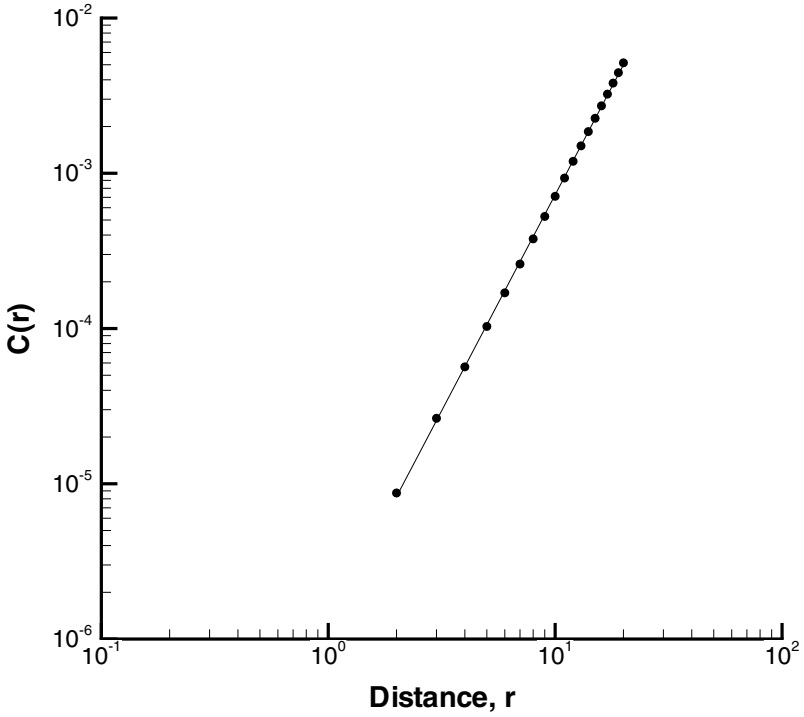

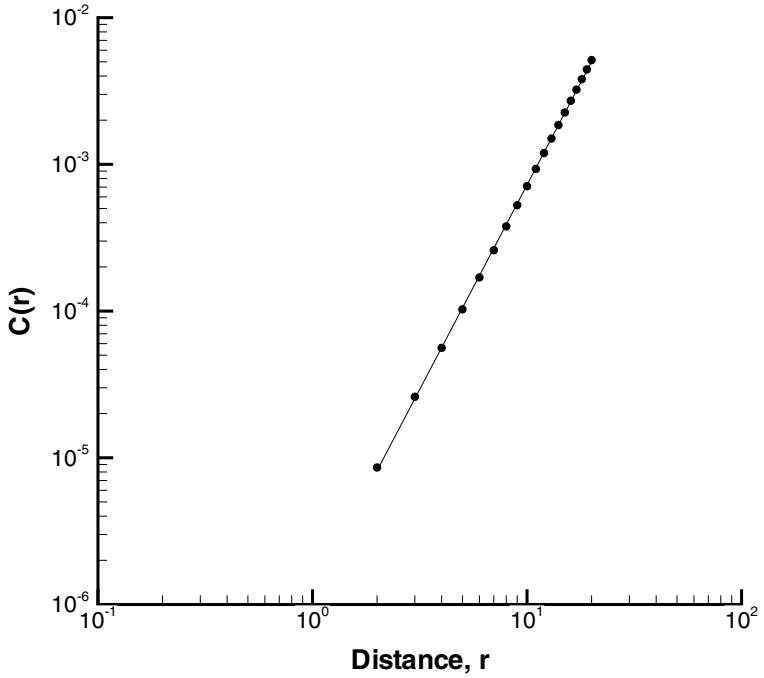

Figure C-10. *The TRUE Block. The correlation function versus distance for two realisations.*

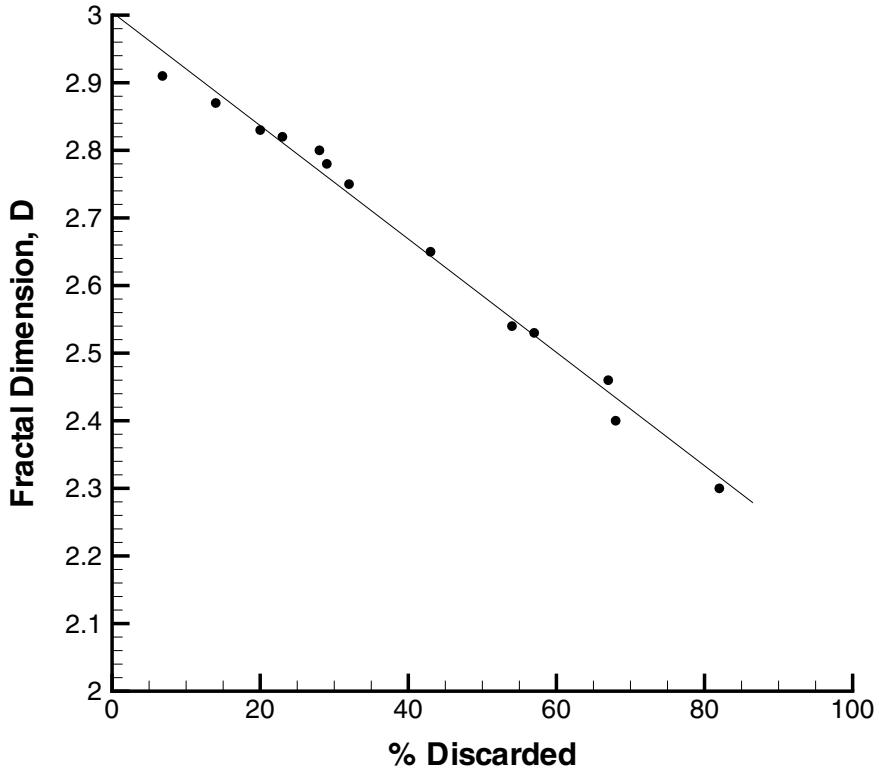

Figure C-11. *Relation between fractal dimension of the generated network and the fraction of fractures* $(0.01L \le l \le 0.05L)$ *discarded in the sorting process.*

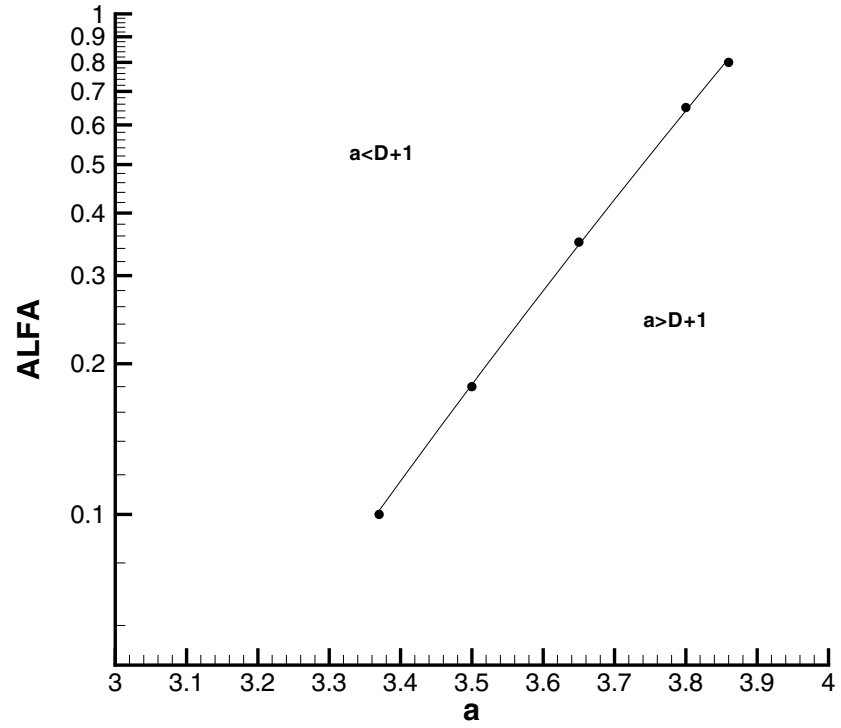

Figure C-12. *Relation between* α_{DT}*, D and a. The line gives the self-similar solution* $\alpha = D+1$.

Concluding remarks

This brief investigation into the generation of fracture networks does not motivate any firm statements. What can be said is that the networks generated by DarcyTools show fractal properties and it also seems possible to generate networks with specified properties (fractal dimension, self-similar, etc).

The bottom line could be quoted from what is often heard at conferences “this paper is now open to discussions”.

References

Bonnet E, Bour O, Odling N, Main I, Berkowitz B, Davy P, Cowie P, 2001. Scaling of fracture systems in geological media. *Rev. Geophys.*, 39, 347–383.

Bour O, Davy P, 1997. Connectivity of random fault networks following a power law fault length distribution. *Water Resour. Res.*, 33, 1567–1583.

Bour O, Davy P, Darcel C, Odling N, 2002. A statistical scaling model for fracture network geometry, with validation on a multi-scale mapping of a joint network (Hornelen Basin Norway), *J. Geophys. Res.*, 107, 2113, doi: 2001JB000176.

Darcel C, 2003. Äspö Hard Rock Laboratory. True block scale continuation project. Assessment of the feasibility of tracer tests with injection in “background fractures” using a model based on a power law fracture length distribution. SKB IPR-03-41, Svensk Kärnbränslehantering AB.

Dershowitz B, Winberg A, Hermanson J, Byegård J, Tullborg E-L, Andersson P, Mazurek M, 2003. A semi-synthetic model of block scale conductive structures at the Äspö Hard Rock Laboratory. SKB IPR-03-13, Svensk Kärnbränslehantering AB.

La Pointe P R, Cladouhos T, Follin S, 1999. Calculation of displacements on fractures intersecting canisters by earthquakes: Aberg, Beberg and Cberg examples. SKB TR-99-03, Svensk Kärnbränslehantering AB.

Sahimi M, 1995. *Flow and transport in porous media and fractured rock.* VCH Verlagsgesellschaft GmbH, Weinheim.

Svensson U, Kuylenstierna H-O, Ferry M, 2004. DarcyTools, Version 2.1 – Concepts, Methods, Equations and Demo Simulations. SKB R-04-19, Svensk Kärnbränslehantering AB.